

TABLE OF CONTENTS

Allen, C. C., Volcano/ice interactions on Mars	1	1/A12
Arvidson, R. E. and Guinness, E. A., Rates of resurfacing of Mars - Constraints on thermal evolution	2	1/A13
Arvidson, R. E. and Jones, K., A year at Mars - Viking Lander imaging results	3	1/A14
Baker, V. R., Morphology of channels on Mars.....	4	1/B1
Balmino, G., Meynet, Roucher, P. and Vales, N., Mars gravity field to degree and order 18: First interpretation	6	1/B3
Baum, W. A., Martin, L. J., Briggs, G. A., and Barnes, J., A review of martian dust clouds and storms	6	1/B3
Bieriann, E., The search for organic compounds in the surface layer and the implications and limitations of the results	7	1/B4
Blasius, K. R., Roberts, W. J. and Glackin, D. L., Topograph. of martian shield volcanoes: comparison of Tharsis and Elysium structures	7	1/B4
Borleries, N., Balmino, G., Castel, L., and Meynet, B., Study and determination of Mars nutations	7	1/B4
Boyce, J. M., Martian subsurface permafrost: evidence from impact craters	8	1/B5
Breed, C. S., and Ward, A. W., Longitudinal dunes on Mars	10	1/B7
Burke, J. D., Mago - A Mars aeroscience-geoscience orbiter	11	1/B8
Carr, M. H., Formation of martian flood features by release of water from confined aquifers	11	1/B8
Casadevall, T., Stoiber, R. and Dzurisin, D., Terrestrial volcanic degassing: a review of mechanisms and magnitudes.....	12	1/B9
Chen, Z. M., The earliest-stage primitive atmospheres of the Mars and the Earth ..	14	1/B11
Chen, Z. M., The structure and oscillation of the martian upper atmosphere.....	14	1/B11
Christensen, E. J. and Balmino, G., Analysis of a twelfth degree and order gravity model for Mars.....	14	1/B11
Chun, S. F.-S., Pang, K. D. and Ajello, J. M., Photocatalytic oxidation of organic compounds in Murchison meteorite under simulated martian conditions	15	1/B12
Cintala, M. J., The effects of subsurface volatiles on martian impact cratering events	16	1/B13
Clark, B. C., Regolith uptake and recycling of volatiles on Mars	16	1/B13
Conrath, B. J., Planetary-scale wave structure in the martian atmosphere	17	1/B14
Coradini, M., A Thermodynamical approach to the study of the martian permafrost...	17	1/B14
Croft, S. K., Kietter, S. W. and Ahrens, T. J., Low velocity impact craters in ice and permafrost with implications for martian crater-count ages	18	1/C1
Cutts, J. A., Blasius, K. R. and Roberts, W. J., Polar geology on Mars: a climatic archive	18	1/C1
Dall'oli, J. F., Environment-organism relations and the interpretation of life-search on Mars.....	19	1/C2
Dowds, R. F., Goldstone radar probes of Mars (1971-1978): A review.....	19	1/C2
Dunne, F. K., Lazarewicz, A. R., Toksoz, M. N., Golin, N., Miller, W. F., Anderson, D. L., Latham, G. V. and Nakamura, Y., A review of the Viking seismology experiment.....	19	1/C2
Dellino, G., Deschamps, M., Duceaux, M., Ksantowaliti, I. V. and Meroz, V. I., Radiometric analysis of Mars from a Sovietic spacecraft	20	1/C3
Farand, J. P., Langevin, Y. and Maurette, M., The Viking imagery, the early history of the martian satellites, and the accretionary tail.....	21	1/C6
Fushary, I. G., Phobos, Deimos and Mars.....	24	1/C7
Dzurisin, D., Casadevall, T. and Stoiber, R., Terrestrial volcanic outgassing: implications for martian atmospheric evolution and surface geology.....	25	1/C8
El Baz, F., Wind erosion in Egypt's Qattara Mountain and implications to eolian on Mars.....	26	1/C9
El Baz, F., Clones of martian light-and dark-colored streaks in the southwestern desert of Egypt.....	26	1/C9

Fanale, F. P. and Cannon, W. A., Mars, implications of capillary condensation and adsorption of CO ₂ on clays for volatile storage and climate change.....	271/C10
Flasar, F. M., Dynamics of thermally driven winds controlled by local topography..	271/C10
Frey, H., Martian rift tectonics.....	281/C11
Friedmann, E. I., Endolithic microbial life in the Antarctic dry valleys: a terrestrial model of martian environment.....	281/C11
Gault, D. D. and Wedekind, J. A., Experimental results for effects of gravity on impact crater morphology.....	291/C12
Gibson, E. K., Andrews, F. J. and Urbanch, M. A., Volatile elements and phase determinations in planetary samples: a proven approach for consideration in future Mars studies.....	301/C13
Goettel, K. A. and Davies, G. F., Present constraints on the bulk composition of Mars and the composition of the martian mantle.....	311/C14
Gooding, J. L. and Keil, F., Relative efficiencies of volatile consumption by chemical weathering reactions on Mars.....	311/C14
Greeley, R., A model for the formation of windblown sand-size particles and related structures on Mars.....	321/D1
Guinness, E. A., Arvidson, R. E. and Lee, S. W., Differential median redistribution rates on Mars.....	331/D2
Hapke, B., The photometric function of martian soil in the vicinity of Viking Lander 1.....	341/D3
Hargraves, R. B., Collinson, D. W., Arvidson, R. E. and Caten, P. M., Viking magnetic properties experiment - results and conclusions.....	341/D3
Honda, K.-I., Leone and compacted soil: two basic units composing the martian surface.....	351/D4
Hansen, K. R., Davis, D. R. and Greenberg, R., Unusual ejecta densities on the martian satellites.....	361/D5
Huyghebaert, K. L., Bond, J. W. and Metcalfe, J. R., Petrologic units on Mars.....	371/D6
Huyghebaert, K. L., Miller, K. J., and Bond, J. W., Mars: chemical reduction of the regolith by frost.....	381/D9
Hunt, G. E., Dust storms and condensation.....	391/D11
Hutton, J. W., Possible oxidant sources in the atmosphere and surface.....	401/D11
Inglis, D. R., Mars: the sedimentary deposits of a Venus-like effect.....	411/D12
Iwamoto, K., Saito, Y. and Akizono, T., Detection and regression of the martian north polar cap in 1975-78.....	421/D12
Jones, P. W., Seasonal behavior of martian polar haze.....	431/D13
Johnson, L. A., Martian solchick: weathering and its relation to water.....	441/D13
Kieffer, H. H. and Anderson, R. P., The climate of the martian polar cap.....	451/D14
Kieffer, H. H. and Anderson, R. P., Global variations of martian surface materials.....	461/E1
Kieffer, H. H. and Anderson, R. P., The role of wind in the martian atmosphere: implications for martian surface.....	471/E2
Klein, D. L., The Viking field experiments: summary and analysis.....	481/E3
Kumar, P. D., Modes of sediment transport by concentrated water flows with ramifications to the erosion of the martian outflow channels.....	491/E3
Kushley, G., Greeley, R. and McKee, D. E., Simulated martian abrasion of soil and basalt under martian conditions.....	501/E4
Kum, G. K., Atreya, S. K. and Postnikov, V. V., Influence of ozone on the thermal structure of the martian atmosphere.....	511/E4
Langevin, Y., An analytical model for the evolution of sand dunes on the martian satellites.....	521/E5
Leitch, D. G., Time scale and patterns of wind erosion on the martian polar regions.....	531/E7

Leach, S., CO ₂ excitation and emission processes in Mars daylight	52	1/E7
Levin, G. V. and Straat, P. A., Status of interpretation of Viking labeled release experiment.....	52	1/E7
Levinthal, E. C., Mars in 3-D.....	53	1/E8
Lyttleton, R. A., Internal structure of Mars.....	53	1/E8
Macris, C. and Petropoulos, B., The martian atmosphere.....	53	1/E8
Malin, M. C., Mars: evidence of indurated deposits of fine materials.....	54	1/E9
Maxwell, T. A., Field investigation of martian canyonlands in southwestern Egypt..	54	1/E9
McCauley, J. F., Breed, C. S., Groller, M. J. and Collins, T., The collar features of the north polar region of Mars.....	55	1/E10
McGord, I. B., Singer, R. B. and Clark, R. N., Mars surface composition from reflectance spectroscopy: a summary.....	56	1/E11
McLosh, B. J., Interior systems on a restricted planet.....	58	1/E13
Moore, B. J., Spitzer, G. B., Coles, P. M., Bradford, K. Z., Scott, R. F., Hutton, K. L., Sherthill, R. A., Surface materials of the Viking landing sites	59	1/E14
Morgan, J. W. and Anders, E., Mars: a cosmochemical-geophysical estimate of bulk composition.....	60	1/F1
Moriyama, S. and Iwashima, T., The spectral model of the atmospheric general circulation of Mars.....	60	1/F1
Mouginis-Mark, P. T., Rampart crater formation on Mars.....	61	1/F2
Mutiso, T. A., Enigmatic landforms on Mars.....	61	1/F2
Nesher, E., Heller, K., Henker, J. and Bolechitel, I., Martian lakes.....	62	1/F2
Nesman, M. J. and Butler, D. M., Cosmic pollution: evidence for recent major martian atmospheric loss.....	62	1/F2
Nye, P. B., Mechanism of dust release on Mars.....	63	1/F4
Okon, L., Origin of volatiles in the martian atmosphere.....	64	1/F5
Phillips, R. J. and Ellis, B. G., Mars: crust and upper mantle structure.....	65	1/F6
Pickerspill, A. O. and Hunt, G. E., On the formation of martian ice waves.....	68	1/F9
Prestel, D. J., McKay, D. S., and Haynes, C. V., Evaporates from the South- western Desert, Egypt: possible martian analogues for the production of sulfuric acid.....	70	1/F11
Rafa, L. L., Danks, C. S., Saunders, R. S. and Lambert, G., Radar morphometry of craters, basins and volcanic landforms on Mars.....	71	1/F12
Russell, C. T. and Scarr, J. L., Mars, the neglected planet: a summary of past deeds and future needs for magnetic and solar wind interaction studies.	71	1/F12
Schubert, E. H. and Gault, D. E., Martian impact craters and their development.....	72	1/F13
Shaffer, P. W., Clark, R. N., and McCollin, T. R., Genesis of martian outflow channels by water-controlled thermal desiccation.....	72	1/F13
Shaw, J. W., Mars: Martian Analogue of warmest southern hemisphere.....	73	1/F14
Shaw, J. W., Gault, D. E., and Clark, R. N., Terrrestrial debris flow deposits as analogs for martian debris flows.....	74	1/F14
Shaw, J. W. and Whorley, K. A., Solis Phlares bright spots.....	75	1/G2
Shaw, J. W. and Whorley, K. A., Solis Phlares bright spots: preliminary results. The 1975-76 period of the solis phlares bright spots.....	75	1/G2
Shaw, J. W., Whorley, K. A., and Gault, D. E., Solis Phlares bright spots: interaction of the solis phlares with the martian atmosphere.....	76	1/G2
Shaw, J. W., Whorley, K. A., and Gault, D. E., Solis Phlares bright spots: interaction of the solis phlares with the martian atmosphere.....	76	1/G3
Shaw, J. W., Whorley, K. A., and Gault, D. E., Solis Phlares bright spots: interaction of the solis phlares with the martian atmosphere.....	76	1/G7
Shaw, J. W., Whorley, K. A., and Gault, D. E., Solis Phlares bright spots: interaction of the solis phlares with the martian atmosphere.....	76	1/G7
Shaw, J. W., Whorley, K. A., and Gault, D. E., Solis Phlares bright spots: interaction of the solis phlares with the martian atmosphere.....	76	1/G8
Shaw, J. W., Whorley, K. A., and Gault, D. E., Solis Phlares bright spots: interaction of the solis phlares with the martian atmosphere.....	76	1/G9

Tillman, J. E., Observations and analysis of frontal systems and periodic processes in the martian atmospheric surface layer.....	82	1/G9
Tokshu, M. N and Hsui, A. T., Internal structure and evolution of Mars.....	83	1/G10
Toon, O. B., History of the martian climate.....	84	1/G11
Veverka, J., Phobos and Deimos: A review of major Viking results.....	85	1/G12
Wall, S. D. and Jones, K. L., Snow on Mars? Quantitative evidence of condensates formed at the Viking Lander 2 site during the martian winter.....	85	1/G12
Warner, J., Oxidation state of martian basalts.....	86	1/G13
Watson, C. C. and Hafl, P. K., Solar wind sputtering of the atmosphere of Mars....	87	1/G14
Wells, R. A., Mantle flow and crustal structure inferred from the low degree harmonics of the martian geopotential.....	88	2/A5
Wise, D. P., Golombek, M. P. and McGill, G. E., Structural sequence, timing and a model for the evolution of the Inarsis province of Mars.....	89	2/A6
Wu, S. S. C., Topographic mapping of Mars.....	90	2/A7

FEB 6 1979

Item 830-H-10

NAS 155:2072

NASA Conference Publication 2072

COMPLETED

Second International Colloquium on MARS

Abstracts for a colloquium held at
the California Institute of Technology
Pasadena, California
January 15-18, 1979

NASA

97

NASA Conference Publication 2072

Second International Colloquium on MARS

**Abstracts for a colloquium held at
the California Institute of Technology
Pasadena, California
January 15-18, 1979**



**National Aeronautics
and Space Administration**

**Scientific and Technical
Information Branch**

1979

**-
I**

PREFACE

This is the second Colloquium devoted to a review of our scientific understanding of Mars. The first Colloquium, held in November, 1973, incorporated the dramatic results of the Mariner 9 orbital mission. The second Colloquium is scheduled at another time of important summation and transition, the end of the Viking mission and the beginning of an intensive Mars Data Analysis Program funded by NASA.

All of the abstracts sent to the Organizing Committee for the Colloquium are included in this volume as submitted. They are arranged alphabetically, by principal author.

TABLE OF CONTENTS

Allen, C. C., Volcano/ice interactions on Mars	1
Arvidson, R. E. and Guinness, E. A., Rates of resurfacing of Mars - Constraints on thermal evolution	2
Arvidson, R. E. and Jones, K., A year at Mars - Viking Lander imaging results	3
Baker, V. R., Morphology of channels on Mars.....	4
Balmino, G., Moynot, Roucher, P. and Vales, N., Mars gravity field to degree and order 18: First interpretation	6
Baum, W. A., Martin, L. J., Briggs, J. A., and Barnes, J., A review of martian dust clouds and storms	6
Biemann, K., The search for organic compounds in the surface layer and the implications and limitations of the results	7
Blasius, K. R., Roberts, W. J. and Glackin, D. L., Topography of martian shield volcanoes: comparison of Tharsis and Elysium structures	7
Borderies, N., Balmino, G., Castel, L., and Moynot, B., Study and determination of Mars nutations	7
Boyce, J. M., Martian subsurface permafrost: evidence from impact craters	8
Breed, C. S., and Ward, A. W., Longitudinal dunes on Mars	10
Burke, J. D., Mago - A Mars aeroscience-geoscience orbiter	11
Carr, M. H., Formation of martian flood features by release of water from confined aquifers	11
Casadevall, T., Stoiber, R. and Dzurisin, D., Terrestrial volcanic degassing: a review of mechanisms and magnitudes.....	12
Chen, Z. M., The earliest-stage primitive atmospheres of the Mars and the Earth ..	14
Chen, Z. M., The structure and oscillation of the martian upper atmosphere.....	14
Christensen, E. J. and Balmino, G., Analysis of a twelfth degree and order gravity model for Mars.....	14
Chun, S. F.-S., Pang, K. D. and Ajello, J. M., Photocatalytic oxidation of organic compounds in Murchison meteorite under simulated martian conditions	15
Cintala, M. J., The effects of subsurface volatiles on martian impact cratering events	16
Clark, B. C., Regolith uptake and recycling of volatiles on Mars	16
Conrath, B. J., Planetary-scale wave structure in the martian atmosphere	17
Coradini, M., A Thermodynamical approach to the study of the martian permafrost...	17
Croft, S. K., Kieffer, S. W. and Ahrens, T. J., Low velocity impact craters in ice and permafrost with implications for martian crater-count ages	18
Cutts, J. A., Blasius, K. R. and Roberts, W. J., Polar geology on Mars: a climatic archive	18
Danielli, J. F., Environment-organism relations and the interpretation of life- search on Mars.....	19
Downs, G. S., Goldstone radar probes of Mars (1971-1978): A review.....	19
Duennebier, F. K., Lazarewicz, A. R., Toksoz, M. N., Goins, N., Miller, W. F., Anderson, D. L., Latham, G. V. and Nakamura, Y., A review of the Viking seismology experiment.....	19
Dollfus, A., Deschamps, M., Duseaux, M., Ksanfomaliti, L. V. and Moroz, V. I., Polarimetric analysis of Mars from a Sovietic spacecraft.....	20
Draud, J. P., Langvin, Y. and Maurette, M., The Viking imagery, the early history of the martian satellites, and the accretionary tail.....	23
Duxbury, T. C., Phobos, Deimos and Mars.....	24
Dzurisin, D., Casadevall, T. and Stoiber, R., Terrestrial volcanic outgassing: implications for martian atmospheric evolution and surface geology.....	25
El Baz, F., Wind erosion in Egypt's Oweinat Mountain and implications to eolian on Mars.....	26
El Baz, F., Clones of martian light-and dark-colored streaks in the southwestern desert of Egypt.....	26

Fanale, F. P. and Cannon, G. A., Mars, implications of capillary condensation and adsorption of CO ₂ on clays for volatile storage and climate change.....	27
Flasar, F. M., Dynamics of thermally driven winds controlled by local topography..	27
Frey, H., Martian rift tectonics.....	28
Friedmann, E. I., Endolithic microbial life in the Antarctic dry valleys: a terrestrial model of martian environment.....	28
Gault, D. D. and Wedekind, J. A., Experimental results for effects of gravity on impact crater morphology.....	29
Gibson, E. K., Andrews, F. F. and Urbancic, M. A., Volatile elements and phase determinations in planetary samples: a proven approach for consideration in future Mars studies.....	30
Goettel, K. A. and Davies, G. F., Present constraints on the bulk composition of Mars and the composition of the martian mantle.....	31
Gooding, J. L. and Keil, K., Relative efficiencies of volatile consumption by chemical weathering reactions on Mars.....	31
Greeley, R., A model for the formation of windblown sand-size particles and related structures on Mars.....	32
Guinness, E. A., Arvidson, R. E. and Lee, S. W., Differential aeolian redistribution rates on Mars.....	33
Hapke, B., The photometric function of martian soil in the vicinity of Viking Lander 1.....	34
Hargraves, R. B., Collinson, D. W., Arvidson, R. E. and Cates, P. M., Viking magnetic properties experiment - results and conclusions.....	34
Horai, Ki-iti, Loose and compacted soils: two basic units composing the martian surface.....	35
Housen, K. R. Davis, D. R. and Greenberg, R., Unusual ejecta dynamics on the martian satellites.....	36
Huguenin, R. L., Head, J. W. and McGetchin, T. R., Petrologic units on Mars.....	37
Huguenin, R. L., Miller, K. J., and Harwood, W. S., Mars: chemical reduction of the regolith by frost.....	40
Hunt, G. E., Dust storms and condensation.....	42
Hunten, D. M., Possible oxidant sources in the atmosphere and surface.....	42
Intriligator, D. S., Mars in the solar wind: implications of a Venus-like interaction.....	43
Iwasaki, K., Salto, Y. and Akabane, T., Formation and regression of the martian north polar cap in 1975-78.....	43
James, P. B., Seasonal behavior of martian polar caps.....	44
Johansen, L. A., Martian splash cratering and its relation to water.....	44
Kieffer, H. H. and Palluconi, F. D., The climate of the martian polar cap.....	45
Kieffer, H. H. and Soderblom, L. A., Global variations of martian surface materials.....	46
Kieffer, S. W. and Simonds, C. H., The role of volatiles in the cratering process: implications for martian surface.....	47
Klein, H. P., The Viking biology experiment: epilogue and prologue.....	48
Komar, P. D., Modes of sediment transport in channelized water flows with ramifications to the erosion of the martian outflow channels.....	48
Krinsley, D., Greeley, R. and McKee, T. R., Simulated aeolian abrasion of quartz and basalt under martian conditions.....	49
Kuhn, W. R., Atreya, S. K. and Postawko, S. E., Influence of ozone on the thermal structure of the martian atmosphere.....	49
Langevin, Y., An analytical model for the regolith evolution of small bodies in the solar system.....	50
Leach, J. H. J., Dune forms and patterns of wind circulation in the north polar regions of Mars.....	52

Leach, S., CO ₂ excitation and emission processes in Mars dayglow	52
Levin, G. V. and Straat, P. A., Status of interpretation of Viking labeled release experiment.....	52
Levinthal, E. C., Mars in 3-D.....	53
Lyttleton, R. A., Internal structure of Mars.....	53
Macris, C. and Petropoulos, B., The martian atmosphere.....	53
Malin, M. C., Mars: evidence of indurated deposits of fine materials.....	54
Maxwell, T. A., Field investigation of martian canyonlands in southwestern Egypt..	54
McCauley, J. F., Breed, C. S., Grolier, M. J. and Collins, P., The eolian features of the north polar region of Mars.....	55
McCord, T. B., Singer, R. B. and Clark, R. N., Mars surface composition from reflectance spectroscopy: a summary.....	56
Melosh, H. J., Fracture systems on a reoriented planet.....	58
Moore, H. J., Spitzer, C. R., Cates, P. M., Bradford, K. Z., Scott, R. F., Hutton, R. E., Shorthill, R. W., Surface materials of the Viking Landing sites	59
Morgan, J. W. and Anders, E., Mars: a cosmochemical-geophysical estimate of bulk composition.....	60
Moriyama, S. and Iwashima, T., The spectral model of the atmospheric general circulation of Mars.....	60
Mouginis-Mark, P. J., Rampart crater formation on Mars.....	61
Mutch, T. A., Enigmatic landforms on Mars.....	61
Neukum, G., Hiller, K., Henkel, J. and Bodechtel, J., Martian ages.....	62
Newman, M. J. and Butler, D. M., Cosmic pollution: evidence for recent major martian atmospheric loss?.....	62
Nummedal, D., Mechanics of fluid release on Mars.....	63
Owen, T., Origin of volatiles in the martian atmosphere.....	64
Phillips, R. J. and Bills, B. G., Mars: crust and upper mantle structure.....	65
Pickersgill, A. O. and Hunt, G. E., On the formation of martian lee waves.....	68
Prestel, D. J., McKay, D. S., and Haynes, C. V., Evaporates from the South- western Desert, Egypt: possible martian analogues for the production of duricrust.....	70
Roth, L. E., Downs, G. S., Saunders, R. S. and Schubert, G., Radar morphometry of craters, basins and volcanic landforms on Mars.....	71
Russell, C. T. and Scari, F. L., Mars, the neglected planet: a summary of past deeds and future needs for magnetic and solar wind interaction studies.	71
Schultz, P. H. and Gault, D. E., Martian impact crater ejecta emplacement.....	72
Schultz, P. H., Glicken, H., and McGetchin, T. R., Genesis of martian outflow channels by crater-controlled intrusions.....	72
Scott, D. H., Mars: Viking Appraisal of mariner geologic mapping.....	73
Shultz, A., Suttner, L. J., and Basu, A., Terrestrial debris flow deposits an analogs of martian strewn fields.....	74
Sjogren, W. L. and Kimberly, R. N., Hellas Planitia gravity anomaly.....	75
Simpson, R. A. and Taylor, G. L., Viking bistatic radar: preliminary results from the north polar region.....	75
Smith, E. J., Mars in the solar wind: Implications of an earth-like interaction.	75
Snyder, C. W., Viking scientific results, September 1977 to September 1978.....	76
Squyres, S., Evolution of the topography of the martian polar laminated deposits.	80
Srnka, L. J., Crustal TRM and the magnetic field of Mars.....	80
Strickland, E. L., Color enhanced Viking lander images of Mars.....	81
Thomas, P., Seasonal and secular behavior of crater-related streaks on Mars: a study of Mariner 9 and Viking Orbiter data.....	82

Tillman, J. E., Observations and analysis of frontal systems and periodic processes in the martian atmospheric surface layer.....	82
Toksz, M. N and Hsui, A. T., Internal structure and evolution of Mars.....	83
Toon, O. B., History of the martian climate.....	84
Veverka, J., Phobos and Deimos: A review of major Viking results.....	85
Wall, S. D. and Jones, K. L., Snow on Mars? Quantitative evidence of condensates formed at the Viking Lander 2 site during the martian winter.....	85
Warner, J., Oxidation state of martian basalts.....	86
Watson, C. C. and Haff, P. K., Solar wind sputtering of the atmosphere of Mars....	87
Wells, R. A., Mantle flow and crustal structure inferred from the low degree harmonics of the martian geopotential.....	88
Wise, D. U., Colembek, M. P. and McGill, G. E., Structural sequence, timing and a model for the evolution of the Tharsis province of Mars.....	89
Wu, S. S. C., Topographic mapping of Mars.....	90

Volcano/Ice Interactions on Mars

C. C. Allen, Department of Planetary Sciences, University of Arizona, Tucson, Arizona 85721

Examination of high-resolution Viking orbital imagery has led to the recognition of martian features probably analogous to table mountains, moberg ridges and pseudocraters.

Table mountains are steep-sided, flat-topped structures resulting from basaltic central-vent eruptions beneath glacial ice sheets. They range from 2-10 km in width, and up to 1 km in height. Many display summit cones and craters.

Moberg ridges are the products of subglacial fissure eruptions. They are generally straight, narrow and steep, with serrated crests. The ridges range from a few hundred meters to tens of kilometers in length, and are several hundred meters high.

Pseudocraters are small cinder and spatter cones which are formed by steam explosions when lava flows over water-saturated ground. Typical features range from a few tens to over 100 meters in basal diameter, while the diameter of the central crater is $1/3 - 1/2$ that of the base.

The proposed martian analogs to table mountains and moberg ridges are common in the northern plains, specifically Amazonis, Chryse, Utopia and most notably Acidalia Planitia. Several lava flows displaying probable pseudocraters also occur in Acidalia Planitia.

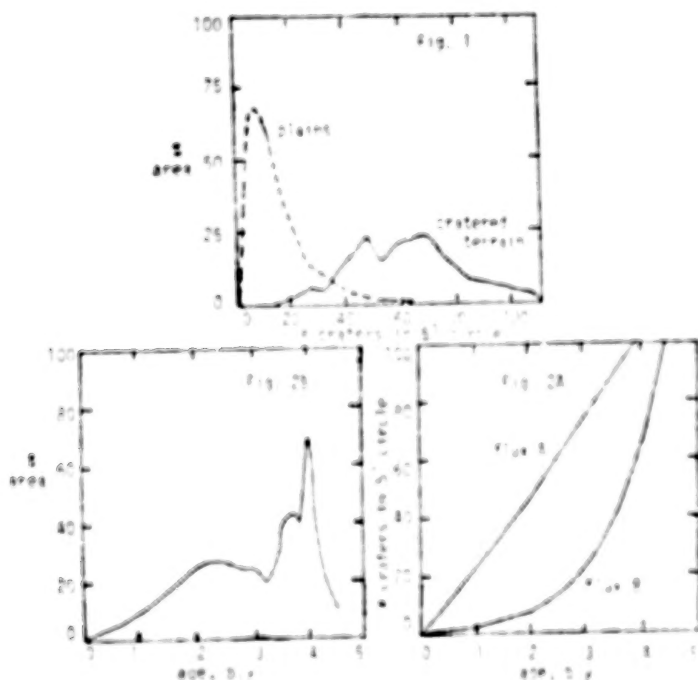
Viking photomosaics (211-5557, 5024) of Acidalia Planitia reveal an extensively cracked terrain with many rampart craters. This unit is topped by a number of mountains and ridges closely resembling the features discussed above. Several "pedestal craters", impact crater whose rampart-style ejecta tops raised platforms, also occur. These craters probably impacted onto a surface uniformly higher than the present one and containing abundant ground ice, as evidenced by the rampart ejecta. Volcanic eruptions into this ice produced the table mountains and ridges. Subsequent erosion stripped the ice-rich layer away, except where crater ejecta acted as a protective cap. The stripping revealed the table mountains and ridges, which appear resistant to erosion.

Several lines of evidence indicate that the lower surface exposed by erosion still contains abundant near-surface ice. The numerous cracks form patterns similar to terrestrial permafrost networks. Rampart craters, as small as 1 km across, may indicate impact into ice-rich material. Finally, several thin lava flows are dotted with small cones similar in size and morphology to pseudocraters. The ice must have been very near to the surface for a lava flow to have heated it sufficiently to produce steam explosions.

Rates of Resurfacing of Mars - Constraints on Thermal Evolution

R. E. Arvidson and E. A. Guinness, Department of Earth and Planetary Sciences, Washington University, St. Louis, Missouri 63130

A rigorous constraint on the thermal evolution of a planet is the mass or volume of volcanic material produced as a function of time. Although we cannot estimate either the volume or the temporal history of volcanic activity with much precision, we have found that a plot of fractional surface area versus age (via crater abundance) provides important information directly related to the planet's thermal evolution history. Figure 1 shows the fractional area within $\pm 30^\circ$ lat. occupied by a given crater abundance, for craters ≥ 8 km in diameter. Qualitatively similar results were obtained for craters between 4 to 10 km in diameter. The data show a bimodal distribution, with cratered terrain extending over a large range of crater abundances, while plains are much more peaked and clustered at low crater abundances. One interpretation is that cratered terrain formed at a low rate over a long period of time, while plains formed rapidly and recently. However, such a scenario would be true only if the rate of cratering on Mars were constant with time (flux A of Fig. 2). The more likely case, is that much of cratered terrain probably began to retain craters during a period of early heavy bombardment (e.g. flux B, Fig. 2A). When such constraints are applied, the effect is to narrow the cratered terrain distribution and to make it considerably more peaked, as shown in Figure 2B. Plains, on the other hand, are extended over a longer period of time and the resurfacing rate is decreased. The important points are that for any reasonable cratering model, (a) the bimodal nature of the data remains and (b) the time range of cratered terrain formation is compressed, while the time scale is extended for plains. Thus, we are left with early, rapid formation of cratered terrain with the plains occurring later and extending over much of geologic time. The exact shape of the re-surfacing curve for plains depends sensitively on the post-heavy bombardment cratering flux and on the age used for the transition between pre- and post-heavy bombardment. Such a scenario is consistent with a thermal evolution history having cratered terrain formed early and rapidly. The only plausible way to get the required large amounts of energy so early in the planet's history is to have cratered terrain be an initial crust solidified from a lunar-like magma ocean formed by accretional melting of the outer few hundred kilometers of Mars. Plains volcanism seems to have followed a somewhat independent time scale that was probably driven by the amount of time needed for the interior of Mars to heat-up and differentiate. Unfortunately, the shape of the re-surfacing curve for plains is sufficiently uncertain so as to provide little information on the timing of peak volcanism.



A Year at Mars - Viking Lander Imaging Results

R. Arvidson, McDonnell Center for the Space Sciences, Washington University, St. Louis,
Missouri 63130

K. Jones, Planetary Research, Inc., Pasadena, California 91106

Throughout the complete Mars year during which they have been on Mars, the imaging systems aboard the two Viking Landers have documented a variety of surface changes. These changes have been used to infer both the dynamic processes which modify the planet's surface and the rates at which these processes are effective. The observed changes result from wind-entrainment of soil materials, formation of a surface layer of H_2O condensates at the VL-2 site, and the accumulation of a thin layer of bright dust at both sites. Dust, brought to the VL-2 site from more southerly latitudes, apparently acted as nucleation center for transporting H_2O in a solid phase. Subsequent solid CO_2 condensation on dust grains above the VL-2 site accelerated their precipitation onto the surface. The remnant surface condensates required well over one hundred sols to return to the atmosphere, suggesting that they consisted exclusively of solid H_2O . Additionally, despite two global dust storms and at least one localized dust storm, the observations of the effects of dust transport have been confined to the surface redistribution of an extremely thin layer of bright dust. Only minimal horizon obscuration by dust is observed. It is now believed that surface erosion rates due to dust redistribution may be substantially less than rates predicted based on pre-Viking observations.

Morphology of Channels on Mars

V. R. Baker, The University of Texas, Austin, Texas 78712

Viking photographs of the martian surface reveal a remarkable density and variety of channels and channel-like forms. Although this variety precludes a rigorous classification, two important groups demand special consideration: (a) dry valley systems, and (b) outflow channels. Considerable variation exists within each major class, and some channels (e.g., Ma'adim Vallis) have features characteristic of both groups.

The dry valley systems of Mars (also termed "microchannels" and "runoff channels") are ubiquitous to the heavily cratered terrain of Mars (1). These relatively small features (widths generally ≤ 1 km, lengths 10-100 km), exemplified by the Margaritifer Sinus and Thaumasia regions, record a very ancient erosional process that conformed to topographic controls (concentric drainage to basins and dissection of ancient crater rims). Although some systems bear a superficial resemblance to terrestrial dendritic valley systems, detailed study has revealed important differences: (a) Generally the high-order (trunk) valleys are much more incised and elongated than the lowest order tributaries. (b) Tributary junction angles to main valleys are much lower than in terrestrial systems and also relatively insensitive to increasing stream magnitude, i.e., valley widening (2). The relationships suggest an immaturity of drainage development. Somewhat analogous terrestrial dry valley systems develop in areas of pronounced climatic change, spring sapping followed by water-table lowering, permafrost or periglacial conditions, and karst or pseudokarstic conditions that divert surface runoff into subsurface aquifers (3). Nirgal Vallis, one of the largest dry valley systems on Mars, displays unusually deep entrenchment that has apparently favored several valley-wall processes: landsliding, debris cones, and sapping.

The outflow channels of Mars are much larger than the dry valley systems. Channel widths range from 10-100 km, and some channel complexes (Maja, Ares, and Kasei Valles) can be traced 2000 km or more. These channels appear full-born at localized sources, usually collapse zones marked by chaotic terrain. They transect terrains of varying age, generally emanating from sources within the heavily cratered terrain, traversing the great "planetary dichotomy" (4), and debouching on to the low-lying sparsely cratered northern plains. Although the majority of outflow channels surround the Chryse Basin (Kasei, Maja, Shalbatana, Simud, Tiu, and Ares Valles), several large outflow channels occur along other portions of the plains-highlands boundary (Mangala and Ma'adim Valles). A variety of outflow channel emanates from collapse troughs in the volcanic lava flow units on the distal flanks of Elysium Mons.

Outflow channel ages are decidedly younger than the dry valley systems. Crater counts for the latter and associated heavily cratered terrains are generally in excess of 10^4 craters ≥ 1 km diameter per 10^6 km², while counts in outflow channels average about 2×10^3 craters ≥ 1 km diameter per 10^6 km² (5). These data imply ages of 2 Gy and about 1 Gy respectively, according to the calibration curve of Soderblom *et al.* (6).

The outflow channels are true channels because the erosive fluid produced a variety of bed forms that often mark the entire valley width. Detailed morphological mapping from Viking imagery of Kasei, Maja, Ares and Tiu Valles (7, 8) has revealed a distinctive assemblage of landforms. The macroforms are related to the overall channel pattern and include the following: (a) a regional anastomosis of channels, (b) discrete source areas (chaotic terrain) displaying a disparity between apparent released fluid volume and downstream trough volume showing fluid-erosional forms, (c) indistinct fluid sink relationships, (d) erosion of diverse rock types thousands of kilometers from probable fluid source areas, (e) residual uplands separating channels, many of which are streamlined by fluid flow, (f) pronounced flow constrictions and expansions, (g) high width-depth ratio, (h) low sinuosity, (i) differential erosion controlled by lithology and structure, including exhumation of pre-flow topography. The bed forms within the channels include the following: (a) longitudinal grooves, (b) inner channels, (c) transverse headcuts (cataracts), (d) scabland, (e) scour marks around flow obstacles, (f) pendant forms, including possible depositional bars, and (g) expansion bar complexes. Although many of the individual features can be explained by the action of fluids other than water, the complete assemblage

of the named landforms and their spatial relationships suggest catastrophic flooding by water as the most likely explanation (9, 10).

The only single terrestrial landscape that contains analogs to all the martian outflow features is the Channeled Scabland of eastern Washington, created by catastrophic flood flows across differentially resistant basalt, loess, and sedimentary rocks (11, 12). Although catastrophic flood erosion generally involves process-response conditions far from equilibrium, some bed forms do show a clear adjustment to process. The streamlined residual uplands have received the most study in this regard. We have now compared 92 streamlined forms in Kasei and Maja Valles to 132 streamlined forms in the Channeled Scabland. The best developed streamlined forms on both planets show similar elongation such that length L , measured parallel to the inferred flow direction, is related to planimetric area A according to $L = 2A^{1/2}$ with $r = 0.94$. The forms are generally elongated to about three times the maximum form width (measured perpendicular to the inferred flow direction). This ideal shape probably results from elongation sufficient to reduce pressure drag in the responsible fluid, but not so long as to create excess skin resistance (13).

Although the same bed forms characterize the martian channels and their scabland analogs, the relative abundances of various bedform types differ. The dominance of erosional grooves on Mars in contrast to butte-and-basin scabland may derive in part from differences in the lithology and jointing of the rock types subject to scour on the two planets. Another important consideration is the different atmospheric conditions that probably prevailed on Mars during the channelling episode. A lower atmospheric pressure on Mars would result in a greater ease in producing cavitation erosion than can be achieved under terrestrial conditions (14). The lower temperature would also have favored a variety of river ice processes. In terrestrial rivers frazil ice forms in supercooled water and transforms to various other ice states. Surface ice is favored at times of extreme cold and may be flushed out as ice drives by upstream warm water flood influxes. Ice jams form at constrictions leading to intense scour when head differences induce breakup (15). If earlier water flows freeze solid, subsequent water moves across the zones of icing thereby inducing abnormal channel widening and erosion high above the normal channel bed (16). The morphological implications of both cavitation and river ice processes have yet to be fully investigated.

Our detailed mapping has focused attention on prominent post-flood modification features that have affected various channels to different degrees. Upper Kasei Vallis has an accentuated floor relief of grooved terrain. Such an "etching" could be achieved by salt weathering and eolian removal of detritus (17). In lower Kasei Vallis wall relief of 2-3 km is associated with prominent mass wastage and sapping features. Spur-and-gully topography (18, 19) landslides, debris fans, and debris cones are locally present. The much lower depth of incision for Maja Vallis is associated with much less wall modification. It appears that steep escarpments exposed by tectonic influences and subsequent flood incision later became the sites of long-term backwearing by mass wasting and sapping. Because the slope forms are most consistent processes that involved ground ice, the outflow channels probably functioned at a time when permafrost was widely distributed on Mars (20).

Viking has revealed a variety of fluvial phenomena on Mars that is as rich and varied as that on the earth. The comparison of these features, their similarities and their differences, will continue to broaden our understanding of river and valley processes. Already the outflow channels have given new relevance to the prophetic words of J. Harlan Bretz (21) as, one-half century ago, he defended his flood hypothesis for the Channeled Scabland: "...it should not be judged by the principles applicable to valley formation, for the scabland phenomena are the product of river channel mechanics."

V. R. Baker...3

References:

- 1) Pieri, D. (1976) Icarus 27, 25-50.
- 2) Pieri, D. and C. Sagan (1978) NASA Tech. Memo 79729, 268.
- 3) Gregory, K. J. and D. E. Waring (1973) Drainage Basin Form and Process, Edward Arnold, London, 456 p.
- 4) Mutch, T. et al. (1976) The Geology of Mars, Princeton Univ. Press, 400 pp.
- 5) Masursky, H. et al. (1977) J. Geophys. Res. 82, 4016-4038.
- 6) Soderblom, L. A. et al. (1974) Icarus 22, 239-263.
- 7) Baker, V. R. and R. C. Kochel (1978) Proc. Lunar Planet. Sci. Conf. 9th, C345-C356.
- 8) Baker, V. R. and R. C. Kochel (1978) Paper presented at 2nd Colloquium on Planet. Water and Polar Processes, Hanover, N. H., Abstracts p. 56-59.
- 9) Baker, V. R. and D. J. Milton (1974) Icarus 23, 27-41.
- 10) Baker, V. R. (1978) Proc. Lunar Planet. Sci. Conf. 9th C383-C401.
- 11) Baker, V. R. (1973) Geol. Soc. Amer. Spec. Pap. 144, 79 p.
- 12) Baker, V. R. (1978) in The Channeled Scabland, V. R. Baker and D. Nummedal, eds., NASA Planetary Geol. Prog., Washington, p. 59-115.
- 13) Baker, V. R. and R. C. Kochel (1978) Proc. Lunar Planet. Sci. Conf. 9th, C403-C413.
- 14) Baker, V. R. (1978) NASA Tech. Memo 79729, 248-250.
- 15) Smith, D. G. (in press) Water Resources Research.
- 16) Smith, D. G. (1978) Paper presented at the 9th Annual Geomorphology Symposium, S.U.N.Y., Binghamton, N. Y.
- 17) Malin, M. C. (1974) J. Geophys. Res. 79, 3888-3894.
- 18) Sharp, R. P. (1973) J. Geophys. Res. 78, 4063-4072.
- 19) Lucchitta, B. K. (1978) J. Res. U. S. Geol. Survey 6, 651-662.
- 20) Carr, M. H. and G. G. Schaber (1977) J. Geophys. Res. 82, 4039-4054.
- 21) Bretz, J. H. (1923) Geol. Soc. Amer. Bull. 39, 643-702.

Mars Gravity Field to Degree and Order 18. First Interpretation

G. Balmino, B. Moynot, P. Roucher, N. Vales, CNES-GRGS, Toulouse, France

A spherical harmonic expansion of the Mars gravity field up to (18,18) has been obtained from two-way Doppler tracking data of Mariner 9, Viking 1 and 2 orbiters. The resolution of this model and the knowledge of the Mars topography (B. Bills et al., 1978) allow some interpretation of the planet upper layers, in terms of Bouguer gravity, deviation from isostasy and crust thickness.

A Review of Martian Dust Clouds and Storms

W. A. Baum and L. J. Martin, Planetary Research Center, Lowell Observatory, Flagstaff, Arizona 86002

G. A. Briggs, Office of Space Science, NASA Headquarters, Washington, DC 20546

J. Barnes, Department of Atmospheric Sciences, University of Washington, Seattle, Washington 98195.

Martian dust clouds tend to occur in particular regions and in a particular season. We summarize the observations obtained with Viking orbiters and with Earth-based telescopes. Active regions are partially correlated with areas of positive vertical velocity predicted by atmospheric circulation models that incorporate large-scale topography, but the role of local slopes is less clear. Dust clouds have also been observed near the edge of the southern polar cap, where winds are doubtless enhanced by the strong temperature gradient. Very few martian dust clouds develop into "global" storms, but patterns of storm development bear some interesting similarities to one another.

The Search for Organic Compounds in the Surface Layer and the Implications and Limitations of the Results

K. Biemann, Massachusetts Institute of Technology, Cambridge, Massachusetts 02139

The results of the Molecular Analysis experiment will be reviewed. The basis and implications of the negative results of the search for organic compounds will be discussed with particular emphasis on the applicability and limitations of the experiment for the various scenarios that have been or are being considered for the chemical environment existing in the martian surface.

Topography of Martian Shield Volcanoes: Comparison of Tharsis and Elysium Structures

K. R. Blasius and W. J. Roberts, Planetary Science Institute, 283 S. Lake Ave., #218, Pasadena, California 91101

D. L. Glackin, Informatics Inc., and Jet Propulsion Laboratory, Pasadena, California 91103

Topographic maps of several martian shield volcanoes in both the Tharsis and Elysium volcanic provinces have been compiled from high altitude stereo image pairs using a semi-automatic digital mapping system developed for the Viking Orbiter Imaging Team at the Image Processing Laboratory, JPL (Ruiz *et al.*, 1977, JGR, 82, 4189 and Blasius, 1977, B.A.A.S., 9, 538). Relief slopes and volume characteristics of the volcanoes are compared. Model mass determinations for Elysium Mons and Olympus Mons (Sjogren 1978, submitted to Science) are combined with new volume estimates to derive model densities.

Study and Determination of Mars Nutations

N. Borderies, G. Balmino, L. Castel, B. Moynot, CNES-GRCS, Toulouse, France

The motion of the Mars polar axis is being studied over long time periods. Very large amplitude nutations have been found by the Lie series method and confirm the results already found by Ward (1973) and Borderies *et al.* (1978). In addition, short period terms have been exhibited with amplitudes ranging from 0.04 to 1.1 arc second. An attempt to determine the largest terms has been made, which used the Earth to Viking Lander 1 and 2 data. We give an account of the method and the first obtained results.

Martian Subsurface Permafrost: Evidence from Impact Craters

J. M. Boyce, U. S. Geological Survey, Flagstaff, Arizona 86001 (present address: NASA Headquarters, SL-4, Washington, DC)

Martian rampart and flow-ejecta craters have been attributed to (1) impact into a subsurface permafrost or water layer (Carr et al., 1977); (2) entrainment of atmospheric gases during impact (Carr et al. 1977; Schultz, 1978); (3) impact by volatile-rich projectiles; and (4) eolian modification of existing craters (McCauley, 1973). Current evidence suggests that the most reasonable of these is impact into a subsurface permafrost or water layer.

It is known that conditions on Mars (water ice polar caps, atmospheric water vapor and ancient river systems) were once favorable for formation of a subsurface permafrost layer. Such features as patterned ground suggest that near-surface ice is indeed present on Mars (Carr and Schaber, 1977). Experimental evidence shows that rampart and flow-ejecta craters are produced only in wet target materials (Gault and Greeley, 1978; D. J. Roddy, personal communication, 1978) and that these two types of craters are genetically related, with the amount of water in the target material controlling the particular morphology.

Entrainment of atmospheric gas probably played only a minor role in ejecta flow, as evidenced by the fact that the earth's atmosphere has little or no effect on experimental or natural crater ejecta (Roddy, 1977). Also, preliminary analyses of impact experiments indicate that there is no correlation of the minimum, or initiation, diameter of flow-ejecta craters with elevation or surface age, which further suggests that atmospheric interaction with the ejecta is unimportant in producing these craters. Impact by volatile-rich (low density) projectiles can play only a minor role in production of rampart and flow-ejecta craters although they may affect other morphologic parameters like depth-diameter ratios. This conclusion is based on two facts: (1) rampart craters are recognized only on Mars, and (2) the initiation diameter of flow-ejecta craters is significantly different from place to place on Mars, which is inconsistent with the random nature of cratering. Morphologically fresh rampart craters with fine-scale features preserved and with no evidence of appreciable erosions are common. These peculiar craters are thus primary landforms and not the result of erosion.

Carr (1978) suggested that some of the water initially outgassed by the planet, or residing in a primitive atmosphere, was lost to the ground-water system. He suggests that as the surface temperature fell, a permafrost layer developed and thickened to form effectively confined aquifers. Allen (1978) showed that young volcanic subsurface water or permafrost must be present even in these terranes. The emplacement in these young rocks has been difficult to explain because, unlike the old terranes, the young terrane show no evidence of being affected by rain (Pieri, 1978), which is needed to charge the ground-water system. The uniform distribution of flow-ejecta craters on the younger surfaces rules out ascent of juvenile water from the deep interior as a source of the permafrost layer, because ascending juvenile waters are usually confined to small areas associated with volcanic vents or fractures. However, the water in the young terranes may have ascended from the old buried terranes. Assuming that the thermal gradient in the shallow part of the martian crust is similar to that of the Earth (temperature is proportional to depth), the permafrost layer in old units should melt in response to burial by young units because of the insulative properties of the young units. The permafrost may also have been melted by heat from young lavas. The melted ground water would migrate upward toward regions of lower pressure. The ascent of the ground water may have been quite rapid because, as pointed out by Carr (1978), volcanic rocks such as those characterizing most young areas are commonly very porous and permeable. The ground water should rise until it freezes again into permafrost. This process may account for the presence of permafrost in both old and young martian rocks.

References:

- Allen, C. C. (1978) Areal distribution of rampart craters on Mars (abs.): NASA TM 79729, p. 160-161.
- Carr, M. H. (1978) Formation of martian flood features by release of water from confined aquifers: NASA TM 79729, p. 260-262.
- Carr, M. H., Crumpler, L. S., Cutts, J. A., Greeley, R., Guest, J. E., and Masursky, H. (1977) Martian impact craters and emplacement by surface flow: *J. Geophys. Res.*, v. 82,

J. M. Boyce ...p. 2

p. 4055-4065.

Carr, M. H. and Schaber, G. G. (1977) Martian permafrost features: J. Geophys. Res., v. 82, p. 4039-4054.

Gault, D. E. and Greeley, R. (1978) Exploratory experiments of impact craters formed in viscous-liquid targets: Analogs for martian rampart craters: Icarus, v. 34, no. 3, p. 486-495.

McCauley, J. F. (1973) Mariner 9 evidence for wind erosion in the equatorial and mid-latitude regions of Mars: J. Geophys. Res., v. 78, p. 4123-4137.

Pieri, D. (1978) Small channels on Mars from Viking Orbiter (abs.): NASA TM 79729, p. 267.

Roddy, D. J. (1978) Large-scale impact and explosion craters: Comparisons of morphological and structural analogs in Impact and Explosion Cratering Planetary and Terrestrial Implications, Pergamon Press, p. 185-248.

Schultz, P. H. (1978) Impact ejecta emplacement on Mars (abs.): Lunar and Planetary Science Conf., 9th Proc. v. 2, p. 1027-1029.

Longitudinal Dunes on Mars

C. S. Breed, U. S. Geological Survey, Flagstaff, Arizona 86001

A. W. Ward, Arizona State University, Tempe, Arizona 85281

Arrays of parallel linear ridges in the equatorial and mid-latitude regions of Mars were described, on the basis of low resolution Mariner 9 and early Viking pictures, as ridge and furrow terrain (yardangs) (McCauley, 1973; Ward, 1978). Newly acquired, high resolution (about 19m) Viking Orbiter pictures reveal that the ridges in the Biblis Patera region are not wind erosion forms, but instead are very large longitudinal dunes. Their identification provides the first conclusive evidence that dunes of the classic longitudinal (linear) type occur on a planet other than Earth.

Linear dunes comprise one of the five basic classes of dunes on Earth, where they cover approximately half the total area of sand seas. They differ significantly in both morphology and mode of occurrence from the barchanoid (crescentic) type of dune which is ubiquitous on Earth. Crescentic dunes were previously known to occur on Mars, particularly in North Polar ergs. They have planet-wide distribution in crater floor dune fields.

Longitudinal dunes, in contrast to the barchanoid type, grow lengthwise to the wind such that their long axes are parallel rather than transverse to the resultant direction of regional winds. On Earth, these dunes are associated with very strong, highly directional and repetitive wind patterns. However, the specific processes by which longitudinal dunes are constructed, and hence their precise relationship to wind regimes are poorly known and remain the subject of controversy (Breed *et al.*, in press).

The largest longitudinal dunes in the Biblis Patera region have a mean length of 8.1 km, a mean width of 0.49 km and a mean wavelength (crest-to-crest spacing) of 1.4 km. They closely resemble compound to complex longitudinal dunes in parts of the Simpson and Great Sandy deserts of central Australia, in the western Sahara of North Africa, and in the southwestern Rub al Khali of the Arabian Peninsula. They appear to be migrating from east to west, climbing and falling across escarpments in a manner similar to dunes observed in terrestrial deserts. The total area occupied by large longitudinal dunes is at least 100,000 km². Fields of barchanoid and complex dunes are visible in surrounding areas of Biblis Patera, and hence it is likely that much of this region is veneered with eolian deposits, and thus is not an erosional surface as previously described.

The discovery of large fields of Earth-like longitudinal dunes close to the martian equator implies that Earth-like atmospheric and geologic processes conducive to dune building have not been restricted to the North Polar region. Unlike the eolian sediments in the north circumpolar region, which are composed of dark material, the Biblis Patera longitudinal dunes have a high albedo, and they are not associated with ice. The broad areal extent, regular pattern of distribution, consistent directional trend, and the large scale of the dunes suggest that strong prevailing winds have persisted in this part of Mars for a rather lengthy time period. Detailed studies of the dynamics of longitudinal dune growth and migration are needed before the relationship of these dunes to the regional martian wind pattern can be defined.

References :

- Breed, C. S., J. F., McCauley, W. J., Breed, C. K., McCauley and A. S. Cotera (in press) Eolian Landscapes in Smiley, Terah (ed.) Landscapes of Arizona - the geologic story, Univ. of Arizona Press, Tucson.
- McCauley, J. F. (1973) Mariner 9 evidence for wind erosion in the equatorial and mid-latitude regions of Mars: *J. Geophys. Res.* 78, no. 20, p. 4123-4137.
- Ward, A. W. (1978) Windforms and wind trends on Mars: an evaluation of martian surficial geology from Mariner 9 and Viking spacecraft television images: Ph.D. Thesis, Univ. of Washington, Seattle, 201 p.

Mago - A Mars Aeroscience-Geoscience Orbiter

J. D. Burke, Jet Propulsion Laboratory, Pasadena, California 91103

This paper describes the objectives and progress of a current study intended to define a relatively low-cost Mars orbital mission for 1986. This independent scientific mission, with geological, geochemical, geophysical, atmospheric and particle-and-field instrumentation, would be an alternative option to doing the same sorts of measurements within the context of a Mars Sample Return program. The study rationale and schedule, assumed scientific objectives, and initial study results will be described.

Formation of Martian Flood Features by Release of Water from Confined Aquifers

M. H. Carr, U. S. Geological Survey, Menlo Park, California

Many large martian channels arise full scale from discrete areas of chaotic terrain. Estimates of peak discharges based on channel dimensions range from 10^6 to 10^8 m³/sec. It is proposed that the large channels were eroded by water released rapidly, under great pressure, from deeply buried aquifers. Early in the planet's history the old cratered terrain was probably highly permeable to depths of several kilometers as a result of its volcanic origin and intense brecciation by meteorite impact. Extensive dissection of the old cratered terrain by fine channels suggests that fluvial action was widespread at that time and that warmer climatic conditions prevailed. Much of the water which cut the fine channels may have been lost not to the atmosphere but to an extensive ground water system. Subsequent global cooling would have trapped the ground water under a thick permafrost layer and formed a system of confined aquifers. The vertical relief of the aquifers and possibly the thickening of the permafrost may have created extremely high pore pressures within the aquifers, particularly in low areas. Episodic break out of water from the aquifers could have been triggered either by impact or by the pore pressure reaching the lithostatic pressure. The rate of outflow would have depended on the aquifer thickness and permeability, its depth of burial, and the diameter of the region over which water had access to the surface. Plausible values give discharges that range from 10^5 to 10^7 m³/sec. Outflow from the aquifer would probably cause undermining of the adjacent areas and collapse of the surface to form chaos. Flow would cease when the aquifer was depleted or when the hydraulic gradient around the chaos, and thus the flow, was so reduced that the flow could freeze. The process could be repeated if the aquifer were recharged.

Terrestrial Volcanic Degassing: A Review of Mechanisms and Magnitudes

T. Casadevall, U. S. Geological Survey, Hawaiian Volcano Observatory, Hawaii 96718

R. Stoiber, Dartmouth College, Hanover, New Hampshire 03755

D. Dzurisin, U. S. Geological Survey, Hawaiian Volcano Observatory, Hawaii 96718

The magnitudes of the contributions made by degassing of subaerial volcanoes to the terrestrial volatile budget are fairly well understood. These estimates are based largely on the study of subaerial volcanoes which represent only 20 to 25% of total terrestrial volcanism.¹ The 75 to 80% of terrestrial volcanic products from submarine activity probably degas less efficiently than subaerial volcanic products.^{2 3 4} For subaerial volcanic eruptions, degassing of magma occurs during four eruptive or post-eruptive processes: 1) vesiculation during effusion;⁵ 2) explosive eruption;⁶ 3) shallow intrusion of magma within the volcanic edifice; and 4) weathering. These four processes produce different proportions of juvenile gases, depending on the chemistry and plate tectonic setting of the volcanic activity.

For the quiescent period in Hawaii from July-October 1978, we have estimates for the annual production of SO₂ from COSPEC measurements (Stoiber and Malinconico, 1978, unpub. data), and analyses of gases (LeGuern and Casadevall, 1978, unpub. data) and condensates for selected fumaroles. The latter measurements allow the total annual flux of Cl and CO₂ from Kilauea and Mauna Loa to be calculated by ratio to SO₂. Data from sea floor basalt⁷ on the concentration of juvenile water in Hawaiian lavas give an indication of the annual contribution of water to the atmosphere by Hawaiian volcanoes (table).

Taken together, these data provide a relatively complete volatile budget for outgassing of Kilauea and Mauna Loa volcanoes. With the appropriate qualifications, this budget can be useful in assessing the impact of volcanic degassing on the atmosphere and surface geology of Mars.

Table

	Volatile Production (Metric Tons per Year X10 ⁵)				
Hawaii (a) (Kilauea & Mauna Loa)	SO ₂	Cl ⁽²⁾	CO ₂ ^(b)	H ₂ O	Lava Production Rate
	0.8	0.24-1.2	0.5-1.1	1	0.1 km ³ /yr
Extrapolation (c) of Hawaiian volatile production to global production	80	24-120	50-100	---	
Estimate of total annual production due to volcanism	100 ⁽⁸⁾	32 ⁽⁴⁾ -70 ⁽²⁾	400 ⁽⁹⁾	---	1-1.5km ³ /yr (subaerial) ⁽¹⁾ 6-8km ³ /yr (submarine) ⁽¹⁾

(a) Hawaiian gas analyses made during February 1975, August 1978, and October 1978 during periods of quiescence at both Mauna Loa and Kilauea.

(b) Assumes CO₂/SO₂ = 1-2; Cl/SO₂ = 0.2-1 (i.e., Cl/SO₂ = 0.3-1.5)

(c) Values for Hawaii multiplied by estimated number (100) of active volcanoes.

References:

1. Nakamura (1974) Utilization of Volcano Energy, Colp and Furumoto (eds.), p. 273
2. Anderson (1975) Rev. Geoph. Sp. Phys., v. 13, p. 37
3. Moore et al. (1977) J. Vol. Geo. Res., v. 2, p. 309
4. Schilling et al. (1978) Nature, v. 273, p. 631
5. Swanson and Fabbi (1973) J. of Res. (USGS), v. 1, p. 649
6. Rose (1977) Geology, v. 5, p. 621
7. Moore (1970) Con. Min. Pet., v. 28, p. 272
8. Stoiber and Jepsen (1973) Science, v. 182, p. 577
9. Bowen (1966) Trace Elements in Biochemistry
10. Buddemeier and Puccetti (1974) EOS (abs.), v. 55, p. 488
11. Swanson (1972) Science, v. 175, p. 169

The Earliest-Stage Primitive Atmospheres of the Mars and the Earth

Z. M. Chen, Institute of Space Physics, Sian, China

The lower and upper limits of the earliest-stage primitive atmospheres of Mars and the earth have been derived from a consideration of the whole history of the protoplanetary cloud and the facts observed. The implications of the presence of such earliest-stage primitive atmospheres in the evolutionary history of the thermal and other conditions of these two planets are discussed.

Present address: P. O. Box 985, Peking, China

The Structure and Oscillation of the Martian Upper Atmosphere

Z. M. Chen, Institute of Space Physics, Sian, China

The structure and oscillation at various time and space scales of the martian upper atmosphere is examined analytically by means of the Green's function, the finite integral transformation and other approaches.

The characteristics of the neutral and ionized upper atmosphere of the Mars have also been analysed and compared with those of the Earth.

Present address: P. O. Box 985, Peking, China

Analysis of a Twelfth Degree and Order Gravity Model for Mars

E. J. Christensen, Member of the Technical Staff, Jet Propulsion Laboratory, Pasadena, California 91103

G. Balmino, Research Scientist, Groupe de Recherches de Geodesie Spatiale, Toulouse, France

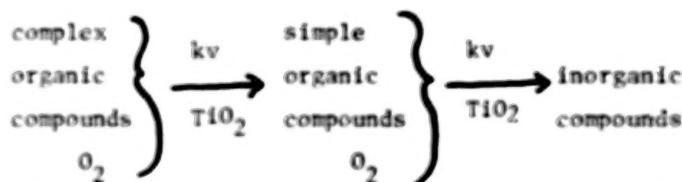
Satellite geodesy techniques previously applied to artificial Earth satellites have been extended to obtain a high resolution gravity field for Mars. Two-way Doppler data collected by ten Deep Space Network (DSN) stations located at three different sites during Mariner 9 and Viking 1 and 2 missions have been processed to obtain a twelfth degree and order spherical harmonic model for the martian gravitational potential. The quality of this model was evaluated by examining the r.m.s. residuals within the fit and the ability of the model to predict the spacecraft state beyond the fit. Both indicators show that the data processed so far has retained some information content and that more data will be required to further refine our knowledge of the martian gravity field. This implies that higher degree and order models will be necessary for future data reductions. The model presented here shows much promise since it resolves local gravity features which correlate highly with the martian topography. An isostatic analysis based on this model shows a lack of compensation on a local (short wavelength) as well as global (long wavelength) scale. These are interpreted to place some bounds on the internal structure of Mars.

Photocatalytic Oxidation of Organic Compounds in Murchison Meteorite under Simulated Martian Conditions

S. F.-S. Chun and K. D. Pang, Planetary Science Institute, 283 S. Lake Avenue., #218,
Pasadena, California 91101

J. M. Ajello, Jet Propulsion Laboratory, Pasadena, California 91103

Chun et al. (Reference 1) proposed a mechanism for the destruction of organics on Mars - UV-stimulated catalytic oxidation. The degradation process from complex organic ultimately into inorganic compounds is:



Powders of Murchison meteorite, rich in a variety of organics, and TiO_2 were degassed in pyrex flasks. The flasks were filled with oxygen at approximately martian surface partial pressure - 0.1 torr. These flasks were then irradiated with UV-visible light. Hard UV light that may cause photolysis was first filtered out. The flasks were rotated on a turning wheel to keep the powder constantly agitated, and inhomogeneities in the radiation field averaged out. The experiment was done at room temperature, equivalent to warmest martian surface conditions. The flasks were examined for changes in gaseous composition using a mass spectrometer. Samples of the powder were pyrolyzed and analyzed using a mass spectrometer. According to our proposed mechanism, an evolution of CO_2 in the flasks, and/or a change in distribution of masses from high to low molecular weights in the solids would mean that UV-stimulated catalytic oxidation of organic compounds has taken place.

After irradiation of four days a copious supply of CO_2 was observed in flasks where all three ingredients, O_2 , TiO_2 and carbonaceous chondrite, were present. The evolution of CO_2 was accompanied by a decrease in O_2 abundance. In flasks where all ingredients, except TiO_2 were present a small but detectable reaction took place. In flasks where all ingredients except O_2 were present, or where the carbonaceous chondrite was replaced by basalt, there was no evolution of CO_2 . Also no reaction was observed in flasks with all ingredients present but kept in the dark.

We interpret the results of the controlled experiment to mean that organic compounds in the carbonaceous chondrite are photocatalytically oxidized. Activation energy, provided by energetic photons, is required for the reactions to take place. A catalyst, TiO_2 , speeds up the reaction, but is not absolutely essential.

Mass spectra of pyrolyzed solid samples were difficult to interpret due to the vast number of peaks present. An alternate way was used to identify and trace the breakdown of high-molecular weight compounds, such as naphthalene, into low-molecular weight compounds.

Reference:

Chun, S. F.-S., Pang, K. D., Cutts, J. A. and Ajello, J. M. (1978) "Photocatalytic Oxidation of Organic Compounds on Mars", *Nature* 274, 875-876.

The Effects of Subsurface Volatiles on Martian Impact Cratering Events

Mark J. Cintala, Dept. of Geological Sciences, Brown Univ., Providence, RI 02912

The method of Gault and Heitowit (1963) has been employed to evaluate the effects of shock heating during martian impact cratering events. Hugoniot data for a mixture of Ottawa sand and H₂O ice ($\rho = 1.72 \text{ g/cm}^3$, dry sand $\rho = 1.65 \text{ g/cm}^3$; Anderson, 1968) were used to simulate the target material, taken to be at 173 K. Calculations were carried out for the normal impact of a 2 km (diameter) basalt body at 15 km/s. It is assumed that both the shock front and the resulting crater cavity are hemispherical in shape. The quantities of mobilized H₂O presented here should be taken as minimum estimates for this target composition since (a) the (-parabolic) transient cavity will almost certainly be less voluminous than this model crater while the absolute amount of sufficiently shocked material should remain relatively constant behind the (-hemispherical) shock front and (b) the Gault and Heitowit approximation tends to underestimate the amount of residual heat acquired by the target (O'Keefe and Ahrens, 1977). If 1/3.6-power energy scaling were to hold for an event of this magnitude, ~0.35% of the excavated mass would consist of vaporized H₂O and--under suitable pressure conditions--an additional 0.25% of the ejected mass would be liquid H₂O; the use of 1/3.5-scaling gives corresponding values of 0.25% H₂O vapor and 0.15% liquid H₂O. Shock heating could thus give rise to a localized transient atmosphere with pressures orders of magnitude greater than those presently observed at the martian surface, given sufficient quantities of volatiles in the target. This high pressure region would limit the lateral ballistic translation of crater ejecta by creating a high-drag environment in the vicinity of the transient cavity. In-flight particle collisions would increase due to preferential aerodynamic deceleration of finer-sized particles, a situation which would further constrain the lateral extent of ballistic ejecta deposition. As the ejecta were deposited, the entrained volatiles could act as lubricants in the development of radial surface flows (Head and Roth, 1976; Carr et al., 1977). In summary, it is possible that shock-released volatiles could both confine ejecta to regions immediately surrounding the crater and aid in producing the observed morphologies of exterior deposits.

Regolith Uptake and Recycling of Volatiles on Mars

B. C. Clark, Martian Marietta Aerospace, Denver, CO 80201

In comparison with terrestrial and lunar soils, and with meteorite matrix materials (excepting C₁'s), the Martian fines are distinctly anion rich (SO₄²⁻, Cl⁻, Br⁻, OH⁻, CO₃²⁻, and possibly NO₃⁻). Crustal degassing events, such as volcanism and impact cratering, will have cycled a large fraction, if not all, of the anionic components through the atmosphere in the gaseous state. Plausible reaction pathways involving regolith minerals can account for the lack of S-, Cl-, and Br-containing species in the prevailing atmosphere. In view of the relatively high rate of UV-catalyzed fixation of CO₂ by basalt powder (Booth and Kieffer, 1977), the presence of 22 g/cm² free CO₂ in the atmosphere becomes enigmatic. Recent experiments demonstrating photocatalyzed reactions of SO₂ + O₂ gas with "dry" carbonates to release CO₂ raises the possibility of a carbon cycle on Mars which maintains the atmosphere in dynamic equilibrium, representing balanced rates of CO₂ fixation and displacement reactions driven by the average planetary degassing rate. Similar considerations suggest nitrogen cycling. The intrinsic ratio of released S/C is critical to the inferred regolith inventories; if 20 times higher on Mars than on earth, as proposed by Anders and Owen (1977) from the observed ⁴⁰Ar/³⁶Ar ratio, then the common presumption of large regolith chemical inventories of C and N may be in error.

Planetary-Scale Wave Structure in the Martian Atmosphere

B. J. Conrath, NASA/Goddard Space Flight Center, Greenbelt, Maryland 20771.

A spectral analysis of atmospheric temperature fields obtained with the Mariner 9 infrared spectrometer has been carried out for a 39-day period corresponding to $L_S = 330^\circ$ - 350° during 1972. A strong apparent zonal wave number 2 component is found to exist in the latitude band 40° - 75° north with maximum wave amplitude occurring at about the 0.5 mb level. Surfaces of constant phase show a westward tilt with height below the 0.5 mb level, but there is little change in phase with height at higher levels, suggesting vertical energy propagation below 0.5 mb and an evanescent behavior above. The latitude band of maximum wave activity corresponds to a region of strong meridional gradient in the zonal mean temperature associated with the polar vortex. The available data coverage does not permit a unique separation of spatial and temporal effects; therefore, the observations are consistent with both stationary planetary waves and traveling baroclinic waves, Doppler shifted by the orbit-to-orbit advance in longitude of the spacecraft. Waves of the latter type are observed in pressure data acquired by Viking Lander 2. The observed vertical structure is compared with a theoretical model of vertical wave propagation in a baroclinic atmosphere.

A Thermodynamical Approach to the Study of the Martian Permafrost

Marcello Coradini, Laboratorio di Astrofisica Spaziale - Planetology Branch 00100 Rome -
Viale dell'Università 11

An outstanding result of the Viking mission has been the detection, both photographic and instrumental of water vapor in the martian environment. The only possible "taak" for the water, where no evidence of surface frost has been detected, is the soil which could contain unexpected amounts of water.

On the Earth, the mixture of water ice and soil, called permafrost, is continuously present in the northern hemisphere in a latitude belt of about 40° around the pole. A comparative morphologic analysis of periglacial terrestrial and martian terrains suggests the permafrost can play an important role in forming many superficial structures as the Valles Marineris landslides or the collapse structures in the volcanic region of Tharsis.

In this paper a study of the thermodynamics which regulate the processes of thawing and freezing of the layers of permafrost on Mars has been carried out. The equation of the heat propagation

$$\frac{\partial T}{\partial t} = K \frac{\partial^2 T}{\partial r^2}$$

has been solved, under martian conditions, both in the case of periodic (daily, seasonal and longer) variations of the surface temperature, and in the case of an anomalous heating of the ground. Such an extra heating could be caused by the presence of a lava flow or by the energy released during a meteoritical impact. Distributions of the temperature as a function of the depth and time have been computed. Possibility of formation of water lenses at some depth in the martian underground has been also checked in order to get a reservoir of liquid water, to be considered as responsible for some collapse features visible in the Viking Orbiter photographs.

Low Velocity Impact Craters in Ice and Permafrost with Implications for Martian Crater-Count Ages

S. K. Croft and S. W. Kieffer, Department of Earth & Space Sciences, University of California, Los Angeles, CA 90024

T. J. Ahrens, Division of Geological & Planetary Sciences, California Institute of Technology, Pasadena, CA 91125

In an effort to understand impact cratering on Mars and the outer solar system satellites, we produced a series of 4-20cm scale craters in targets composed of "permafrost" (saturated sand/water mixture frozen to -70°C), super-cooled ice (pure water ice cooled to -70°C) and temperate ice (pure water ice near 0°C). The craters in these targets were generally bowl-shaped, with depth/diameter ratios of ~ 0.4 to 0.5 .

The projectiles used were standard 0.22 and 0.30 caliber rifle bullets fired at velocities ranging from 0.3 to 1.5km/sec. Impact velocities and energies, ranging from 1×10^9 to 4×10^{10} ergs, were calculated from published ballistic data. The following relation between impact energy (E) and diameter (D) was determined by least-squares fit for the craters in permafrost:

$$D(\text{cm}) = 2.36 \times 10^{-3} E(\text{ergs})^{0.36 \pm 0.02} \quad (1)$$

Ice craters appear to have a similar E vs. D relation, but too few data were obtained for a reliable least-squares fit. The relation derived by Gault (1973, *The Moon*, 6, 32-44) for hyper-velocity impacts in basalt in the same energy range is:

$$D = 1.1 \times 10^{-3} E^{0.37 \pm 0.01} \quad (2)$$

Comparison of the coefficients of eqs. 1 & 2 show that at a given energy, craters in permafrost are ~ 2 x larger than craters in rock. Craters in ice are ~ 3 x larger than those in rock. A model has been constructed which explains the size differences in terms of the effective tensile strengths of the materials.

Because Mars has been postulated to have a thick permafrost layer covering large portions of its surface, this strength effect could significantly alter estimated ages of Martian features. If the dependence of crater size on strength persists to large hyper-velocity impact craters, then given rock and permafrost surfaces of equal age and identical flux histories, the crater-count age of the permafrost surface would be greater than that of the rock surface because there would be more large craters in the permafrost. Of particular interest to Martian problems is the observation that the tensile strength of permafrost is a strong inverse function of temperature (Tsytovich, N. A., 1975, *The Mechanics of Frozen Ground*, Scripta Book Co.), so that Martian crater E vs. D scaling may be a function of latitude. The magnitude of the strength scaling effect is comparable to the effects of gravity and impact velocity scaling calculated by Hartmann (1973, *Icarus* 31, 260-276) for use in determining relative interplanetary chronologies. Inclusion of the strength effect in such calculations would reduce the absolute ages of Martian events compared to events on the other terrestrial planets.

Polar Geology on Mars: A Climatic Archive

J. A. Cutts, K. R. Blasius, W. J. Roberts, Planetary Science Institute, 283 S. Lake Avenue, #218, Pasadena, California 91101

The martian polar layered deposits, first recognized in images returned by the spacecraft Mariner 9, have long been suspected to contain a rich record of martian climatic history. However, with the recent discovery in Viking Orbiter images of undulating terrain - a wave-like topographic relief on north polar surfaces previously supposed to be flat plains - it may be possible to unravel martian climatic history by purely photogeologic means. Furthermore, undulating terrain may be the key to solving a martian polar enigma - the origin of the large scale curvilinear frost-free bands that dominate the structure of the perennial ice caps. In this paper, mechanisms for the generation of depositional layering, undulating terrain topography and the large scale frost-free troughs are presented and evaluated. The implications of these features to climate change on Mars is also considered and the role of future missions in further probing the climatic history of Mars is discussed.

Environment-Organism Relations and the Interpretation of Life-Search on Mars

J. F. Danielli, Worcester Polytechnic Institute and The Center for Theoretical Biology

Studies of data obtained by the Viking landers, and of the complexity of organism-environment relationships in the ecological niches available for exploration by the landers, show that the present Viking data cannot be interpreted definitively, either for or against the presence of life in the samples examined.

Goldstone Radar Probes of Mars (1971-1978): A Review

G. S. Downs, Jet Propulsion Laboratory, Pasadena, California 91103

Range-Doppler data obtained during the 4 oppositions since 1969 covers selected latitude bands between -22° and 11° . The data has been used for ever-improving ephemerides of Mars, was part of the landing site certification process for Viking 1, and has provided details of topographic variations with an E-W resolution of 8 km. Surface roughness and reflectivity have been provided also with a resolution of 8 km. Preliminary comparisons of the topographic results with the M9 and Viking images of Mars have been made. A more extensive comparison involving also the roughness and reflectivity is planned.

A Review of the Viking Seismology Experiment

F. K. Duennebier and A. R. Lazarewicz, University of Hawaii, Honolulu, HA 96822
M. N. Toksoz and N. Goins, Massachusetts Institute of Technology, Cambridge, MA 02139
W. F. Miller and D. L. Anderson, California Institute of Technology, Pasadena, CA 91125
G. V. Latham and Y. Nakamura, University of Texas, Galveston, TX 77550

The purpose of the Viking Seismology experiment was to determine the seismicity of Mars and collect data to constrain the current models for the internal structure of Mars. The seismometer on Lander 1 failed, while the one on Lander 2 successfully returned data for 577 Earth days. 88 Earth days of data were collected during relatively quiet periods when marsquakes could be detected. Two events of unknown origin have been identified, and marsquakes are among the possible sources.

Mars is generally considered as having no active plate tectonics. Assuming Martian seismicity is comparable to Earth's intraplate seismicity, reasonable estimates for the seismic propagation properties of Mars, and the known instrument response, 2-3 local events would be observed during the quiet periods.

Important considerations and experimental design concepts for future extra-terrestrial seismology experiments will be presented.

Polarimetric Analysis of Mars from a Sovietic Spacecraft

A. Dollfus, M. Deschamps, M. Duseaux, Observatoire de Meudon, France
L. V. Ksanfomaliti and V. I. Moroz, IKI, Moscow, USSR

A polarimetric analysis of the light reflected by planet Mars was achieved with photo-electric polarimeters on board of spacecrafts (Fig. 1).

The Soviet cosmic craft MARS-5 was equipped with two photopolarimeters designated VPM'73-I and II. These instruments were designed in the Soviet industry by the Institute of Cosmic REsearch IKI of Moscow; a flight model was transferred to France in 1972 for test and calibration. The spacecraft was launched by the end of 1973 and placed into orbit around planet Mars in February 1974; measurements were transmitted through telemetry for 6 orbital revolutions during which the planet was each time scanned along a track of almost 7,000 km. The data from VPM-I included intensity, amount of polarization and azimuth of polarization for a phase angle of 60° and for 9 wavelengths covering from 3420 Å to 7490 Å. VPM-II produced these parameters for the phase angle 90° , for only one wavelength at 5920 Å, but with more details.

The raw data recorded on the Soviet magnetic tapes were transmitted to the department Mathematics of CNES for decoding and the results were sent back to Observatoire de Meudon after April 1976 for the scientific analysis in co-operation with Drs. Moroz and Ksanfomaliti from Institute of Cosmic Research IKI in Moscow.

A rather large number of polarimetric measurements were previously recorded on Mars with telescopes during 15 years, including particularly those measurements recorded during the month preceding the orbital spacecraft data. These telescopic measurements are more global and limited to phase angles smaller than 40° . Their combinations with the results of the instruments VPM-I and II produced the complete curve of polarization of Mars surface at 6000 Å reproduced in Fig. 2. This curve is unambiguously diagnostic of a soil which is a layer of small but very absorbing grains. However, some small localized areas produce anomalies with higher polarizations (Fig. 3) which are indicating the presence of rocky surfaces clean of dust.

During the limb scanning, the polarization by the atmosphere and its aerosols overtake the measurements and enable computations on the scattering properties of the aerosols and cloud layers.

The Soviet photographs of Mars surface disclose on certain areas of the planet some localized hazes or white clouds; their scanning with the photopolarimeters produces sharp peaks of polarization with steep increases towards the shorter wavelengths (Fig. 4).

The polarimeter detects also some minima of polarization in UV, which decrease towards the red and are apparently produced by small localized dust storms on areas covering 100 to 200 km only, for instance, in the mountainous area Ogygis Rupes (Fig. 5).

These preliminary results are still under study at Meudon Observatory.

References:

- Dollfus, A. and M. Grosjean (1973) "Polarimètre spatial soviétique VPM'73: Etude des caractéristiques de fonctionnement et calibration à l'Observatoire de Meudon" Rapport au CNES, 1er Septembre 1973.
- Ksanfomaliti, L. V., V. I. Moroz and A. Dollfus (1975) "Une expérience polarimétrique sur Mars-5 (en Russe) "Kosmicheskie Issledovaniya 13, No 1 pp 92-98.
- Ksanfomaliti, L. V. and A. Dollfus (1976) "Polarimetry and Photometry of Mars from Mars-5 Station" Space Science XVI (COSPAR) pp. 975-981.
- Dollfus, A., L. V. Ksanfomaliti and V. I. Moroz (1977) "Simultaneous polarimetry of Mars from Mars-5 Spacecraft and ground-based telescopes" Space Science XVII (COSPAR) pp. 667-671.

Figure 1

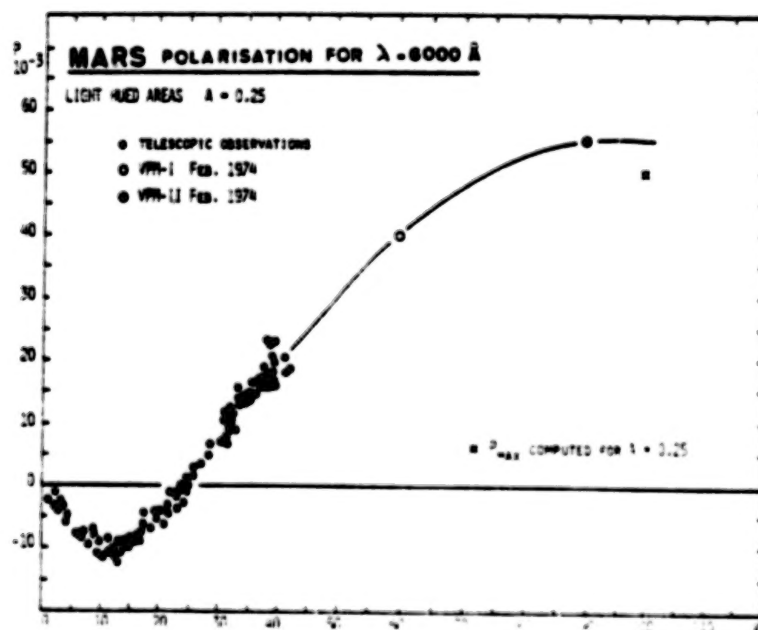
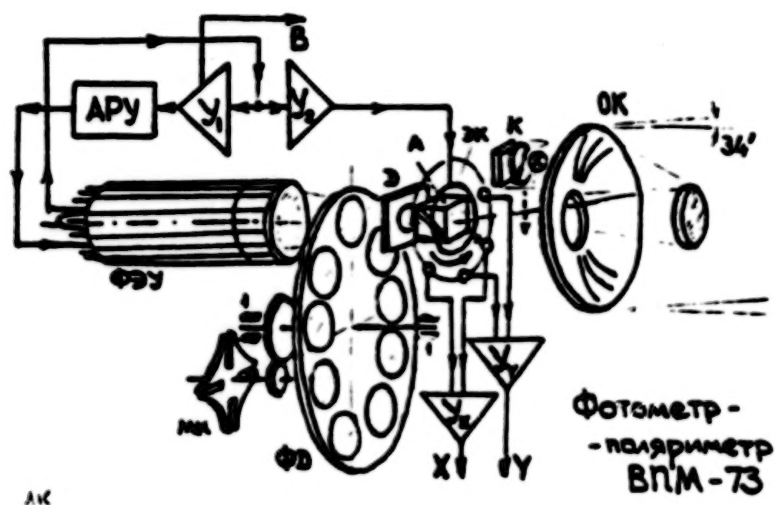
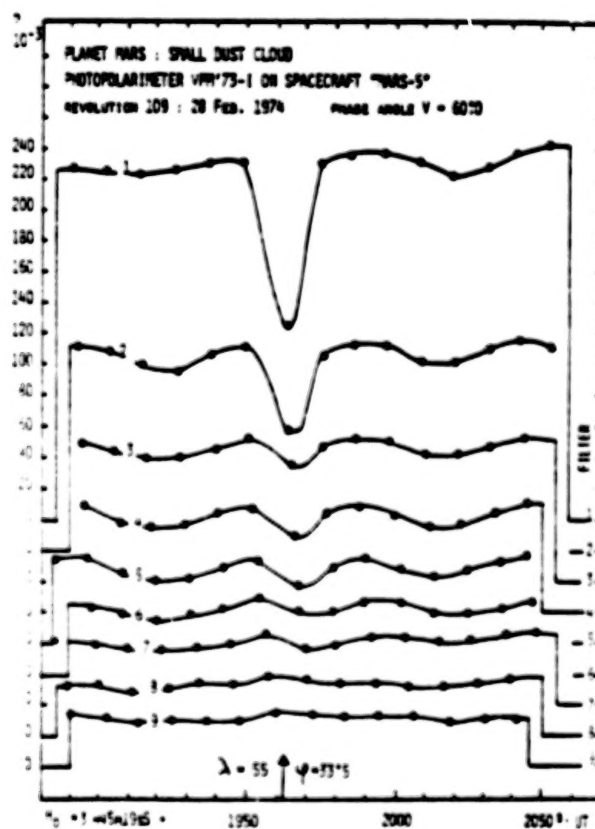
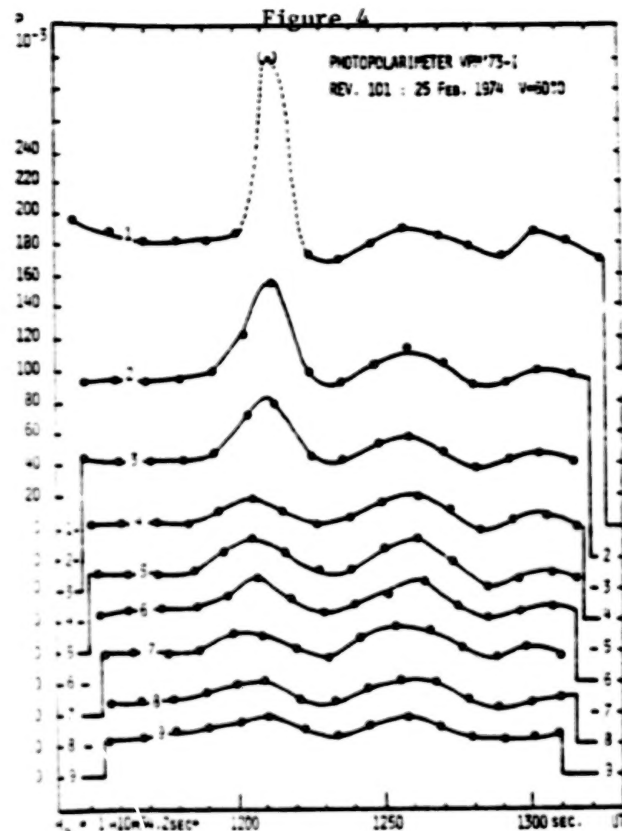
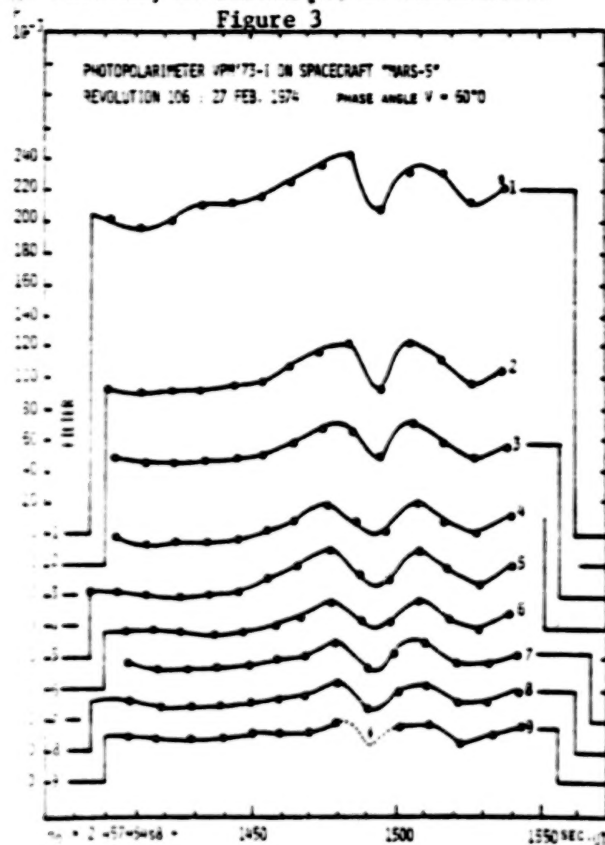


Figure 2



The Viking Imagery, The Early History of the Martian Satellites, and the Accretionary Tail

J. P. Duraud, Laboratoire Rene Bernas - 91406 ORSAY and Service de Chimie-Physique du Cea,
91120 GIF SUR YVETTE

Y. Langevin and M. Maurette, Laboratoire Rene Bernas - 91406 ORSAY

I. INTRODUCTION

In reference 1 we presented an analytical model of regolith evolution for a small martian satellite with a radius, R_s , which allows to compute 3 distinct types of regolith thickness, Δ : 1. $\Delta \sim R_s/50$ is an upper limit of Δ , obtained by supposing that all material ejected upon impact is reaccruted and that the satellite has been bombarded with the maximum integrated flux of meteorites, beyond which the satellite is fragmented; 2. the equilibrium thickness, $\Delta \sim 2$ m, is evaluated just by assuming that the material ejected with the escape velocity is completely lost for the formation of the regolith; 3. the "normal" value, $\Delta \sim 5$ to 10 m, corresponds to a situation already observed on lunar maria, where both all the ejected material is reaccruted and the surface is exposed during ~ 4 by to a meteoritic flux similar to the present day flux. As shown in the next section these values of Δ_f , Δ_e , Δ_o help in interpreting either important features observed on the pictures of Phobos, that put severe constraints on any model of regolith evolution, or the thickness of the regolith presently observed on lunar highlands.

II. THE VIKING IMAGERY OF PHOBOS AND THE EARLY HISTORY OF THE MARTIAN SATELLITES

First the observation of the superb pictures of Phobos taken at a distance of 40 km by the Viking imagery system reveals a flat bottomed crater and this indicates that the "experimental" thickness, Δ_{exp} , of the regolith of a martian satellite with a radius of ~ 10 km is about 100 m. This value, when compared to both Δ_e and Δ_o gives the following clues concerning the early history of the martian satellites: 1. Δ_{exp} is much larger than $\Delta_e \sim 2$ m. We thus conclude that Phobos (and probably Deimos) reaccruted a very large fraction of the ejected material. 2. But Δ_{exp} also greatly exceeds $\Delta_o \sim 5$ to 10 m and this has the following implications: i. Phobos was in fact bombarded with an integrated flux of meteorites much larger ($\times 100$) than that corresponding to a 4 by exposure of its surface in the present day meteoritic flux. This flux could possibly originate either from a swarm of small bodies first in orbit around Mars, and then subsequently accreted by Phobos, or from the accretionary tail, i.e. the flux of "debris" still not accreted into large bodies, and which pervaded the early solar system. The large crater density observed on lunar highland as well as the almost complete erasure of lunar geological features older than 4 by is also best interpreted by assuming a large increase in the meteoritic flux intensity during the early history of the Moon (2). The simultaneous observations of the effects of these very high fluxes of meteorites on the Moon and Phobos would rather support their filiation to the accretionary tail. This in turn strongly suggests that Phobos was already locked in orbit around Mars more than 4 by ago; ii. As a result of being exposed to the accretionary tail the martian satellites should present a "megaregolith" similar to that observed on lunar highland. But since the cessation of the accretionary tail ~ 4 by ago only the most superficial layer of the martian satellites, that we define as their "normal" regolith, should have been frequently gardened down to a depth $\Delta \sim 5$ to 10 m, in being thus similar to the regolith observed on lunar maria. Consequently, although our steady rain sedimentation model predicts no stratification in such normal regoliths (1), we would rather expect an horizontal boundary delineating this limit of normal gardening. Indeed the mass spectrum of the present day meteoritic flux could be different from that of the accretionary tail, and this could trigger a marked change in the size distribution of the megaregolith grains. In addition the exposure time of these grains on the top surface of the satellite was certainly much shorter during the accretionary tail, and this would act as to considerably decrease their space "weathering"; iii. As $\Delta_{exp} \sim \Delta_f$, Phobos has "almost" being exposed to the maximum integrated flux of meteorites beyond which fragmentation occurs.

Various other features in the pictures of Phobos are quite compatible with some of these conclusions. For example, the large crater Stickney ($r \sim 5$ km) is surrounded by an extensive network of lines extending up to a distance of ~ 10 km and which have been interpreted as fracture lines (3). This clearly indicates that Phobos has almost been fragmented. Verveka has also reported the observation of a clear horizontal boundary at a depth ~ 20 m in one of the crater of Phobos (4), which is compatible with our limit of normal gardening. Such a limit, if confirmed by further work, should in turn gives interesting clues about either the mass spectrum of the accretionary tail or the effects of space weathering on regolith

evolution.

Finally the high resolution pictures of Phobos show both rock boulders and impact craters presenting a continuous range of degree of burial, which is well illustrated by the "filled up snowprint" appearance of the buried features. These features are thus well compatible with our steady rain model for the deposition of material on the surface of the small martian satellites.

III. LUNAR HIGHLAND REGOLITH AND THE ACCRETIONARY TAIL

In the previous section we already argued for the existence of the accretionary tail in the early solar system, which has left various types of prints on both the lunar highlands and the surface of Phobos. We now try to infer the value, Ψ_{lh} , of the integrated flux of meteorites received by lunar highlands during the accretionary tail by relying on experimental evaluation of the thickness of their regolith ($\Delta_{lh} \sim$ a few km).

In reference 1 we evaluated the equilibrium thickness of the regolith of a small body, $\Delta_e \sim 0.05 R_s/R_M$, where R_s and R_M are the radius of the small body and that of the Moon, respectively. For a large body like the Moon, exposed to a sufficiently high integrated flux of meteorities, the value, $\Delta_e \sim 40$ km, has to be considered as a low limit of Δ_{lh} . Indeed, in the computation a large fraction of the ejected material is lost to space whereas 99.9% of this material is reaccreted by the Moon. But the estimated value of Δ_{lh} (\sim a few km) is in fact much smaller than Δ_e ! By using formula derived from our model of regolith evolution we thus conclude that the Moon has not been subjected during its early history in the accretionary tail to an integrated flux of meteorite, $\Psi_e \sim 300,000 \Psi_0$, sufficiently high to trigger the formation of an equilibrium thickness (Ψ_0 corresponds to the bombardment of the lunar surface during 4 by in the present day meteoritic flux).

With more elaborated computations the value of Δ_{lh} can indeed be used to infer an estimate $\Psi_{lh} \sim 10,000 \Psi_0$, for this earlier flux of meteorite which was mostly active ~ 4 by ago. If confirmed by further works this high value of Ψ_{lh} will put on firmer grounds interesting speculations presented by others, and dealing for example with the various effects of the accretionary tail on the early Earth (Formation of the Ocean basins; injection of extraterrestrial organic matter on the Earth; evolution of the primitive atmosphere of the Earth; etc....)

References

- 1) Langevin, Y., this Conference Proceedings.
- 2) Lunke, J. C. et al (1973) Geochim. Cosmochim. Acta, Suppl. 4, p. 1725.
- 3) Veverka, J. et al (1977) J. Geophys. Res. 82, 4213.
- 4) Veverka, J. (1978) Nasa Conf. Publication 2053, p. 207.

Phobos, Deimos and Mars

T. C. Duxbury, Jet Propulsion Laboratory, California Institute of Technology, Pasadena, CA 91103

Visual photometric properties (color, albedo, phase functions) of the surfaces suggest a great similarity between Phobos and Deimos. However, mean densities (1.9 ± 0.5 gm/cm³ for Phobos and 1.4 ± 0.6 gm/cm³ for Deimos) as well as physical appearances suggest marked differences between the two moons of Mars. Physical appearance differences include the abundance of grooves and sharp craters on Phobos but not on Deimos and the abundance of bright material around craters on Deimos but not on Phobos. The low densities suggest a Class I carbonaceous chondritic or high ice content composition found in asteroids or comets. Possibly Phobos and Deimos are captured bodies which accumulated regoliths of similar material after capture. The regolith on Phobos appears to be hundreds of meters thick while the regolith on Deimos appears to be meters or tens of meters thick. Impacts on Deimos may have exposed the original surface of Deimos by removing the much thinner regolith resulting in the brighter material visible around these impacts. Imaging of Phobos, Deimos and their shadows against Mars has yielded information on Mars. Validations as well as improvements to map coordinates of craters and Viking Lander 1 have been obtained from these pictures. Additionally, limits can be set on the internal dissipation function, Q , of Mars by observing the secular acceleration in the longitude of Phobos.

Terrestrial Volcanic Outgassing: Implications for Martian Atmospheric Evolution and Surface Geology

D. Dzurisin and T. Casadevall, Hawaiian Volcano Observatory, Hawaii 96718

R. Stoiber, Dartmouth College, Hanover, New Hampshire 03755

Planetary thermal models suggest that the martian interior experienced a post-accretion temperature increase owing to radiogenic heating.¹ This phenomenon may have been responsible for the initiation of surface volcanism recorded most notably by the large volcanoes of the Tharsis Plateau. By analogy with the terrestrial case, Tharsis outgassing presumably released large volumes of volatiles to the atmosphere. This reasoning combined with photo-geologic evidence of relatively recent, intense surface-atmosphere interactions on Mars led Malin and Murray (1974) to assess the potential role played by a late-evolving atmosphere in modifying the martian surface.

The volatile budgets of Kilauea and Mauna Loa volcanoes on Hawaii have recently been determined by direct measurement.² Given the tentative identification of some Tharsis volcanoes as basaltic shields, the data on Hawaiian volatiles provide a rational framework for re-assessing the potential importance of recent volcanic outgassing on Mars. Planetary accretion models and analyses of meteorites presumably derived from the asteroid belt suggest that the initial volatile inventories of Mars and Earth were roughly comparable.³ It follows from the Hawaii data that degassing of lavas comprising the Tharsis Plateau produced SO_2 , Cl, CO_2 , and H_2O in greater amounts than currently observed in the martian atmosphere and polar caps.

Fanale (1971) argued that the combined effects of exospheric escape, solar wind sweeping, and regolith storage could plausibly account for the current paucity of observable volatiles on Mars. Reconstruction of the history of surface-atmosphere interaction since the beginning of Tharsis volcanism depends critically on the relative rates of volcanic outgassing and volatile removal processes. If removal processes proceeded more rapidly than outgassing, surface modification would have been minor and restricted to the immediate vicinity of the volcanoes (e.g., fumarolic activity), and no significant global atmospheric pressure change would have occurred. However, if outgassing temporarily exceeded volatile removal processes, a significant secondary atmosphere (as opposed to the primary atmosphere produced by accretion and early differentiation) could have been produced. Increased atmospheric pressure owing to degassing could have been responsible in part for the high rates of eolian transport implied by polar sedimentary blankets. The hypothesis of a late-evolving atmosphere on Mars is thus consistent with the volatile budget of Hawaiian volcanoes, and may help to explain the observation derived from detailed geologic mapping⁴ that the oldest recognizable eolian deposits on Mars are roughly coeval with Tharsis volcanism.

References:

1. Johnson, McGetchin, and Toksöz (1974)
2. Casadevall, Stoiber, and Dzurisin (1979)
3. Fanale (1971)
4. As synthesized by Scott and Carr (1978)

Wind Erosion in Egypt's Oweinat Mountain and Implications to Eolian Erosion on Mars

Farouk El Baz, National Air and Space Museum, Smithsonian Institution, Washington, DC 20560

The formation of pits in solid rock was studied along the northern slopes of the Oweinat Mountain at the southwestern corner of Egypt. Emphasis was placed on the wind-facing northern slopes. Near the base of these slopes tafoni abound, where honeycombing of the sandstone rock occurs by moisture.

At higher levels of the slopes another type of pits form by wind erosion. Smallest are the vortex pits that form on the surface of hard quartzitic rock. Deeper and larger pits appear to form by plucking of individual grains from the sandstone. These become the host for wind-carried sand grains which move about the pits as the wind gusts. Such erosive action increases the size of the pits. These are very similar to the pits in rocks of the Viking 2 landing site. They were observed not only in sandstone and quartzite, but also in dense and fine grained basalt, trachyte, granite, and hematite exposures.

At the highest levels of the wind-facing scarps, the pits form in rows. As the number and size of the pits increases, grooves are formed. Parallel rows of grooves produce a distinctly fluted surface.

Clones of Martian Light- and Dark-Colored Streaks in the Southwestern Desert of Egypt

Farouk El-Baz, National Air and Space Museum, Smithsonian Institution, Washington, DC 20560

Light- and dark-colored streaks abound in the southwestern part of the Western Desert of Egypt. In Apollo photographs and Landsat images, they appear similar to the streaks photographed by Mariner 9 and Viking spacecraft on Mars.

Field investigation indicates that light-colored streaks are made of sand accumulations in the form of dunes and sand sheets. The sand is derived from the Great Sand Sea to the north of the streaks. Sand grains are distinguished by a red color due to the presence of hematite as surface coating and microfracture fill. The red sand color gives the locality a Mars-like appearance.

Dark-colored streaks are usually sand-free zones in the lee of topographic highs. Behind these highs the streaks form teardrop shapes that taper downwind. Other dark streaks are caused by light-colored zones on either side. The dark surfaces are made of lag. In most areas the lag is immature with numerous angular rock fragments. Beneath the rock fragments and quartz grains there is usually a layer of extremely fine sand.

Mars: Implications of Capillary Condensation and Adsorption of CO₂ on Clays for Volatile Storage and Climate Change

F. P. Fanale and W. A. Cannon, Jet Propulsion Lab, California Institute of Technology, Pasadena, CA 91103

We have compiled a set of data describing the interaction of CO₂ and nontronite over the full range of probable martian surface and subsurface conditions. This data has allowed us to modify and sharpen our previously published models for CO₂ storage and atmospheric exchange on Mars (J. G. R. 79, 3397-3402, 1974; 83, 2321-2325, 1978) which were based mainly on basalt data. Our original three basic contentions--(1) that regolith adsorption is the main storehouse for atmosphere-exchangeable CO₂ on Mars, (2) that considerable long-term variations in atmospheric pressure ($\sim \times 10$) could result from insolation-driven pumping of the regolith, and (3) that very high pressures (> 100 mb) could have existed early in the history of Mars providing the regolith was much smaller--remain unaltered. Our added conclusions, based on the new nontronite data are: (1) Smectites may well be the best adsorbers occurring in nature and, if the Mars regolith is at all smectite rich, those minerals will dominate all adsorptive and exchange effects. (2) The same exchange and storage effects we previously postulated for a 1 km regolith can be achieved with a < 100 m smectite-containing regolith. (3) The dominance of exchange effects in the high latitudes over those in the middle and low latitudes is much stronger than we previously supposed owing to a very sharp (and well understood) increase in adsorption and capillary condensation of CO₂ on smectites at temperatures $< 180^\circ\text{K}$. If the very cold deposits in the layered terrain and surrounding debris mantle are mostly smectite clays, each meter of that regolith would contain about as much CO₂ as the entire atmospheric column directly overlying that regolith.

Dynamics of Thermally Driven Winds Controlled by Local Topography

F. M. Flasar, NASA/Goddard Space Flight Center, Greenbelt, MD 20771

Diurnal slope-wind circulations, associated with basins and valleys on Mars having horizontal scales $< 10^3$ km, are analyzed. A large class of these features has circulations which are characterized by an "interior", comprising most of the atmosphere within the basin, and a multi-structured boundary layer adjacent to the surface. The interior flow is determined by a balance between thermal advection and radiative driving; buoyancy effects do not enter to lowest order. The circulation is so efficient as to maintain isentropes and isobars horizontally, quite unlike the radiative equilibrium solution. The slope winds themselves, which are buoyantly driven, are confined to a narrow "inertial" boundary layer near the surface. Within this layer is imbedded another, in which eddy diffusion is important and alters the velocity profile so as to satisfy the surface drag boundary condition on tangential velocities. The relevance of these flows to dust movement, and to the morning fogs often observed in canyons and craters will be discussed.

Martian Rift Tectonics

H. Frey, Geophysics Branch, NASA Goddard Space Flight Center, Greenbelt, MD 20771, and
Astronomy Program, University of Maryland, College Park, MD 20742

The major extensional fractures of Mars are the graben-like canyons of the Valles Marineris. Although significantly modified by erosional activity, it is possible to infer from resistant portions of the canyon walls a likely reconstruction of the bounding scarps. Major trends in these inferred scarps are radial to the Tharsis Uplift but secondary orthogonal trends imply some association with a smaller uplift at Thaumasia. Doming in these two regions may account for many but not all of the structural trends along which the troughs have developed. Comparison of the individual canyons of Mars with individual rifts of East Africa on the Earth reveal the following: (a) Martian canyons and African rifts both have similar distributions in lengths, measured in units of planetary radius. This suggests a common mechanism of formation on both planets and one that scales with planetary radius. (b) Martian rifts are significantly wider than African rifts, probably indicating a greater thickness of martian crust at the time the canyons formed. (c) Martian scarps are straighter for longer distances, and the overall pattern of inferred fractures is much simpler than for African rifts. This reflects the relatively simple tectonic history of Mars prior to formation of the Valles Marineris. Although eolian features are common in the deep floors of the rifts of Mars, actual blanketing of floor morphology is at most a thin veneer. There is no evidence of the extensive fault swarms or central volcanism which characterized the late state evolution of the African rifts in Kenya in any of the martian canyons. This is probably due both to the greater thickness of the martian crust and the lower degree of internal mantle activity on Mars.

Endolithic Microbial Life in the Antarctic Dry Valleys: A Terrestrial Model of Martian Environment?

E. I. Friedmann, Dept. of Biological Science, Florida State Univ., Tallahassee, FL 32306

The dry valleys of Southern Victoria land, Antarctica, probably the closest terrestrial analog to the surface of Mars, have a harsh climate that is hostile to life. Yet, endolithic microorganisms are able to survive within the inner airspace systems of porous rocks. Algae and fungi that form a primitive lichen association, cyanobacteria and non-photosynthetic bacteria colonize the rocks and appear as a visible dark zone a few mm below the surface crust. The occurrence of these microbial layers is widespread and they are usually present under the surface of porous Beacon sandstone in favorable (Northern) exposures. The microbial biomass was estimated from Kjeldahl N, ATP and chlorophyll fluorescence determinations.

Measurements indicate that temperature and water conditions inside the rocks are significantly different from the hostile outer climate. Comparative studies show that the endolithic microenvironment in the dry valleys is less extreme than in hot deserts. In the Antarctic polar desert, endolithic microorganisms are able to exist by withdrawing into a physically protected microscopic niche rather than through special physiological adaptations.

Experimental Results for Effects of Gravity on Impact Crater Morphology

D. E. Gault, Murphys Center of Planetology, Box 833, Murphys, CA 95247

J. A. Wedekind, NASA, Ames Research Center, Moffett Field, CA 94035

Craters formed under the limiting conditions of virtually zero (0.0003 - 0.0008) " g " on Phobos and Diemos provide valuable comparisons with other planetary gravity environments and, for present purposes, some previously unreported results for impact craters formed in quartz sand for " g " = 1.0 to 0.073 . These experimental results indicate that crater shape as defined by depth-diameter ratio and rim height can be expressed as a function of rim diameter D_r and " g " in the form $d/D_r = K_0 + K_1 D_r^a g^b$ where K_0 is the crater depth referenced to the undisturbed surface, and the second term describes the height of rim above the reference surface. We have shown previously (Gault and Wedekind, 1977) that over the range of experimental data the interior shape of the bowl-shaped craters remains unchanged with " g " so that K_0 can be taken to be constant (≈ 0.193). It has since been determined that for the rim height, $a=0.12$, $b=0.157$, and K_1 is approximately 0.05 (cgs units). Although the values of these empirical constants probably depend on the material properties to a greater or lesser degree, the laboratory values should provide a good first approximation for most planetary applications, especially for regolith type materials. The empirical relationship indicates a weak functional dependence for d/D_r on " g ", less than about 10-percent difference between Phobos and Diemos as compared to the Moon, a result consistent with observations of Thomas (1978) and Pike (1974). In contrast, however, such subtle effects of " g " on d/D_r are the result of major changes in rim height, 25- and 75-percent reductions relative to terrestrial craters for, respectively, lunar and martian satellite craters. Although the experimental results could not distinguish between changes in rim heights due to ejecta thickness or structural uplift, the constancy of interior morphology ($K_0 = \text{constant}$) strongly suggests that the primary cause of the reduction in rim height with decreasing " g " is thinning of the ejecta deposits. The empirical indication of a $2/3$ reduction in rim height for craters on Phobos and Diemos with respect to the Moon is consistent with the observations of Thomas (1978) and portends important re-evaluations of ejecta-thickness estimates for the Moon.

References

- Gault, D. E. and Wedekind, J. A., (1977), Experimental hypervelocity impact into quartz sand-II, Effects of gravitational acceleration, in *Impact and Explosion Cratering*, eds. Roddy, Pepin, and Merrill, Pergamon Press, 1231-1244.
- Pike, R. J., (1974), Depth/diameter relations of fresh lunar craters: revision from spacecraft data, *Geophys. Res. Lett.*, **1**, 291-294.
- Thomas, P. C., (1978), The morphology of Phobos and Diemos, Cornell University Center for Radiophysics and Space Research, CRSR 693.

Volatile Elements and Phase Determinations in Planetary Samples: A Proven Approach for Consideration in Future Mars Studies.

E. K. Gibson, SN7, NASA-JSC, Houston, TX

F. F. Andrews, Lockheed Electronics Co., Houston, TX

M. A. Urbancic, Univ. of Illinois, Urbana, IL (Formerly a Lunar and Planetary Institute Summer Intern)

Water and other volatiles have been recognized as important factors affecting the past and present states of Mars. Despite this fact, analytical methods for the determination of water and associated volatiles have not been fully utilized in studies conducted to date. Pyrolysis mass spectrometry and/or pyrolysis gas chromatography are proven analytical techniques which can be used for the determination of water and other volatiles (e.g. CO_2 , CH_4 , N_2 , CO , SO_2 , etc.) in samples from Mars either in returned samples or *in situ* studies.

Our laboratory has had a decade of experience in analyzing volatiles in extraterrestrial samples using the techniques of pyrolysis mass spectrometry and/or gas chromatography. The analytical results clearly demonstrate the power of such methods in characterizing the volatile phases and components found in extraterrestrial samples. The gas release technique identifies the nature and abundances of the volatiles present in the samples and distinguishes between: adsorbed species, chemically bound species (e.g. hydrates, sulfates, etc.), products from the decompositions of mineral phases which evolve a volatile component, chemical forms of the released volatiles (e.g. H_2S vs SO_2 vs SO_3 , CO vs CO_2 , SO_2 vs S_2 , etc.), and vapor or gaseous phases trapped within vesicles and inclusions. The instrument operating conditions and parameters drastically affect the analytical results obtained. For example, the decomposition temperature of calcium carbonate can be changed by 500-600°C depending upon the pressure and composition of the gaseous species in the pyrolysis chamber. The rates at which the samples are heated during pyrolysis also affect the analytical results and can lead to erroneous interpretation of the presence or absence of a particular volatile phase. Knowledge of such behavior is critical in the design and operation of any analytical instrument and for the interpretation of results obtained. The application of this proven technique for the study of volatiles in terrestrial and extraterrestrial samples can be demonstrated for a variety of samples including: basalts, volcanic glasses, clays, carbonates, sulfates, hydrates, meteorites, and lunar samples.

Present Constraints on the Bulk Composition of Mars and the Composition of the Martian Mantle

K. A. Goettel and G. F. Davies, Dept. of Earth and Planetary Sciences, Washington Univ.,
St. Louis, MO 63130

Present data are not adequate to specify uniquely the composition of Mars or the composition of the Martian mantle. The observed mean density and calculated moment of inertia factor of Mars place constraints on the three basic parameters of simple Mars models: core density, mantle density, and core size. However, independent knowledge of one of these three parameters is required to specify uniquely the other two: at present the requisite data do not exist.

Solar system abundances suggest strongly that only five plausible core forming elements are likely to be sufficiently abundant to be major core constituents in Mars: Fe, Ni, S, O, and Si. Therefore, the zero pressure densities of high pressure polymorphs of plausible core-forming phases for Mars must fall in the range between pure Ni (8.9 g/cm^3) and Fe_3O_4 (5.2 g/cm^3). Within this range of core densities, the allowed range of mantle densities is very large: from nearly terrestrial to densities requiring large FeO enrichments relative to the terrestrial mantle. Within the narrower, and perhaps more plausible, range of core compositions from FeS to $\text{Fe}_{85}\text{S}_{15}$ corresponding mantle densities range from 3.47 to 3.58 g/cm^3 (1). If Mars has the solar proportions of major rock-forming elements and Fe-FeS core, then the mantle density is about 3.50 g/cm^3 (2).

It appears probable that the Martian mantle is denser and enriched in FeO relative to the terrestrial mantle. However, this conclusion, which may not be absolutely required by present Mars data, depends also on the equations of state chosen for Martian constituents (cf. (1) and (3)). In any case, the degree of enrichment of FeO in the Martian mantle is highly model-dependent. Therefore, development of models for petrologic evolution of Mars, based on a single value for the density of the Martian mantle, must be approached with considerable caution.

References

- 1) D. H. Johnston and M. N. Toksoz (1977), Internal structure and properties of Mars, *Icarus* **32** 73-84.
- 2) K. A. Goettel (1978), The Composition of Mars, in NASA TM 79729 116-117b.
- 3) E. A. Okal and D. L. Anderson (1978), Theoretical models for Mars and their seismic properties, *Icarus* **33** 514-528.

Relative Efficiencies of Volatile Consumption by Chemical Weathering Reactions on Mars

J. L. Gooding and K. Keil, Dept. of Geology and Institute of Meteoritics, Univ. of New Mexico,
Albuquerque, NM 87131

In principle, four types of chemical weathering reactions, involving primary rock-forming minerals, are available for the incorporation of O_2 , H_2O , and CO_2 into the Martian regolith. These are (a) oxidation by O_2 , (b) oxidation by H_2O , (c) hydration by H_2O , and (d) carbonation by CO_2 . Assuming that all iron is oxidized to Fe^{3+} , hydration forms goethite and clay minerals, and carbonation produces carbonates of Ca, Mg, Fe, Na, and K, upper limits for the relative volatile-consuming efficiencies of alternative reaction schemes can be calculated. For (a)-(d), limiting reaction capacities (grams volatile consumed/gram mineral reacted) are: olivine ($\leq 0.08a$, $\leq 0.09b$, $0.09-0.3c$, $0.4-0.6d$), clinopyroxene ($\leq 0.03a$, $\leq 0.04b$, $0.03-0.04c$, $0.2-0.4d$), orthopyroxene ($\leq 0.06a$, $\leq 0.07b$, $0.04-0.07c$, $0.3-0.4d$), feldspar ($0a,b$, $0.06-0.13c$, $0.08-0.16d$), feldspathoid ($0a,b$, $0.04c$, $0.15d$), magnetite, ilmenite ($0.03-0.05a$, $0.04-0.06b,c$, $0.2-0.3d$). In general, (a) and (b) are equally efficient for a given mafic mineral although (a) is thermodynamically preferred. For felsic minerals, only (c) and (d) are possible. Simultaneous or competitive operation of (a)-(d) should lead to lower efficiency values than those cited here. Petrologically translated, one gram of basalt can consume, by weathering, $\sim 0.01 \text{ g O}_2$, $0.05 \text{ g H}_2\text{O}$, and 0.1 g CO_2 .

A Model for the Formation of Windblown Sand-size Particles and Related Structures on Mars

R. Greeley, Department of Geology and Center for Meteorite Studies, Arizona State University, Tempe, AZ 85281

Knowledge of aeolian features and related processes on Mars has been advanced considerably by Viking Orbiter and Lander results. A problem, however, has arisen by two sets of observations that appear to be in conflict. Features interpreted to be dunes are observed from orbit in many regions of Mars; deposits of presumed windblown particles are observed at Viking Lander sites to have bedding structures typical of dunes. Both of these observations suggest the presence of sand-size (.06 to 2.0 mm) particles, because the physics of aeolian processes generally prohibits smaller and large particles from forming dunes, even under martian conditions. However, Viking observations also indicate the lack of sand particles at the lander sites and the prevalence of particles a few microns in diameter and smaller. This is partly attributed to the self-destructing, or "kamikaze" effect of saltating grains in the 150 μ m size range (Sagen et al., 1977). Furthermore, grains in the atmosphere are estimated to be smaller than a micron or so in diameter (Pollack et al., 1977). Thus, the question arises as to how structures such as dunes originate that require sand-size particles for their formation. Several possibilities can be suggested: 1) The dunes are "fossil" features that formed some time in the history of Mars when sand-size particles were common, 2) The calculations for martian aeolian processes requiring sand-size particles for dune formation are incorrect, or 3) There is a mechanism of dune formation that does not require individual sand-size grains. Laboratory and windtunnel studies of the electrostatic effects on grains (Greeley and Leach, 1978) and analysis of possible terrestrial analogs suggest the latter possibility, as follows: Electrostatic charges and other interparticle forces appear to be an effective means of holding aggregates of very fine particles together to form sand-size "particles"; in addition, nucleation around ice particles in the atmosphere may enable the formation of large particles (Pollack et al., 1977). These particles would then behave as "sand" in the aeolian environment to produce dunes and other typical sand structures as suggested by Moore et al., (1977). Although it is not known if the strength of the aggregates is sufficient to survive saltation of Mars, the presence of silt-clay dunes on Earth suggests an analog. These features, such as those in Clark Dry Lake in Southern California (Roth, 1960) involve aggregates of fine sediments that behave as sand-size particles and are emplaced, as "sand" to form dune-like structures. Internal bedding characteristic of sand dunes also develops and is preserved. On Mars, after the aggregates are emplaced, the forces holding the tiny grains together may be lost (e.g. the electrostatic charges may be balanced or may "leak" to the atmosphere), destroying the aggregates and the grains would once again behave as very fine grained material. Thus, in this model, the observation of sand-like large scale features and the presence of fine grained materials are not in conflict.

Differential Aeolian Redistribution Rates on Mars

E. A. Guinness, R. E. Arvidson and S. W. Lee, Department of Earth and Planetary Sciences, Washington University, St. Louis, MI 63130

Data acquired during the Viking mission have provided an opportunity to examine the effects of aeolian processes on Mars integrated over billions of years, tens of thousands of years, and over the course of a single year. The effect on aeolian activity can be sampled over geologic timescales by examining the extent of modification of features large enough to be seen by the Viking Orbiters. The degree of preservation of the impact craters and wrinkle ridges at the Viking Lander 1 (VL1) site implies that rock breakdown and removal has been limited to meters in depth. Using the crater abundances within a 100 km radius of the landing site we obtain an age for the surface of about 3.5 billion years, within a factor of 2 or 3. Despite the age uncertainty, the computed rock breakdown and removal rate of meters per billions of years is surprisingly small, $\sim 10^{-3}$ microns per year. In contrast, there has been several hundred meters of wind erosion within a few hundred kilometers of the Viking Lander 2 (VL2) site, based on the relief between pedestal craters and the surrounding fine-grained aeolian deposits. The pedestal crater abundances indicate that the partially stripped deposits are about the same age as the VL1 site. The erosion rate for the aeolian deposits, averaged over such a lifetime, would be a few tenths of a micron per year, which is two orders of magnitude greater than the computed rate of rock removal at VL1. Such a large difference in erosion rates between rock and soil is in fact mandatory if the pedestal craters have resisted stripping due to a bouldery surface. Windblown drifts seen at both landing sites may provide information on the intensity of aeolian processes averaged over tens of thousands of years. The drifts have morphologies indicative of accumulation during a prevailing north to south wind regime - the situation prevalent during the annual global dust storms occurring near perihelion. Due to precessional effects the subsolar latitude at perihelion (SLP) migrates $\pm 25^\circ$ in latitude about the equator with a 50,000 year period. Because of the enhanced stripping associated with regions close to the SLP, it seems probable that the drifts at VL1, with their strictly north to south trend, must have accumulated since the SLP was last over the landing site latitude (24° N. lat.), which would have been about 15,000 years ago. If this line of reasoning is accepted, then an average accumulation rate of about 10 centimeters (mean drift thickness) per 15,000 years, or several microns/year, can be computed. A redistribution rate of microns per year is also consistent with the observations made by the Lander cameras over the past year. A thin layer (microns thick) of dust was deposited at VL2 site during the second of the two global dust storms observed during the mission. Conditions at VL1 have been similarly quiet, with the removal of a thin, bright dust layer, again probably only microns in thickness, being the dominant activity.

In summary, results for the Viking landing sites indicate that little rock breakdown and removal by wind has occurred over approximately the past 3 billion years. On the other hand, relatively rapid redistribution of friable or loose, fine-grained materials has occurred. Many of the landforms seen in higher resolution Viking Orbiter frames covering other parts of Mars are consistent with such interpretations. Many volcanic flow fronts, well preserved crater populations, and other features indicative of little to no significant modification can be discerned. In other regions, the surface has been stripped, yardangs have formed, and in general the topography appears to have largely been configured by aeolian activity. Such regions must be composed of friable deposits, such as volcanic ash or older aeolian materials. Finally, the similarity of redistribution rates for aeolian deposits averaged over three vastly different time-scales implies that roughly the present aeolian environment has been operative for a significant fraction of geologic time.

The Photometric Function of Martian Soil in the Vicinity of Viking Lander 1

B. Hapke, Department of Earth and Planetary Sciences, Univ. of Pittsburgh, Pittsburgh, PA 15260

A special photometric sequence of images was taken by Viking Lander 1 throughout the Martian day on sol 29. In the raw images the photometric function of the soil appears quasi-Lambertian. However, after correcting for effects of the sky aerosols, the photometric function is found to be strongly backscattering. The backscatter parameter which describes the opposition effect has the value $h = 0.5$, which is comparable to the moon. This large opposition effect is apparently partially masked by the atmospheric dust in earth-based photometric observations of Mars. The soil is inferred to have a normal albedo (phase angle = 5°) in the green of 0.18.

Viking Magnetic Properties Experiment - Results and Conclusions

- R. B. Hargraves, Dept. of Geological and Geophysical Sciences, Princeton University, Princeton, NJ 08540
D. W. Collinson, Institute of Lunar and Planetary Sciences, School of Physics, University of Newcastle upon Tyne, England
R. E. Arvidson, McDonnell Center for Space Science, Dept. of Earth and Planetary Sciences, Washington University, St. Louis, MO 63160
P. M. Cates, Jet Propulsion Laboratory, California Institute of Technology, Pasadena, CA 91103

During the Viking primary missions the magnets on the sampler backhoe of both landers established the presence of a strongly magnetic mineral in the Martian surface. Magnetic particles were also attracted from the atmosphere by the RTC magnets on top of each lander.

During the extended missions picture-differencing of images of the VL-1 RTC magnet on Sols 151 and 475 show that more atmospheric particles were attracted to the magnet in this period, presumably reflecting the additional sampling activity and the dust storms. On Sol 502 the backhoe magnets on VL-2 were cleaned. Imaging after each of three subsequent insertions of the magnets into the surface shows that the magnets become essentially saturated after the first insertion. This result is further evidence for uniform distribution of the magnetic mineral throughout the surface material.

The effective magnetic susceptibility of the particles suggest that they are composite, consisting of a non-magnetic phase with a small admixture of highly magnetic mineral. Spectral data and the apparently highly oxidized condition of the surface material suggest that the magnetic mineral is maghemite $\gamma\text{-Fe}_2\text{O}_3$.

Loose and Compacted Soils: Two Basic Units Composing the Martian Surface?

Ki-iti Horai, Lamont-Doherty Geological Observatory of Columbia Univ., Palisades, NY 10964

Laboratory measurements of the thermal conductivity of lunar and terrestrial soils under simulated lunar and martian surface conditions suggest that loose and compacted soils are two basic units composing the martian surface. The measurement of the thermal conductivity on lunar soil samples and their terrestrial analogs under simulated lunar surface conditions shows that the thermal conductivities are $0.2 - 0.6 \times 10^{**(-5)}$ cal/cm sec K for loose soil samples and $2.1 - 2.6 \times 10^{**(-5)}$ cal/cm sec K for compacted soil samples. These values correspond, respectively, 1) to the thermal conductivity in the top 2 cm of the lunar regolith and 2) the stratum directly underneath, inferred from the lunar surface brightness temperature observations made by Apollo 15 and 17 heat flow experiments. The inference is consistent with a model of the lunar regolith structure that a thin layer of loose soil is underlain by a substratum of compacted soil.

The same samples, when measured under a simulated martian surface condition, yield thermal conductivities of $3.1 \pm 0.1 \times 10^{**(-5)}$ cal/cm sec K (loose soil) and $10.1 \pm 1.0 \times 10^{**(-5)}$ cal/cm sec K (compacted soil). These values are converted to thermal inertias of $2 - 3 \times 10^{**(-3)}$ cal/cm² sec^{1/2}K (loose soil) and $5 - 6 \times 10^{**(-3)}$ cal/cm² sec^{1/2}K (compacted soil). These coincide with the two peak values of the martian surface's thermal inertia as observed by the infrared radiometric measurements from Viking 1 and 2 orbiters. The bimodal distribution of the observed martian surface's thermal inertia may be explained by aeolian activity. Compacted soil, being more resistant, may be exposed in the area of aeolian erosion, whereas loose soil will constitute the surface layer of the aeolian depositional area. The laboratory values of thermal inertia for loose and compacted soils which agree with the two most frequently observed values of the martian surface's thermal inertia suggest that these two types of soil are most widely exposed on the martian surfaces.

Unusual Ejecta Dynamics on the Martian Satellites

K. R. Housen, University of Arizona, Tucson, Arizona

D. R. Davis and R. Greenberg, Planetary Science Institute, Tucson Arizona

The Martian satellites, particularly Phobos, provide an unusual dynamic environment due to their location deep within the gravity field of Mars. We have studied the dynamics of material ejected from the satellites, which are modelled as homogeneous triaxial ellipsoids ($\rho=1.9$) in the Martian gravitational field. The effective surface gravity on Phobos varies by a factor of 2.5 from a minimum of 0.28 cm/s^2 at the sub-Mars point to a maximum of 0.73 cm/s^2 at the rotational poles. At the present position of Phobos, the normal component of surface gravity is everywhere directed inward so that any regolith is gravitationally bound. However, when Phobos has tidally evolved inward by $\sim 25\%$ of its current orbital radius, the normal component of gravity at the sub-Mars point will be directed outward allowing surface material to leak off the satellite. Even at Phobos' present position, impact ejecta follow unusual trajectories. Ejecta patterns that might otherwise be symmetric are often quite distorted (Fig. 1). Note that a given launch velocity and launch angle can result in quite different ballistic ranges depending on the launch direction. The open contours in Fig. 1 for some launch speeds reflect the variation of escape speed with azimuth, i.e., it is easier to escape in certain preferred directions. Escape speeds on Phobos, which lead to independent orbits about Mars, vary from a minimum of 3.6 m/s to a maximum of 16 m/s . The regolith depth on Phobos is thought to be of order 100 m (Thomas, 1978). Impacts into this uncohesive material produce mainly low velocity ejecta (Fig. 2). Thus, most material ejected from craters smaller than $\sim 500 \text{ m}$ will be retained by the satellite. Larger craters will penetrate through to a presumably more solid substrate and thus will eject most material at velocities greater than the typical escape velocity. On Deimos, located a greater distance from Mars, the surface gravity (0.29 cm/s^2 to 0.36 cm/s^2) and escape speed are more nearly uniform and ejecta contours are quite symmetric.

Figure 1: Ejecta contours for a launch angle of 45° at the points (0,270E) and (0,315E).

The contours are impact loci which correspond to ejection velocities of $0.5, 1, 1.5, 2, 2.5, 5,$ and 7 m/s .

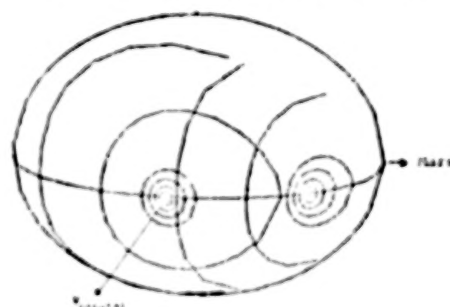
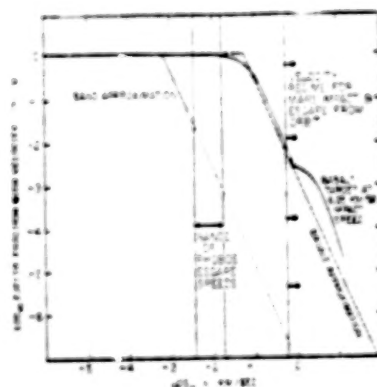


Figure 2: Representation of the ejecta velocity distribution for hypervelocity impacts into basalt and sand. Curves constructed from the work of Gault et al. (1963) and Stoffler et al. (1975). Also shown is the range of speeds required to impact on Mars or to escape Mars and the range of surface escape speeds on Phobos. Deimos escape speeds overlap the lower part of the Phobos range.



References

- Gault, D. E., E. M. Shoemaker, and H. J. Moore (1963), NASA TN D-1767.
- Stoffler, D., D. E. Gault, J. Wedekind, and G. Polkowski (1975), JGR 80, 4062.
- Thomas, P. C. (1978), Cornell Univ. CRSR Report No. 693.

Petrologic Units on Mars

R. L. Huguenin, Department of Physics/Astronomy, Univ. of Massachusetts, Amherst, MA 01003
J. W. Head, Department of Geological Sciences, Brown University, Providence, RI 02912
T. R. McGetchin, Lunar and Planetary Institute, Houston, TX 77058

Earth-based reflectance spectra (0.3-1.1 μm) of 200-400 km diameter areas (1) and spectral vidicon images (200 km resolution) (2) reveal that a large fraction of the martian surface is covered with a mantle of high albedo dust (3). This dust is remarkably uniform in composition everywhere, and it is apparently composed of weathering products of basaltic to ultrabasic rocks. The dust does not mantle the entire surface of Mars, however. Reflectance spectra show that the martian dark areas are windows through the dust mantle to crustal rocks, and that the surface mineralogy in these areas varies from region to region (1, 2). Most of the dark areas for which both spectra and vidicon coverage have been obtained are located in the Margaritifer Sinus (0 to 30° latitude, 0 to 45° longitude) and Copratés (0 to -30° latitude, 45 to 90° longitude) Quadrangles of Mars. Spectra for some areas were measured with a photometer (1) while spectra for other areas were derived from vidicon ratio images (2). The vidicon ratio images were formed by dividing each of the images measured at 20 wavelengths (0.35 - 1.03 μm) by the 0.566 μm image, thus providing 20-point spectra for each spatial resolution element. In addition to providing spectra, the ratio images also revealed the spatial extents of numerous geochemical units. Ten distinct units are visible in the Margaritifer Sinus and Copratés quadrangles and they are presented in Fig. 1. Interpretations of unit mineralogy are primarily those of Huguenin et al. (3), although they have been extended here to include gross estimates of relative mineral abundance. Interpretations are still being refined by laboratory modeling.

Units 1 and 2. Unit 1 corresponds closely in spatial extent with the dark area Margaritifer S. Unit 2 corresponds to a higher albedo dark area Pyrrhae R. The spectrum of Unit 2 shows absorption bands at 0.87 - 0.90 μm , 0.93 - 0.97 μm , and beyond 1 μm . The 0.87 - 0.90 μm band is stronger than the other two and it is probably due to a mixture of enstatite and ferric oxide (from contaminant dust). The band at 0.93 - 0.97 μm is of roughly equal strength to the band longward of 1 μm ; it can be attributed to pigeonite or augite. The band beyond 1 μm is probably due to olivine or basaltic glass. Opaques cannot exceed ~10 wt.% since the bands are relatively unmasked. Since olivine and glass produce much weaker bands than pyroxenes, we conclude that olivine (or glass) is the dominant phase in Unit 2, followed by the enstatite, and the clinopyroxene (pigeonite-augite). Unit 2 has weaker absorption features between 0.93 and 1.03 μm and slightly stronger features between 0.45 and 0.65 μm than Unit 1. The stronger absorption at 0.45 - 0.65 μm indicates contamination by ferric oxide in Unit 2, but probably not enough to account for the weakness (by band masking) of the absorptions beyond 0.93 μm . With the similarity of band strengths at 0.87 - 0.90 μm , it appears that Unit 1 contains more olivine (or glass), somewhat more clinopyroxene, and less orthopyroxene than Unit 2. In summary for Unit 1 $\text{ol (or glass)} > \text{cpx} > \text{opx}$ while for Unit 2 $\text{ol (or glass)} > \text{opx} > \text{cpx}$ (pigeonite-augite).

Unit 3 corresponds to a region in the eastern part of Erythraeum M. Comparison of its spectrum with those of Units 1 and 2 suggests that $\text{ol (or glass)} > \text{cps} \approx \text{opx}$.

Unit 4 occurs in the central part of Erythraeum M. The spectra show absorption characteristics of titaniferous augite or diopside with bands at 0.96 - 1.00 μm and a strong 0.6 - 0.77 μm $\text{Fe}^{2+} \rightarrow \text{Ti}^{4+}$ charge transfer band. There is also strong absorption beyond 1 μm , while absorption at 0.87 - 0.93 μm is conspicuously absent. Comparisons with Unit 1-3 spectra indicate that $\text{ol (or glass)} > \text{cps}$ (Ti-augite or Ti-diopside; $\text{TiO}_2 > 1\%$) \gg opx.

Unit 5 is in the western third of Erythraeum M. and its spectrum indicates that $\text{ol (or glass)} > \text{cpx}$ (augite) \approx opx.

Unit 6. Spectra in the dark areas Solis Lacus and Meridiani Sinus are quite similar; thus both regions have been assigned to Unit 6. Their spectra suggest that cps (diopside-salite) $>$ ol (or glass) opx and/or pigeonite.

Units 7, 8, and 9. Each of these units is a distinct albedo and spectral unit, but masking of silicate absorption bands by contaminant dust precludes identification of any of the phases present.

Unit 10. This is part of the global dust mantle, which Maderazzo and Huguenin (4) proposed is composed of 72-78% silicate clay, 13% $MgSO_4$, 6-10% $FeOOH$, 3-5% opaques, and minor amounts of carbonates, salts, and oxides.

It has been proposed independently by McGetchin and Smyth (4) and Maderazzo and Huguenin (4) that martian primary magmas should be picritic basalts (normative: 37-38% ol, 20-32% plag, 20-29% cpx, 4.4-7% mt, 2.5-5% neph, 0.6-2.4% or, trace il, and no opx). The unit mineralogies derived here are consistent with differentiation of the proposed primary melts by any of several possible mechanisms, including ol or ol + mt separation and/or partial melting. The o + 2px mixes suggest a possible differentiation sequence of ol → opx → cpx, with progressive Si-enrichment, and such differentiation of ultramafics can lead to late stage melts enriched in cpx and TiO_2 (S. Haggerty, personal comm.), which is consistent with the observations here (cf. Unit 4).

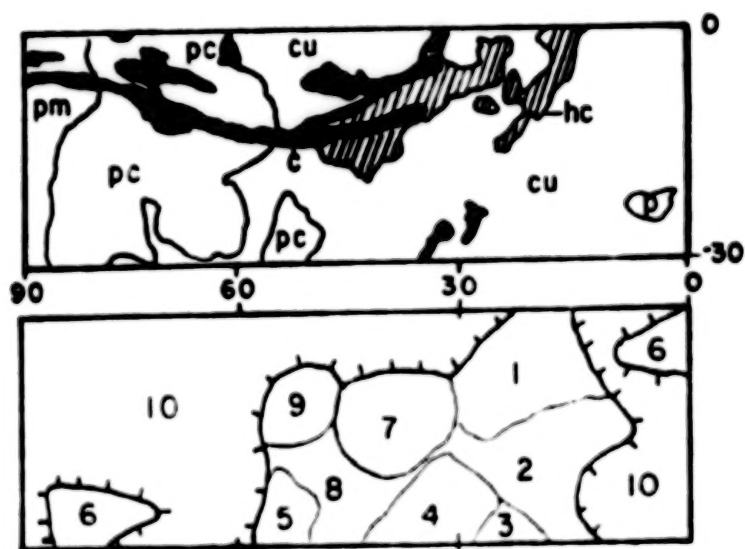
The petrologic units correlate closely with albedo units in these two quadrangles. Units 7, 8 and 10 are covered with dust and have medium-high to high albedos, while Units 1-6 have exposed Fe^{2+} - silicates and are medium-dark to dark. Unit 9 (Aurorae S.) is normally dark, but it was obscured by a dust cloud during our observations. Within Units 1-6 there is a further correlation with albedo; the darkest units (Units 1, 4, and 6) have the lowest opx/cpx + ol (or glass) ratios, while the lightest of the dark units (Unit 2) has the highest opx/cpx + ol (or glass) ratio. The medium dark units (Units 3 and 5) have ratios that are intermediate to these extremes. This suggests that differentiation may possibly involve ol separation and not ol + mt separation. If true, this suggests that the magmas may have formed in low f_{O_2} environments. A low f_{O_2} combined with the possibility of a high magmatic sulfur content (high observed soil sulphate content) further suggests the possibility that the opaque phase could be a sulfide rather than magnetite.

Correlations with geologic units are not straightforward. The boundaries of Unit 5 correlate with those of a densely cratered plains unit (pc), while Unit 6 comprises both densely cratered plains (Solis Lacus) and cratered uplands (Meridiani S.). Units 1-4 are within cratered uplands. Units 1 and 4 contain major channels and chaotic terrain while Units 2 and 3 do not. It may or may not be significant that Units 1 and 4 (with channels) have low opx/cpx + ol (or glass) ratios (late stage differentiates), while Units 2 and 3 (few channels) have high opx/cpx + ol (or glass) ratios. The possible significance of this correlation is enhanced by the observation (5) that Solis Lacus (Unit 6, with a low opx/cpx + ol (or glass) ratio) contains an anomalous contemporary reservoir of H_2O . If the correlation is real, it raises the possibility that the darker, more cpx-rich units may have a greater capacity, for H_2O storage (possibly containing more cracks, vesicles, or lava tubes for example). It is interesting to note that in a planet-wide survey of channel distribution, D. Pieri (private comm.) also noted that the darkest units generally contained the highest density of channels.

References

- 1) McCord, T. et al. (1977) *Icarus* 31, 25
- 2) McCord, T. et al. (1977) *Icarus* 31, 293
- 3) Huguenin, R. et al. (1977) *Lunar Science* VIII, 478
- 4) Smyth, J. et al. (1978) *Lunar and Planetary Science* IX, 1077
- 5) Huguenin, R. et al. (1978) *Proc. 2nd Coll. Planetary Water and Polar Processes* (in press)
- 6) Mutch, T. et al. (1976) *Geology of Mars*, Princeton Press, 354 pp.

Figure 1. Geologic map (6) and units derived from spectra and vidicon images. p = plains (m = moderately cratered, d = densely cratered); cu = cratered terrain; c = channels; hc = hummocky/chaotic. Hachures point toward regions obscured by dust mantle.



Mars: Chemical Reduction of the Regolith by Frost

R. L. Huguenin, K. J. Miller and W. S. Harwood, Department of Physics/Astronomy, Univ. of Massachusetts, Amherst, MA 01003

The occurrence of ferric oxides and oxidants (inferred by the Viking biology experiments) in martian soil has been generally construed as evidence for a highly oxidized regolith. While oxidation has clearly occurred, it cannot be concluded that oxidation dominates the weathering process, however. It has already been shown that the oxidation of Fe^{2+} in minerals does not require an oxidizing atmosphere on Mars: it is forced by solar UV and can occur in highly reducing atmospheres containing only trace amounts of $\text{O}_2(1)$. Indeed we now report laboratory studies that indicate that the oxidants in the soil may be byproducts of the chemical reduction of mafic silicates by H_2O frost and ice, and show that chemical reduction may possibly dominate the regolith weathering processes.

The mineral olivine is apparently a principal component of martian rocks(2) and we therefore chose it as the mineral for our first experiments. Samples were pulverized and exposed to H_2O vapor at -11 to -22°C , simulating the martian nighttime and subsurface daytime formation of frost on freshly cleaved mineral surfaces. Upon reaching -22°C the coolant was turned off and the sample warmed to room temperature. After about 30 minutes the frost in the sample began to melt and the chamber pressure rose rapidly to 9×10^{-2} torr. The rate of gas evolution tapered off and slowly rose to 2 torr after 120 hours. The gas was analyzed by gas chromatography to be principally O_2 , amounting to 7×10^{19} O_2 molecules per gram of sample (after 120 hours). In a second experiment we pulverized a sample of olivine in the presence of H_2O vapor at -11 to -22°C , and again turned off the coolant and after ~ 30 minutes the frost began to melt. At this point 5 ml of 0.1M HCOONa solution was injected into the sample and the chamber pressure increased to 1.8 torr in ~ 1 hour. The gas chromatogram registered two peaks, one corresponding to O_2 and the other corresponding to 1.8 torr CO_2 . The amount of CO_2 produced (6.5×10^{19} molecules g^{-1}) was very close to the number of formate ions available for oxidation (3×10^{20} molecules) and it represented nearly complete (43%) conversion to CO_2 in ~ 1 hour. Numerous control experiments were performed which indicate that the source of the O_2 and CO_2 was a species produced by the simple exposure of freshly cleaved olivine to frost.

We have attempted to identify the source of the chemical activity using a variety of chemical indicators. One of the tests gave positive results, and it indicated that a peroxide, probably H_2O_2 , had been formed on our frost-treated olivine samples. The samples were injected with an aqueous solution containing dilute FeCl_3 and a trace of $\text{K}_3\text{Fe}(\text{CN})_6$. Upon exposure to the sample this yellow solution turned colorless and a white precipitate formed. The formation of the "Berlin White" precipitate without a blue or green precipitate (as we observed) is a specific and sensitive indicator for peroxide in the presence of an adsorbate substrate. H_2O_2 apparently chemisorbed as $\text{HO}_2^-(\text{ads})$ (at metal ion sites) and $\text{H}^+(\text{ads})$ (at surface O^{2-} sites), and when the frost melted the peroxide apparently went into solution as $\text{FeO}_2\text{H}^{2+} + \text{FeOH}^{2+} + \text{HO}^- + \text{H}^+$.

We propose that the peroxide was produced from chemisorbed H_2O as a result of the reduction of the substrate olivine, i.e. hydrogen was removed from the surface H_2O and incorporated in the silicate. In particular we propose that upon exposure to the freshly-cleaved surfaces, H_2O vapor dissociatively adsorbed as $\text{OH}^-(\text{ads})$ and $\text{H}^+(\text{ads})$. Following this, a fraction of the H^+ were drawn into the crystal by the attractive force of negatively-charged lattice defects (eg. metal ion vacancies or Al^{3+} substituted for Si^{4+}) where they combine with oxide ions to form lattice hydroxyl ions. Incorporation of the protons at negative defects gives the crystal a net positive charge, while the surface layer of adsorbed H_2O has a net negative charge (excess OH^- relative to H^+). Charge balance is restored by transfer of electrons from $\text{OH}^-(\text{ads})$ to positive lattice defects (eg. anion vacancies or Fe^{3+} substituted for Fe^{2+}) and the resultant surface OH radicals combine to form the more stable hydrogen peroxide molecules ($\text{H}_2\text{O} + \text{O}_2^{2-}(\text{o}, \text{Al}^{3+}) + \text{Fe}^{3+}(\text{o}) \rightarrow \text{OH}^-(\text{o}, \text{Al}^{3+}) + \text{Fe}^{2+}(\text{o}) + 1/2 \text{H}_2\text{O}_2(\text{ads}) - 33.9 \text{ kcal mole}^{-1}$). The H_2O_2 should actually chemisorb in the dissociated state ($\text{HO}_2^-(\text{ads}) + \text{H}^+(\text{ads})$) and it would be metastable, i.e. it should decay with time to adsorbed oxygen ($\text{H}_2\text{O}_2(\text{ads}) \rightarrow \text{H}_2\text{O}(\text{g}) + \text{O}(\text{ads}) + 42.4 \text{ kcal mole}^{-1}$). The activation energy for the decay should correspond to the O^-OH^- bond strength in HO_2^- , which is $\sim 34 \text{ kcal mole}^{-1}$. A large surface potential energy should develop during the proton incorporation and peroxide production reactions which would not

develop if the H_2O occurred as a liquid instead of frost. Subsequent exposure of the surface layer to liquid H_2O would release the surface potential energy, and produce the observed avalanche-like ejection of peroxide and metal ions into solution. The species that get released to solution include FeO_2H^{2+} , $FeOH^{2+}$, $HO\cdot$, and H^+ which react to form $O_2(g)$ and which can efficiently oxidize formate ions to $CO_2(g)$.

Our experimental results closely mimicked the chemical activity of the martian soil samples during the active cycles of the Viking Gas Exchange (GEx) and Labeled Release (LR) biology experiments, although the activity of our samples was more intense than the martian samples. In addition the model proposed here predicts the unusual thermal and storage behavior of the GEx and LR experiments. In particular, the ability of the martian oxidant to oxidize organic substrate to CO_2 gas during the LR experiment was inhibited by sterilization at 45-50°C and 160°C and by prolonged storage at 10-15°C, while the release of O_2 gas from the GEx samples was not appreciably affected by either sample sterilization or storage. Levin (3) constructed an Arrhenius plot of the LR thermal and storage data and derived an activation energy for destruction of the martian oxidant to be 35-43 kcal mole⁻¹. This is remarkably close to the ~ 34 kcal mole⁻¹ activation energy derived here for the decay of adsorbed peroxide to $O_{(ads)}$ and it strongly suggests that chemisorbed peroxide may have been the active species in the unsterilized GEx and LR samples. The end product of the decay, $O_{(ads)}$, should be stable to a temperature of $\sim 580^\circ C$ at Fe^{2+} sites in the absence of liquid H_2O (4), while subsequent exposure to liquid H_2O should rapidly release the $O_{(ads)}$ as $O_2(g)$ (4). We thus propose that $O_{(ads)}$ derived from the decay of chemisorbed peroxide may have been the principal source of $O_2(g)$ in the heat-sterilized GEx samples. The results of the LR and GEx experiments provide strong support for the olivine reduction model proposed here, and they indicate that the martian soil is actively undergoing a chemical reduction. Photochemical oxidation processes are also predicted to be active in the contemporary martian environment (1), however, and a major question then is whether surface weathering is producing a net oxidation or net reduction.

The answer to this depends in large part on the mineralogy of the unweathered material, which varies regionally and is not well known (2). It also depends on the population of defects in the constituent minerals, and this too is not well known. A crude estimate can be made, however, if one assumes that the average crustal mineralogy can be approximated by the primary mantle melt normative mineralogy derived from the Viking XRF data and mantle thermal models (3): 37-38% olivine (Fe_{44}), 20-29% diopside (Wo_{50} , En_{28} , Fs_{22}), 20-32% plagioclase (An_{60}), 2.5-5% nepheline, 0.6-2.4% orthoclase, and 4.4-7% magnetite. If it is assumed that one oxygen is incorporated per two Fe^{2+} during oxidation, then complete oxidation of the above basalt would incorporate $.4 - 6 \times 10^{21}$ oxygens per cm^3 . The number of H^+ incorporated depends on the number of negative defects and their percent occupancy. The principal negative defect in semiconductor solids are cation vacancies which typically have abundances of $10^{20} - 10^{22} cm^{-3}$ in pure synthetic specimens, and in natural minerals the number of defects should be greater. The number of hydrogens incorporated on our olivine sample after exposure to frost was $3 \times 10^{20} cm^{-3}$ which represents $\sim 12\%$ occupancy of the defects. Repeated exposures to frost would have increased the occupancy, since the number of H^+ incorporated was limited by the number of chemisorption sites on the mineral surface (4). If it is assumed that full occupancy of the defects can be attained and that there are (conservatively) $10^{20} - 10^{22} defects cm^{-3}$ in the above basalt, then the number of hydrogens incorporated per cm^3 could be comparable or even exceed the number of oxygens incorporated per cm^3 . Clearly there are too many uncertainties to determine whether surface weathering is a net oxidation or net reduction process. Earth-based measurements of the reflectance spectra of small areas (200-400 km diameter) indicate that the rock types vary from region to region and they are quite different than the basalt used in the above calculation (2). Weathering of these different basalts would have different relative oxidation and reduction rates, and the net oxidation and reduction rates would have changed over geologic time as new and different basalt units erupted onto the surface.

One of the most important effects of surface weathering is its effect on atmospheric evolution and oxidation state. Imbalances in the oxygen and hydrogen incorporation rates can have important effects on the oxidation state of the atmosphere (4). In particular a net oxidation of the regolith would produce a gradual decrease in the O_2/CO rate, while a

net reduction of the regolith would produce a gradual increase in the atmospheric oxidation state. These changes in O_2/CO would be buffered somewhat by adjustments in the surface photooxidation rates, atmospheric chemistry, and exospheric escape rates, but the long term effects could potentially be appreciable (4). In addition current changes in the atmospheric oxidation state may be very different than they were in the past, since the crustal mineralogy has probably undergone significant changes over geologic time.

References

- 1) Huguenin, R. L. (1974) *J. Geophys. Res.* 79, 8495
- 2) Huguenin, R. L., Head J. W. and McGetchin, T. R. (1976) *NASA TM79729*, 118
- 3) Levin, G. (1978) presentation at 2nd Conf. on Simulated Mars Surf. Prop., NASA Ames, 17-18 August
- 4) Huguenin, R. L., Prinn, R. G., and Maderazzo, M. (1977) *Icarus* 32, 270.

Dust Storms and Condensation

G. E. Hunt, Laboratory for Planetary Atmospheres, Department of Physics and Astronomy, Gower Street, London WC1E 6BT, England.

The thin martian atmosphere possesses an active meteorological system which, in particular seasons, gives rise to a variety of major disturbances which may be observed through dust storms and condensate clouds. Throughout the Viking mission, many types of clouds have been observed by the Imaging and IRTM instruments on the orbiter. Information on the opacity of these phenomena have been obtained both from the lander imaging and IRTM instruments, so that their effects on the radiative transfer of the martian system may be assessed. CO_2 clouds have also been thought to be present at particular times and locations on the planet. The effects of all these cloud types and their effects upon the martian meteorology will be discussed.

Possible Oxidant Sources in the Atmosphere and Surface

D. M. Hunten, University of Arizona

Photolysis of H_2O in the atmosphere near the surface is a copious source of OH, HO_2 , and probably superoxides, some of which are likely to condense on the surface and migrate through the pores. The processes have been modeled in detail for their atmospheric interest. The models successfully account for the rarity of CO and O_2 , the notable variability of ozone, and the escape flux of hydrogen. Though only qualitative estimates can be made of surface deposition rates and lifetimes, the suggested amounts are in the range inferred by Viking. The OH rapidly destroys any organic molecules that are present as vapors.

Analogous reactions involving adsorbed water have been studied by Huguenin. These processes can be driven by the much larger photon fluxes at longer ultraviolet wavelengths. The suggested explanations, and many of the experiments, make it likely that peroxides, superoxides, and adsorbed OH are all present. Both kinds of process, and their combinations, seem in principle able to explain the absence of all organic molecules and the variety of observed oxidants. Since they operate planetwide, there is a strong suggestion that the observed conditions are typical. "Oases" of higher than average humidity may in fact be even more hostile than the average region, because water under Martian surface conditions is anything but benign.

Laboratory simulation of the atmospheric processes must pay careful attention to scaling.

Curiously, similar OH densities occur at the Earth's surface. The notable differences are food for thought, and ideas about the origin of life may be particularly affected.

References

- Atmospheric: Hunten, *Rev. Geophys.* 12, 529 (1974) (summarizes earlier work); Liu & Donahue, *Icarus* 28, 231 (1976); Kong & McElroy, *Icarus* 32, 168 (1977), *Planet. Sp. Sci.* 25, 839 (1977).
- Surface: Huguenin, *JGR*, 78, 8481, 8495 (1973), 79, 3895 (1974), *Icarus* 28, 203 (1976); Huguenin, Prinn & Maderazzo, *Icarus* 32, 270 (1977).

Mars in the Solar Wind: Implications of a Venus-like Interaction

D. S. Intriligator, Physics Department, University of Southern California, Los Angeles, California 90007

Observations by plasma analyzers and magnetometers on one US and several USSR spacecraft in the vicinity of Mars provide evidence for the existence of a martian bow shock. There are two possible basic modes of interaction between the solar wind and Mars: a Venus-like interaction where the solar wind may interact directly with the atmosphere and an earth-like interaction where the planetary magnetic field is strong enough to hold off the incident solar wind. In this paper, I will briefly summarize the theoretical models associated with these modes of interaction, and then as a complement to the presentation by E. J. Smith, discuss the implications of a Venus-like interaction of the solar wind with Mars. Our recent Pioneer Venus observations will be used to discuss the possible direct interaction of the solar wind with the atmosphere of Mars, the scavenging of ions by the solar wind from the atmosphere, and the existence of magnetospheric-tail associated phenomena. The controversy concerning the USSR plasma measurements in the vicinity of Mars will be briefly reviewed. The presentation will conclude with a brief description of the measurements needed to resolve these issues and how they may be obtained on future missions to Mars.

Formation and Regression of the Martian North Polar Cap in 1975-78

K. Iwasaki and Y. Saito, Kwasan Observatory, Univ. of Kyoto, Yamashina, Kyoto, 607, Japan
T. Akabane, Hida Observatory, Univ. of Kyoto, Kamitakara, Gifu-Ken, Japan

In the photographic observations of Mars at the Kwasan Observatory and at the Hida Observatory during the 1977-78 apparition, the north polar cap was first observed at $L_s=14^\circ$ and the latitude of the edge of the cap was about $65^\circ N$. This edge of the cap changed little until $L_s=50^\circ$ and then it started to shrink. The edge was observed near $74^\circ N$ at $L_s=70^\circ$. The same tendency is seen with the data of the Lowell Observatory (Baum et al., 1973) and the data of the Kwasan Observatory (Miyamoto, 1963). Therefore, observed constancy of the dimension of the north polar cap before $L_s=50^\circ$ appears to be a regular phenomenon in the behavior of the north polar cap. In the observations at the Hida Observatory during the 1975-76 apparition, red-light photographs taken in winter did not show a north polar cap, but revealed a dark surface of the polar region through the polar hood. In our observations during the 1977-78 apparition, the north polar cap first observed at $L_s=14^\circ$ on red-light photographs. According to the visual observation by Miyamoto during the 1960-61 and the 1962-63 apparitions, the north polar cap first observed at $L_s=0^\circ$ and 2° , respectively (Miyamoto, 1974). In the Mariner 9 observations of the north polar region, the picture acquired before the northern vernal equinox show no clear-cut boundary of the north polar cap. The north polar cap has been generally believed to be formed in winter under the polar hood covering the north polar region. However, these ground-based observations and the Mariner 9 observations would suggest that the north polar cap is formed not in mid-winter, but near the northern vernal equinox.

Seasonal Behavior of Martian Polar Caps

P. B. James, Physics Dept., Univ. of Missouri, St. Louis, MI 63121

Seasonal changes of the martian polar caps are sensitive to insolation, to atmospheric processes, and to the distribution of volatiles on the planet. The annual polar cap cycle therefore reflects the current climate of Mars, and clues to climate changes may be recorded in the polar regions. Astronomical records suggest uniformity in seasonal cap variations from year to year, although telescopic measurements of the caps are difficult and possibly subject to systematic errors. Mariners 7 and 9 made polar observations; these data, confined to restricted seasons, were consistent with terrestrial observations. Viking orbiters have acquired data on the martian polar regions which span more than a full year. A particularly complete set of data, acquired by VO-2, portrays the spring-summer recession of the south polar cap. The regression curve obtained departs significantly from the curves based upon telescopic observations. The retreat observed by Viking was slower than those previously seen; the magnitude of the retardation at summer solstice is quantitatively estimated to be 12.5° in L_s . A comparison of Viking and Mariner 9 pictures of the south polar region in summer confirms this conclusion; these data also suggest that some CO_2 frost may have survived the summer season viewed by Viking. The retardation of the polar recession may be related to a global duststorm observed by Viking at an unusually early date relative to the classical duststorm season. Dust aerosols may affect the polar energy balance directly by reducing the heat absorbed at the surface and indirectly by modifying meridional heat transport by the atmosphere. Data relevant to other seasons are less complete than for the one discussed above because of orbital constraints and cloud cover. Several observations of the north polar cap during its sublimation phase agree well with terrestrial data and with Mariner 9 observations.

Martian Splish Cratering and its Relation to Water

L. A. Johansen, Jet Propulsion Laboratory, California Institute of Technology, Pasadena, CA 91103

Mapping of Maritan crater morphology types from Viking Orbiter imagery provides information from which a model of water distribution can be derived. This model involves the presence of water ice layers increasing in volume to the poles and is consistent with predicted locations of ground ice in equilibrium with the atmosphere.

Certain crater types have ejecta that appear to be the result of fluid-like flowing associated with impact. The frequency of occurrence of these "splish" craters varies strongly with latitude. If water is the agent responsible for fluidizing the ejecta, then water is more common in the Martian regolith in these zones. This distribution is consistent with an equilibrium model of volatile distribution. This latitude relation implies volatile redistribution over time in response to thermal conditions. Given this relation, the location of subsurface ice or water at the time of meteor impact may be determined.

Water has probably played a substantial role in the formation of the Martian splish craters.

The Climate of the Martian Polar Cap

H. H. Kieffer, U. S. Geological Survey, Flagstaff, AZ 86001

F. D. Palluconi, Jet Propulsion Laboratory, Pasadena, CA 91103

Observations of the polar regions over a complete Martian year by the Infrared Thermal Mappers (IRTM) on the Viking Orbiters have shown the two poles have quite different behavior, but both endure marked, but opposing effects by global dust storms, that the two permanent polar caps may be of different composition, and that the circumpolar soil in the North is probably saturated while that in the South may be dessicated.

In the winter, polar cap brightness temperatures at 20 μm (T_{20}) drop to and below the CO_2 frost point; there is a general temperature decrease toward the geometric pole, with local areas becoming as cold as 125K; some local thermal features are associated with craters. Polar stratospheric temperatures, sensed in the 15 μm CO_2 band with a weighting function that peaks near 0.5 mbar, decrease toward the pole, approaching T_{20} , but undergo profound changes during the dusty periods. During the second global dust storm, T_{15} at 65°N rose rapidly to over 230K while T_{20} at the same location remained near 150K and continued to exhibit local colder areas. These temperatures imply remarkable vertical stability in the polar night and indicate the global dust storms produce a major increase in meridional circulation carrying heat toward the winter pole.

In the summer, north polar ice temperatures reach 200 to 210K (based on observations made in 1976 and 1978), the level expected for material with the observed bolometric albedo 0.5 to 0.4; the residual north polar cap is a dirty water ice. In contrast, maximum observed south polar summer temperatures are lower even though Mars is near perihelion, and show strong spectral contrast, ranging from 160K at 20 μm to 196K at 9 μm . The explanation of the southern summer observations involves warm soil lanes intruding into the frosted areas, and considerable thermal infrared opacity of the then dust-laden atmosphere; the inferred surface temperatures are consistent with a CO_2 surface layer remaining throughout the year.

The hemispheric polar differences apparently depend on the timing of the global dust storms. The dust storms occur near perihelion; in the southern summer the scattering properties of dust in the atmosphere decrease the insolation which reaches the surface. This effect overrides the increased downgoing thermal radiation due to the infrared opacity of the dust. Little dust appears to be incorporated into the subliming cap. In the northern winter, both heat, H_2O and dust are carried into the polar night. The seasonal asymmetry in atmospheric dust content results in the south pole having a more favorable annual energy budget for retention of solid CO_2 . The condensation that occurs in the north during dusty periods results in the sweeping out of dust from the atmosphere and its incorporation into the northern winter cap. This dust remains on the surface during the sublimation phase and may eventually be mobilized to constitute the extensive northern dune fields. During the south polar growth period the atmosphere around that cap is remarkably clear; it is uncertain when or how much dust is incorporated into the permanent south polar ice. Dust resting on CO_2 frost in the sublimation phase should rapidly sink into the frost, as the same enhanced solar absorption that would make it visible causes it to supply additional heat to sublime the CO_2 locally supporting it. A process such as this may be responsible for the substantial changes in albedo observed over the south polar cap in the summer.

A probably secondary result of the asymmetry of polar summer temperatures is a dichotomy in the circumpolar subsurface H_2O abundance. The warming of the north polar water ice saturates the polar atmosphere and water vapor will diffuse at relatively high partial pressures into any permeable soils in the north polar region. In the winter, the cold surface will act as an effective barrier to H_2O , even if permeable because of the enormous decrease in the saturation vapor pressure of H_2O at CO_2 condensation temperatures. Over long times, the average partial pressure in the soil will approach the annual average partial pressure in the polar lower atmosphere; this exceeds the saturation pressure at the annual average soil temperature so there will be net increase in the soil H_2O content until it becomes impermeable. This may explain the origin, stability and morphology of the north polar dune fields; they are glued together with permafrost. In the south polar region, the presence of a permanent polar ice cold trap will act to remove water vapor from the polar atmosphere, and lower the mean annual vapor pressure below that in equilibrium with the mean circumpolar soil temperature resulting in gradual dessication of the ground.

The preceding discussion is based on the coincidence of southern summer and perihelion, when maximum equatorial diurnal thermal variations initiate the annual dust storms. Periodic variation in spin axis direction and orbital elements will reverse the perihelion summer hemisphere every 50,000 years, and the asymmetry of the dust-circulation-condensate cycle would also be expected to switch hemispheres. The observation that the circumpolar geomorphologies of the two hemispheres, which presumably reflect a much longer history, are very different suggests that there is adequate stability in the residual caps to survive the isolation variation or that hemispheric differences in geology and/or topography have sizable effects on the seasonal processes. The positive feedback stability of high albedo - clean CO₂ frost lessening its own sublimation rate in the summer implies that the polar cap with the more favorable annual energy environment will grow at the expense of the other through the coupling provided by the total atmospheric pressure. Thus, there can be only one permanent polar cap composed of the major atmospheric component.

All existing models of Martian polar cap behavior predict that CO₂ frost will not remain throughout the summer. The major parameter in these models is the bolometric albedo of the frost. For at least the south cap, large spatial and temporal variations in apparent albedo are observed; no good explanation of this exists. Although there have been attempts to determine the existence of a regolith absorbed CO₂ reservoir by its buffering effect on the seasonal total pressure variation, the simplicity of current polar condensate budget models prohibits a reliable determination of this secondary effect. Preliminary to future modeling, the apparent absorbed insolation and emitted radiation budgets should be compiled for the polar regions through a Martian year. Future models should then incorporate the effects of a seasonably dusty atmosphere, meridional transport of energy by the atmosphere, and the probable drifting of solid CO₂.

Global Variations of Martian Surface Materials

H. H. Kieffer and L. A. Soderblom, U. S. Geological Survey, Flagstaff, AZ

The Viking Orbiter spacecraft were each equipped with two instruments (infrared thermal mapper and the orbiter imaging system) capable of providing information on the nature and distribution of surface materials on Mars. Using color imaging obtained during approach to Mars (resolution 30 km) and apoapsis predawn temperature observations (resolution 120 km), the Martian surface can be categorized in terms of visual reflectance (0.42 - 0.64 μ m), color, and thermal inertia; and are referred to as "albedo, color, thermal inertia", for example "bright, red, low".

There are generally good correlations of these three parameters with geologic units, although marked counter examples exist. Examples of abrupt contacts in all three parameters correspond to sharp, pronounced geologic contacts. Strong correlations exist in dark equatorial regions. The bright regions are more varied, probably the result of the surficial-mobile nature of the bright material, and considerable structure below the resolution of this study.

In these parameters, "dark, red, low" terrain is common in the equatorial region and represents old cratered terrain on which fluvial features are common. Crater rims are exceptionally red, while crater interiors have relatively higher thermal inertia. The immediate age volcanics are "dark, blue, high" and are usually devoid of fluvial features. Large, elongated regions of both units trend northwest across the southern equatorial region. The youngest volcanic constructs are all "dark, red, very low".

Color is interpreted as an index of either chemical weathering (red corresponding to increased oxidation of iron), or mineralogical separation, as likely in obvious eolian deposits. Thermal inertia is related primarily to the physical nature of the surface, increasing with mean grain size or intergrain bonding. Brightness may represent either intrinsic mineralogical differences or enhanced scattering associated with very fine particles.

While generally corroborating the geologic mapping of Mars based on Mariner 9 data, unusual local variations of these parameters in opposition to the general correlations have no obvious geologic cause.

New data is becoming available in the form of apoapsis color images (resolution 1 km), northward extension of the apoapsis temperature mapping to +50° latitude, and isolated low altitude (resolution 5 to 20 km) thermal maps.

The Role of Volatiles in the Cratering Process: Implications for Martian Surface

S. W. Kieffer, U.S.G.S., Flagstaff, AZ 86001

C. H. Simonds, Northrup Services, P. O. Box 34416, Houston, TX 77034

In an effort to understand shock processes and products on hydrous vs. anhydrous planets, we have constructed a cratering model based on theoretical calculations and field observations to account for the roles of both lithology and volatiles in cratering mechanics. We have focused on the influence of lithology and volatiles on melt production because a survey of published descriptions of 32 of the least eroded large terrestrial impact structures reveals that the amount of melt formed in craters in crystalline rocks appears to be approximately 2 orders of magnitude greater than the amount formed in craters in sedimentary rocks. This observation implies either that melt is not generated during impacts into sedimentary rocks or that it is destroyed by some process during or after the cratering event. The proposed cratering model is used to examine the cratering process for 3 impact velocities (6, 17, 24.6 k sec⁻¹): for a variety of meteorites (iron; diabase and basalt to represent stony meteorites; permafrost and ice to represent porous chondrites or comets); and for a variety of target lithologies (diabase, basalt and granite to represent terrestrial or planetary anhydrous crystalline rocks; carbonate to represent terrestrial limestones or possible Martian carbonates; dry Coconino Sandstone and water-saturated permafrost to represent dry and wet or frozen regoliths; ice to represent terrestrial oceans, polar caps, Martian polar caps or Jovian satellite surfaces; and dry sand and aluminum to calibrate our results against previous laboratory experiments). We calculated crater volume, depth of penetration of the meteorite, scaled depth of burst, radii to various peak-pressure isobars, volume of silicate melt, and volume of water (or, in the case of carbonate, carbon dioxide) vapor produced.

The calculations show that the volume of material shocked to pressures sufficient for melting should not be significantly different in sedimentary and crystalline rocks. We are forced to conclude that shock melt formed by impacts into volatile-containing lithologies is destroyed by the cratering process, and we propose that it is finely dispersed by the large volume expansion of shocked volatiles upon release from high pressure. In addition, any unit produced probably reacts chemically to clay minerals penecontemporaneously (i.e., while ejecta units are cooling) so that any original melt is unrecognizable.

We propose that during terrestrial cratering events volatile (vapor)-lubricated flows are formed at craters in volatile-rich rocks and that such flows are the "suevite" units observed in the field. They are approximately equivalent stratigraphically, but not mechanically or thermally, to the melt sheets found at craters in crystalline rocks; however, they contain material from a much wider range of pressures and temperatures than the melt sheets and contain hydrated clay minerals instead of glass or devitrified glass. Similar dispersal of melt by volatile expansion may account for the lack of observable melt sheets on the Martian surface. Melt sheets on the Martian surface are probably replaced by suevite-like vapor-lubricated flows or ash clouds which originate in that part of the crater shocked to ~ 100 kb and by liquid-lubricated flows which originate in that part of the crater where the permafrost is melted. Together, these two units may make up the flows observed at the Martian rampart craters.

A cratered Martian regolith, therefore, should contain not the mixture of unshocked and shocked crystalline fragments and glass characteristic of the lunar regolith, but rather a mixture of unshocked and shocked hydrous crystalline material. Impact glass will be virtually absent on the Martian surface.

The Viking Biology Experiment: Epilogue and Prologue

H. P. Klein, NASA-Ames Research Center, Moffett Field, CA 94035

The three Viking biology instruments that probed samples of the martian surface at Chryse and Utopia were predicated on several different hypothetical models of martian biology. They utilized assay systems designed to test for metabolic activity by measuring the uptake or release of biologically important gases. After analysis of all of the Mars data (from 26 separate experiments), it is generally agreed that only one of the instruments—that was used in the Labeled Release (LR) experiments — yielded data resembling that expected from a metabolizing system. The other two instruments also gave results indicative of chemical reactions whenever martian samples were incubated in these systems, but the characteristics of these reactions do not fit the criteria for metabolism. That even the LR data is the result of non-biological reactions seems likely (although not proven) in view of (a) evidence suggestive of the production of oxidants in the martian atmosphere, (b) direct evidence for oxidants in the regolith samples, and (c) the absence of any organic matter in these samples as determined by the highly sensitive GCMS instrument. Over the course of the last two years, the general conclusions, derived from the Viking biology investigation, have stimulated numerous ground-based studies which are directed toward a better understanding of the active components or processes accountable for the Viking results. One approach has been to expose terrestrial materials to activation by UV, oxygen plasmas, or other sources of excitation in order to determine whether oxidants can be generated in situ. Another has been to test the ability of postulated oxidants, including H_2O_2 , superoxides, and iron oxides, to promote reactions simulating those seen on Mars. A third line of research has utilized different types of clays in attempts to catalyze reactions postulated to have occurred on Mars. By and large, the ground-based studies have provided insight into plausible mechanisms for the more significant observations seen on Mars, but it is not yet feasible to arrive at a unified concept to explain all the Mars data, and many fine details remain to be duplicated in simulation experiments.

Modes of Sediment Transport in Channelized Water Flows with Ramifications to the Erosion of the Martian Outflow Channels

P. D. Komar, School of Oceanography, Oregon State Univ., Corvallis, Oregon 97331

Comparisons are undertaken between the hydraulics of channelized water flows on Mars, those which presumably eroded the large outflow channels, and large rivers, the catastrophic floods that formed the Channeled Scablands, and deep-sea turbidity currents. Like the Lake Missoula floods, turbidity currents are catastrophic in character, being formed by the slumping of large masses of sediments in the ocean; repeated flows have been formed deep-sea channels similar in scale and overall morphology to the Martian outflow channels. Expected bottom shear stresses, velocities and discharges, flow powers, and other parameters are computed for Martian water flows and for the three types of flows on Earth. Sand transport rates and the times required for channel erosion are estimated for Mangala Channel. These calculations indicate that turbidity currents and the Lake Missoula floods were similar to channelized water flows on Mars in their flow characteristics and in their abilities to erode and transport sediments. The criteria for quantitatively determining which grain-size ranges are transporting in terrestrial rivers as bed load, suspended load and wash load (autosuspension) are applied to an analysis of sediment transport in the large Martian outflow channels. Of importance is the balance of the effects of the reduced Martian gravity on the water flow velocity versus the reduction in grain settling velocities. Analyses were performed using grain densities ranging from 2.90 g/cm^3 (basalt) to 1.20 g/cm^3 (volcanic ash). The results show that nearly all sand-sized material and finer would be transported in auto-suspension and thus could be transported in nearly unlimited quantities as the autosuspended load requires no net expenditure of the water-flow power. A comparison with terrestrial rivers indicates that concentrations as high as 60-70% by weight of sediment could prevail in the Martian water flows, resulting in the very rapid erosion of the channels.

Simulated Aeolian Abrasion of Quartz and Basalt under Martian Conditions

D. Krinsley, R. Greeley, and T. R. McKee, Department of Geology, Arizona State University, Tempe, AZ 85281

Abrasion of crushed quartz and basalt sand sized particles has been simulated at Martian pressures and velocities in an aeolian erosion device; surfaces were examined with the scanning electron microscope (SEM). At velocities less than 20 meters sec^{-1} and 5 mb pressure, mechanical aeolian textures which appeared were similar to those found on natural sands in Earth deserts and to those produced in simulation experiments at low velocities. However, at velocities greater than 20 meters sec^{-1} , plastic deformation and/or melting may have occurred on basalt and quartz sand grains. Abrasion surfaces became progressively smoother with the elimination of all aeolian mechanical features. Fragments of this smooth crust tended to break off the surface; new crust was created as bombardment progressed.

To determine if plastic deformation had actually occurred, micron sized particles of quartz, produced both by crushing and simulated aeolian erosion, were examined with selected area electron diffraction (SAED) via the transmission electron microscope (TEM); surfaces were studied with the SEM. After viewing with SAED, it was found that the crushed quartz was completely crystalline, while the structural deformation observed in the abraded material suggested plastic deformation.

This data suggests that mineral and rock surfaces on Mars may consist of surfaces that have been plastically deformed and/or melted, and if true, physical and chemical weathering on that planet should proceed more rapidly than on Earth. Additionally, the presence of structurally damaged debris indicates that a fresh study should be made of possible mineralogies on that planet.

Influence of Ozone on the Thermal Structure of the Martian Atmosphere

W. R. Kuhn, S. K. Atreya, S. E. Postawko, Dept. of Atmospheric and Oceanic Science, Univ. of Michigan, Ann Arbor 48109

The column abundance of ozone in the terrestrial atmosphere down to the level of maximum ozone heating by solar radiation is only 13 micrometers, comparable to the total amount of ozone (0 to 57 micrometers) in the Martian atmosphere. We calculated radiative equilibrium temperature profiles for Martian high latitude winter conditions to determine whether or not ozone might influence the Martian thermal structure. For an ozone abundance of 57 micrometers the temperature is some ten degrees higher in the height range of 10 to 30 km than for a pure carbon dioxide atmosphere. The carbon dioxide ice-vapor equilibrium occurs in the region of the computed radiative equilibrium temperatures. Thus ozone may exert some control on the rate of deposition of carbon dioxide ice and the Martian atmospheric pressure.

Y. Langevin, Laboratoire Rene Bernas - 91406 Orsay, France.

I. INTRODUCTION. In the present paper we extrapolate a model of lunar regolith evolution (1,2) based on mass transport phenomena triggered by the meteoritic rainfall to a test body with a radius, $R_s \sim 10$ km, injected either in the asteroidal belt or in orbit around Mars. In this way we simulate the regolith evolution of both small asteroids and the martian satellites, Phobos and Deimos. In two companion papers (4), we then show how these predictions when constrained by various experimental observations give clues about the early history of the martian satellites and the origin of gas-rich meteorites.

II. PRELIMINARY REMARKS. All models of regolith evolution so far reported in the literature including ours (2,4) used as input data a few basic functions which are the meteoritic mass spectrum, $\phi(m > m_0) = A m_0^{-\gamma}$, the production rate of impact crater with a radius, r , $N(r > r_0) = K r_0^{-\beta}$, and the radius and depth of a crater, $r = B m^{-\lambda}$ and $D = C m^{-\lambda'}$. In these expressions, $A, B, K, C, \gamma, \beta, \lambda, \lambda'$ are considered as constant within a given range of mass.

In this short paper we can neither derive in detail the mathematical formulation used in our computations nor rigorously justify all the assumptions of our model of regolith evolution. The space environment of the small bodies considered in our work (martian satellites, asteroids) is different from that of the Moon. One of the major problems for "evolutionists" is to fix the values of both $\phi(m)$ and $N(r)$, which are still very poorly known beyond the Earth's orbit, whereas the values of the crater shape parameters (r, D) are considered as much more reliable as a result of extensive laboratory experiments dealing with the physics of impact phenomena. In this context our simple analytical model of regolith evolution differs from the models previously reported as we have tried to develop a model essentially based on the physics of impact phenomena, and intended to make prediction as much independent as possible from the absolute values of $\phi(m)$ and $N(r)$. In fact the only major assumption used in our derivation of the regolith thickness Δ_e and Δ_f (see below) is that in the mass range $< 10^{-2}$ g (which plays the major role in the growth and the "gardening" of a regolith) $\phi(m)$ can be represented by a power law spectrum in a given mass range. When an absolute evaluation of $\phi(m)$ was required (determination of \dot{A}_0 , for example), we considered that Hartmann (5) gives a good estimate of the variation of the intensity of the asteroidal component of the meteoritic flux with the heliocentric distance. Consequently, $\phi(m)$ is about 1.3 and 10 times higher near Mars and the asteroids, respectively, than on the Moon.

In addition to the effects expected from the different values of these basic functions the regolith evolutions of a small body differs from that of the Moon with regard to the following points: i. the acceleration of gravity ($g_s \sim 1 \text{ cm.s}^{-2}$) is much smaller than on the Moon. Consequently most of the material ejected upon meteoritic impact has a velocity exceeding the escape velocity, and this mass will be lost for the formation of a regolith. In addition, the small value of g_s triggers a drastic change in the extent and thickness of the blanket of material ejected from the crater interior, whereas both the radius and the depth of the craters are only slightly affected in a predictable way; ii. it is generally assumed that the lifetime of a small body via fragmentation by a large meteorite producing a crater with a critical radius, r_f , markedly decreases with R_s . This in turn should limit the integrated duration of the meteoritic bombardment of the surface and consequently the growth of a regolith.

III. THE DYNAMICAL EVOLUTION OF ASTEROIDAL REGOLITH. Let us consider a regolith with a thickness, Δ , which is spread on the constituent bed rocks of a small asteroid with a radius, $R_s \sim 10$ km. Only the craters that penetrate through the bed rocks contribute to the formation of "fresh" regolith material. In addition there is a critical radius, $r_c = R_s^2/R_M$ (the subscripts s and M will constantly refer to the small body and the Moon, respectively), such as 50% of the excavated material is ejected with a speed exceeding the escape velocity. The regolith will then only grow when the r_c -craters will inject an amount of bed rock material larger than that of regolith material lost to space. It can be shown that this condition implies that Δ reaches an equilibrium thickness, Δ_e , such as $(r_c - 4\Delta_e)^3 / r_c^3 \sim 0.5$. Finally, $\Delta_e \sim 0.005 R_s^2/R_M$.

This expression of Δ_e , which is independent of any assumption on $\phi(m)$, therefore shows that a regolith can be formed on small asteroids, as $\Delta_e \sim 2$ m, when $R_s \sim 10$ km. This general prediction, that we already derived 3 years ago (6), is in good agreement with both the more

complex "model dependent" computations of Housen et al. (4) relevant to larger asteroids and the telescopic observations of several asteroids showing in particular a negative branch in their polarization curves (7).

Upon meteoritic impact this limiting thickness will recess toward the interior with a rate, dR_s/dt , which is a function of the absolute value of $\phi(m)$. For R_s values \lesssim a few tens of km, dR_s/dt , can be approximated by the following simple expression:

$$dR_s/dt \sim AB^2C \log m_f/m_c \quad \text{II}$$

where A, B, C, are the constants defined in the previous section and m_f and m_c the mass of a meteorite capable of fragmenting the asteroid and producing a crater with a radius, $r_c = R_s^2/R_m$, respectively.

With the values of $\phi(m)$ derived by Hartmann we finally deduce the following scenario for the evolution of asteroidal regoliths, which is only valid for an intensity of the ancient meteoritic flux similar to the present day value (in this paper we thus exclude very exotic speculations based on the existence of a much more intense meteoritic flux $\gtrsim 4$ b.y. ago): for $R_s \sim 10$ km the value $\Delta_e \sim 2$ m is reached in $\lesssim 100$ m.y. and the regolith subsequently recesses to the interior with a speed of ~ 10 m/b.y. When R_s increases up to 100 km, $\Delta_e \sim 200$ m, and dR_s/dt , which has to be inferred from a formula different from that just quoted, decreases to about 2m/b.y.

In sharp contrast to the lunar regolith which presents a stratified structure, no stratum should be expected in the regolith of a small asteroid, except in the immediate vicinity of a large crater. In fact as a result of the small value of g_s , the ejecta blanket is spread over a distance which is $\sim R_M/R_s$ times greater than on the Moon. Consequently the thickness of the strata varies as R_s^{-2} , and they cannot be observed when $R_s < 0.3 R_M$. The regolith grains of a small asteroid ($R_s \sim 10$ km) are thus deposited individually via a steady rain and this is a profound implication concerning their space weathering (4) when they reside in the most superficial layers of their parent regolith.

IV. THE REGOLITH OF THE MARTIAN SATELLITES. As already pointed out by Pollack (8) the material ejected from a small satellite in orbit around Mars could efficiently be reaccreted and Δ should be larger than the equilibrium value, $\Delta_e \sim 2$ m, evaluated for an asteroid. On the other hand Δ cannot exceed an upper limit, Δ_f , corresponding to the exposure of the satellite surface to the maximum integrated flux of meteorites beyond which the satellite is fragmented by an impact crater with a critical radius, $r_f \sim R_s/2$. With this value of r_f and by imposing that all the ejected material is reaccreted, the value of Δ_f can be obtained first by computing the volume of material accreted per unit of time and per cm^2 , $d\Delta/dt$. Then this expression has to be integrated up to the time when an impact crater with a radius, $r_f \sim R_s/2$ is formed. We thus obtain:

$$d\Delta = \frac{R_s/2}{4E} K.5.R^{(-5-1)\pi/6} . (R-4E)^{-5} dR \quad \text{III}$$

By taking a reasonable range of δ values > 3 this expression can be easily integrated in giving a value of $\Delta_f \sim R_s/50$ that only slightly depends on δ ($\Delta_f = R_s/60$, $R_s/45$ and $R_s/30$ when $\delta = 3.2$, 3.4 (lunar value) and 4.0, respectively) and which is also independent of the absolute values of both $\phi(m)$ and $N(r)$.

More detailed computations give the following useful predictions concerning the regolith evolution of a small satellite around Mars, which will be used in reference 3. i. the "normal" regolith thickness, $\Delta_0 \sim 5$ to 10 m, computed by assuming that the satellite surface was exposed during ~ 4 b.y. to a meteoritic flux similar to the present day flux, is both much smaller than $\Delta_f \sim 200$ m, and comparable to that observed on lunar maria; ii. the ejecta blankets are too thin to generate a stratified regolith, and the deposition of material on a martian satellite can also be described by a steady rain operating like on asteroids.

REFERENCES: (1) Borg, J. et al. This Conf. Proceedings; (2) Langevin, Y., Arnold, J. (1977) Ann. Rev. Earth Plan. Sci. 5, 449; (3) Housen, K. et al (1978) Lunar Sci. IX, p. 54; (4) see Duraud, J.P. et al. This Conf. Proceedings; (5) Hartmann, W.K. (1977) Icarus 31, 260; (6) Borg, J. et al. (1975) Meteoritics 10, 365; (7) Zellner, B. et al. (1976) Icarus 28, 117; (8) Pollack, J.B. (1977) Planetary Satellites, p. 319, U. Ariz. Press, Tucson.

Dune Forms and Patterns of Wind Circulation in the North Polar Region of Mars

J. H. J. Leach, Univ. of Melbourne, Parkville, 3052. Australia

There are three main dune types which occur in the Martian north polar region. They are the transverse dunes, barchan dunes, and longitudinal snow dunes. A study of their form and orientation can determine the direction of the wind that formed them and provides an overall wind circulation pattern for the region.

The longitudinal snow dunes indicate a wind direction that is consistent with the model of them having been formed by katabatic winds which spiral off the ice cap in a clockwise direction under the influence of Coriolis force. The spiral pattern that they indicate has the opposite sense to that of the dark bands seen in imagery of the ice cap.

Transverse and barchan dune forms along the floor, and at the mouth, of the Chasma Borealis and in other smaller but similar valleys indicate that strong, low-level winds flow along these valleys. This is consistent with katabatic winds being channelled by topography.

The orientation of the transverse dunes of the circumpolar dune field, and of the barchan dunes at its periphery, indicate that away from the influence of the katabatic winds near the ice cap the atmospheric circulation is in an anti-clockwise direction.

Thus the atmospheric circulation in the north polar region of Mars consists of a polar cell of katabatic wind spiralling off the ice cap in a clockwise direction which is surrounded by a girdle of winds travelling in an anticlockwise direction. This is analogous to the wind circulation around the Antarctic ice cap on Earth.

CO₂⁺ Excitation and Emission Processes in Mars Dayglow

S. Leach, Laboratoire de Photophysique Moléculaire du CNRS, Université de Paris-Sud, 91405 Orsay, France

Interpretation of the $B^2\Sigma_u^+ \rightarrow X^2\Pi_g$ and $A^2\Pi_u \rightarrow X^2\Pi_g$ CO₂⁺ emissions in the Martian dayglow observed by Mariners 6, 7 and 9 requires a knowledge of $B^2\Sigma_u^+$ and $A^2\Pi_u$ state excitation and subsequent emission processes. Photoionization, fluorescent scattering and photoelectron impact excitation mechanisms used in previous model calculations are critically examined in the light of recent spectroscopic data. The excited state production rates are shown to require modification. The emission rates are affected by intramolecular coupling which is shown to exist between the $B^2\Sigma_u^+$ and $A^2\Pi_u$ states. Revised values are derived for the various contributions to the CO₂⁺ emission intensities in the Martian dayglow.

Status of Interpretation of Viking Labeled Release Experiment

G. V. Levin and P. A. Straat, Biospherics Incorporated, Rockville, MD

Further experiments have been carried out in the laboratory to assist in the interpretation of the signals returned from Mars by the Labeled Release (LR) life detection test. Although the radiorespirometric responses from active Mars samples and from "heat-sterilized" portions of the same sample satisfy the pre-Mission criteria for life, doubt in the biological interpretation remains because of other Viking findings. The theory that a strong oxidant on Mars is responsible for the LR data is being rigorously examined. Of the possible oxidants, hydrogen peroxide remains the best candidate after testing in the laboratory and in the flight-like LR instrument. However, significant obstacles to this theory exist and although data with hydrogen peroxide are suggestive, complete duplication of the LR Mars data has not yet been achieved. The new hydrogen peroxide data and their impact on interpretation of the LR experiment are presented. From the alternative standpoint, attributes of Antarctic endolithic algae are extrapolated to a possible biological model for the LR data. Results of an LR-type experiment with these organisms are presented.

Mars in 3-D

E. C. Levinthal, Genetics Department, Stanford University, Stanford, California 94305

An important part of the photographic record of the exploration of Mars is conveyed by the three dimensional character of its surface. The stereo movie Mars in 3-D, starts with scenes taken by the Viking Orbiter cameras of the teardrop shaped plateaus and channels that characterize the Chryse Planitia region, the faulting north of Olympus Mons, the spectacular relief of Candor Chasma, and the canyon walls of Ius Chasma. The second portion of the movie shows the operation of the Science Test Lander at JPL. The final half of the movie is devoted to stereo scenes of Chryse Planitia and Utopia Planitia taken by the Viking Lander cameras. The ridges, outcrops, and eroded drifts of the Lander One terrain are clearly shown. The closing scenes show the rock types and troughs that surround Lander Two.

In addition to the narration, the sound track includes a specially composed score of computer-generated stereo music.

Internal Structure of Mars

R. A. Lyttleton, Jet Propulsion Laboratory, Pasadena, CA 91103

The central pressure in Mars is only $0.28 \times 10^{12} \text{ dyn cm}^{-2}$ (reached at 750 km depth in the Earth), so a phase-change corresponding to the 20° -discontinuity will exist in Mars. With radioactive heating, this phase-change requires greater pressure and therefore greater depth. Material will be converted back to the lower-pressure form, and the planet will expand to cause rifting of the outer layers.

The radius and mass of Mars rule out the possibility of any high-density core whether of nickel-iron or of a high-pressure phase-change to a metallic liquid-form. No core-produced dipole magnetic field can therefore be expected. Nor will there be any folded and thrust mountains, since these would require a phase-change core steadily growing through conversion of solid material to the denser liquid-phase by radioactive heating to give a contracting planet. (The same theory implies that such mountains will have been formed on Venus.)

These several correct predictions were made on the basis of the phase-change theory of the terrestrial core prior to the Mariner-4 flypast of Mars.

References

Monthly Not. Roy. Astron. Soc. 129, 21, (1965).
Proc. Roy. Soc. A 287, 471, (1965).

The Martian Atmosphere

C. Macris and B. Petropoulos, Research Center for Astronomy and Applied Mathematics, Academy of Athens

The physical parameters of the martian atmosphere have been computed for different molecular distribution and from 0 to 200 km altitude. The computed pressures and densities for different altitudes, have been compared to the measured for the same altitudes by Viking 2. From this comparison we have concluded the probable molecular distribution of the martian atmosphere as a function of the altitude. For the above computation we have used the following data measured by Viking 2.

a) The pressure and the temperature near the surface b) The chemical composition near the surface c) The temperature distribution as a function of the altitude.

The hydrostatic model has been used for the computation. We have used the above results in order to give a model of the martian atmosphere.

Mars: Evidence of Indurated Deposits of Fine Materials

M. C. Malin, Jet Propulsion Laboratory, Cal. Inst. of Technology, Pasadena, CA 91103.

Recent Viking Orbiter images of the equatorial and temperate latitudes of Mars show a variety of erosional landforms suggesting materials initially deposited unconsolidated and subsequently lithified. These landforms, including serrated-edged plateaus and elongate, closely spaced yardangs (see, e.g., Ward, 1978), are suggestive of those produced by wind-pluck-and-scour of indurated deposits of granular materials such as sandstones and ignimbrites. A most conspicuous deposit on Mars occurs in a restricted latitude zone ($\sim 5^{\circ}\text{S}$) spanning about 40° of longitude ($160\text{--}200^{\circ}\text{W}$) from an area southwest of Olympus Mons and due west of Pavonis Mons to approximately 1000 km west of Apollinaris Patera. Covering more than $2 \times 10^6 \text{ km}^2$, these deposits range to 3000 m in thickness and display conspicuous terracing inferred to result from differential erosion of layers. Morphology of impact craters suggests craters formed prior to deposition are well preserved and undergo only modest modification during exhumation, whereas craters formed within the deposits have a subdued initial morphology and can be completely eroded away during the disintegration of the deposits. Owing to the intense erosion, a younger limit on the age of the deposits cannot be set. An upper limit can be set stratigraphically, as the deposits superimpose a plains unit with numerous mare-like ridges and a moderately high density of 4-10 km diameter craters (approximately Lunae Planum equivalent). Crossing patterns of yardangs suggest either variations in principal direction of eroding winds, internal jointing and fracturing, or both. The deposits are interpreted to be volcanically derived ash-fall and -flow units associated with the early volcanism in the Apollinaris Patera-Tharsis Ridge volcanic zone (see, e.g., Mutch and Saunders, 1976, pp. 37-39).

References:

- Mutch, T.A. and R.S. Saunders (1976) *Space Sci. Rev.*, **19**, 3-57.
Ward, A.W. (1978) *Bull. Am. Astro. Soc.*, **10**(3), Part 2, 557.

Field Investigation of Martian Canyonlands in Southwestern Egypt

T. A. Maxwell, National Air and Space Museum, Smithsonian Institution, Washington, D.C. 20560.

Investigation of the dissected canyonlands of the southern part of the Gif Kebir plateau in southwestern Egypt has provided one of the closest analogs to martian canyons on the south side of Valles Marineris. As viewed on Landsat images, these distributary canyons lack integrated drainage on the top of the plateau, and are characterized by blunt upstream ends and branching patterns that are in part structurally controlled. Although the gross morphology and scale are similar, the ratio of valley floor width to total canyon width is much greater in the Gif Kebir than on Mars. This is most likely due to both more active slumping of the canyon walls on Mars, and fluvial undercutting and erosion on Earth.

In addition to marked morphologic similarities, identical modes of origin have been proposed for both areas. In 1938, R. A. Bagnold recognized the importance of cliff sapping in the formation of canyons of the Gif Kebir, and suggested this as the dominant mode of canyon formation. Preliminary field investigations support this hypothesis, although sheetflooding on the plateau surface has not been ruled out. The present-day hyper-arid climate and active eolian regime provide the basis for interpretation of fluvial landforms modified by wind.

The Eolian Features of the North Polar Region of Mars

J. F. McCauley, C. S. Breed, M. J. Grolier, and P. Collins, U. S. Geological Survey, Flagstaff, AZ 86001.

Viking Orbiter-2 pictures show enormous seas of dunes covering hundreds of thousands of square kilometers around the north polar region of Mars. The shapes, wavelengths and apparent amplitudes of these dunes are similar to those in the central parts of the great mid- and low-latitude deserts on Earth. The circumpolar dunes apparently are composed of material that has behaved in a fashion similar to the materials in terrestrial sand seas. The martian sand seas contain kilometer-size barchanoid dunes comparable to dunes in the Sahara that required at least 10,000 years to form under terrestrial conditions (Wilson, 1971). The dunes on Mars emerge "full grown" from beneath the retreating polar cap and therefore cannot be the seasonal redistribution products of the layered terrain as supposed by some investigators.

Under the current climatic regime, the martian dunes are almost surely inactive. The preservation beneath the polar ice cap of such fragile landforms, which can be built only under a limited set of conditions, is geologically significant. On Earth, dunes representative of prior climatic conditions may be preserved beneath covers of vegetation, evaporites, or lake sediments (Grolier et al., 1976). Such situations are indicative of short or long term climate changes in the geologic record. Conditions far more favorable for eolian transport must have existed in the past on Mars. These more favorable conditions required a much denser atmosphere, freedom of movement of the dune-forming materials and a far more dynamic wind regime than now observed.

The characteristic pattern of dune and interdune plains in sand seas on Earth is due to the marked separation of the suspension, saltation, and creep loads within the eolian transport regime. Dunes on Earth are built of a very narrow range of sand sizes, while most of the dust-size particles, and the gravels, are confined to the interdune flats. The same types of dunes and interdune plains are clearly recognizable on Mars (Breed et al., 1977, 1978b). The striking similarity that we have observed among dune patterns on Mars and Earth strongly suggests that a similar range of processes has operated with the same degree of sedimentary selectivity on both planets. This similarity has important implications for the global transport of surficial sediments.

The marked regularity of the sand sea patterns on Mars is believed to reflect long-term, long-distance transport of surficial materials by wind. On Earth, most of the material in the sand seas of all of the desert regions is derived, by wind, from fluvial, glacial, or marine sediments. It is reasonable to assume that the dune sediments on Mars were also secondarily derived even if most of the material involved (the martian resistates) consists of basaltic ash or the mechanical disintegration products of basalt.

The problem of source materials for the dune sediments is critical to an understanding of the surficial history of Mars. Relationships between eolian erosional and depositional processes and the development of the north polar ice cap are far more complex than previously recognized. Our observations indicate that the north circumpolar dunes predate the development of the present ice cap. The change from a former dune-building environment to the present glacial environment may have important solar system-wide climatic implications.

References:

- Breed, C. S. (1977) Terrestrial analogs of the Hellespontus dunes, Mars, *Icarus* 30, 326-340.
- Breed, C. S., Ward, A. W., and McCauley, J. F. (1978b) Windform patterns on Earth and on Mars: Implications for similarities of eolian processes on two planets: NASA TM 79729, p. 228-229.
- Grolier, M. J., Ericksen, G. E. and McCauley, J. F. (1976) Wind-furrowed sandstone, north-eastern margin of the Sechura Desert (Peru): Proceedings, International Colloquium of Planetary Geology, Rome 1975, p. 317-325.
- Wilson, I. G. (1971) Desert sandflow basins and a model for the development of ergs: *Geographical Journal*, v. 137, pt. 2, p. 180-199.

Mars Surface Composition from Reflectance Spectroscopy: A Summary

T. B. McCord, Institute for Astronomy, Univ. of Hawaii, Honolulu, HA 96822.

R. B. Singer and R. N. Clark, Dept. of Earth and Planetary Sciences, Mass. Inst. of Technology, Cambridge, MA 02913; and Institute for Astronomy, Univ. of Hawaii, Honolulu, HA 96822.

Definition and characterization of Mars surface units are fundamental to understanding the evolution and current state of the planet. Surface compositional and mineralogical information is required to properly define and characterize units. It will be necessary to use remote sensing techniques to derive this information on regional and global scales, even if an Apollo- and Luna-like sampling program were carried out (Head et al., 1978). The only techniques so far applied to Mars are reflectance spectroscopy and its daughter multispectral mapping (emission spectra of dust clouds yielded some compositional information of airborne material). Some multispectral mapping has been done by Viking (Soderblom, 1978; Arvidson, personal communication) and low resolution reflectance spectra have been obtained by the Viking lander cameras (Arvidson, 1977). Most of the reflectance spectra and some multispectral maps have been obtained from groundbased telescopes. This will continue to be the case at least until the Galileo spacecraft passes Mars in 1982 on its way to Jupiter and possibly until the next Mars mission in the mid to late 1980's. Application of other techniques, such as x-ray spectroscopy, must await the next Mars mission.

It is the purpose of this paper to discuss the available reflectance spectra, some new, and outline the future prospects. It is assumed that the Viking multispectral maps and spectra will be discussed elsewhere in this program, but we will place them in context in our presentation.

McCord and Adams (1969), reviewed available data to that date. Binder and Jones (1972) presented IR spectrophotometry with spectral resolution too low to yield much compositional information. McCord and Westphal (1971); McCord et al. (1971, 1977, 1978a) presented reflectance spectra (0.3-1.1 and 0.6-2.5 μm) for a total of 33 areas 100-500 km in diameter. McCord et al. (1978b) have 11 new spectra (0.6-2.5 μm) of 1500 km diameter areas. Space telescope will not help this effort except for multispectral maps for no appropriate spectrometer is provided. Spacelab could carry such an instrument.

Bright area spectra are characterized by a steep slope from the UV to 0.75 μm with a slope change at about 0.6 μm and a weaker absorption near 0.86 μm . These features are attributed to a ferric oxide content of about 5 to 8% (Huguenin et al., 1977). From the band minimum, near 0.86 μm , to about 1.3 μm the spectrum slopes upwards slightly. Between 1.4 and 1.7 μm there is an absorption which has been interpreted as H₂O in a hydrate or ice. From 1.8 to 2.2 μm the spectrum is dominated by a deep Mars atmospheric CO₂ absorption. Removal of a model CO₂ atmosphere yields a fairly flat spectrum from 1.7 to 2.5 μm . Laboratory modeling has produced fair simulation of this spectrum with mixtures including goethite and/or hematite and clays such as montmorillonite, although the exact makeup of the bright material is not yet known and is the subject of continued research.

Dark area spectra are substantially different. The slope from UV to red is reduced, compared to the bright region spectra; the absorption near 0.86 μm is also weaker. This implies a lower Fe³⁺ content. In addition, dark area spectra show broad Fe³⁺ absorptions centered around 1.0 μm . These vary with location on the planet and are thought to represent differences in mafic mineralogy (pyroxene, olivine, glass). In sharp contrast to bright area spectra, dark area spectra slope fairly uniformly downwards from 1.1 to 2.5 μm . Adams and McCord (1969) showed that bright and dark area spectra could be modeled by more and less oxidized basalt.

Reflectance spectra of the bright regions from 0.3 to 1.1 μm have been shown to be very similar to dust cloud spectra, which correlates with other evidence that the bright material is fairly homogeneous eolian dust (McCord et al., 1977). Dark areas shown less uniformity and are less oxidized (weathered), so they may represent materials closer in petrology and physical location to primary martian crust.

Based on the knowledge that many dark regions have extensive coverage by bright streaks, we have applied a simple additive or checkerboard model to investigate the effects of bright spectrum contamination of dark region observations. An upper limit of about 40% areal coverage of observed dark regions by bright material has been found. Removal of bright spectra

from observed dark spectra further reduces the depth of the UV to 0.75 μm Fe^{3+} absorption, and increases the downward slope to 2.5 μm .

In related work a number of spectra of spots intermediate between bright and dark were manipulated by scaling and bright spectrum removal to see if it was possible to reproduce a dark area spectrum. In no case was a perfect match obtained; in the case of one spectrum roughly midway in characteristics between bright and dark, the best match was quite poor. These results show that a two component surface model with only large scale mixing (bright or dark size \gg mean optical path length) is not sufficient to explain observed spectral reflectance. We conclude from this that the actual case for the martian surface probably includes a combination of: a) a variety of compositions (spectral types) besides bright dust; b) large scale (additive) mixing of spectral types; c) fine scale (multiplicative) mixing of spectral types.

All martian IR spectra observed so far show a drop in reflectance from 1.3 to 1.4 μm . This drop is greater for bright areas than dark areas. In order to understand the reason for this drop, we modeled the reflectance of Mars with spectra typical of iron oxide or oxidized basalt. The light areas were modeled with a spectrum typical of a thick oxidation layer and the dark areas with a spectrum typical of an oxidation layer about 1 micron thick over basaltic material. These spectra were normalized in the same manner as the telescopic spectra and have a smooth reflectance beyond 1.1 μm . To these spectra, an ice spectrum was added in small amounts to match the apparent 1.4 μm drop observed in the martian spectra. The ratio of the martian spectra and the simulated spectra show absorption features which correlate with the expected martian atmospheric CO_2 bands. The simulations fit the bright area spectra better than the dark spectra and indicate that the relative band intensities are weaker and different for dark areas than bright areas. This is also apparent from the weak 1.23 μm water associated band. The results show that water is present in the martian surface in different forms but we cannot yet determine the actual forms based on the present knowledge of reflectance spectroscopy. We conclude that bright areas contain more water than dark areas.

A spectrum of the north polar cap of Mars shows very strong water ice bands. Modeling the spectrum by an ice spectrum and a grey spectrum (same reflectance at all wavelengths) shows that 60% is due to light reflected by ice and 40% by grey. The actual amount of water present is difficult to determine because of the variation in grain size and/or hydration state. However, we do not see any evidence for CO_2 ice in this spectrum taken in the northern spring ($L_s=50^\circ$) with the extent of the cap to about 60°N . There is good evidence that there was no polar hood or clouds present at the time of this observation.

References:

- Adams, J. B. and T. B. McCord (1969) *J. Geophys. Res.* 74, 4851-4856.
- Binder, A. B. and J. C. Jones (1972) *J. Geophys. Res.* 77, 3005-3019.
- Huck, F. O., D. J. Jobson, S. K. Park, S. D. Wall, R. E. Arvidson, W. R. Patterson, and W. C. Benton (1977) *J. Geophys. Res.* 82, 4401-4411.
- Huguenin, R. L., J. B. Adams and T. B. McCord (1977) *Lunar Science VIII*, 478-480.
- McCord, T. B. and J. B. Adams (1969) *Science* 163, 1058-1060.
- McCord, T. B. and J. A. Westphal (1971) *The Astrophys. J.* 168, 141-153.
- McCord, T. B., R. Clark and R. L. Huguenin (1978a) *J. Geophys. Res.*, in press.
- McCord, T. B., R. Clark, R. B. Singer and R. L. Huguenin (1978b) in preparation.
- McCord, T. B., J. H. Elias and J. A. Westphal (1971) *Icarus* 14, 245-251.
- McCord, T. B., R. L. Huguenin, D. Mink and C. Pieters (1977) *Icarus* 31, 25-39.
- Soderblom, L. A., K. Edwards, E. M. Eliason, E. M. Sanchez and M. P. Charette (1978) *Icarus* 34, 446-464.

Fracture Systems on a Reoriented Planet

H. J. Melosh, Div. of Geological and Planetary Science, Cal. Inst. of Technology, Pasadena, CA 91125.

Both geologic and free air gravity data suggest that the positive mass anomaly associated with the Tharsis volcanoes may have reoriented Mars' lithosphere by as much as 30° . Since Mars is oblate (with flattening $f \approx 0.005$), rotation of the lithosphere over the equatorial bulge by 30° produces membrane stresses of several kilobars, large enough to initiate faulting. These stresses were first evaluated by Vening-Meinesz (1947) who treated the lithosphere as a thin elastic shell. The fracture patterns which result from these stresses are determined by the relation between stress and faulting proposed by E. M. Anderson (1951).

Plots of the magnitude and direction of stresses in a reoriented planet show that near Tharsis the dominant fault type should be north-south trending normal faults. This normal fault province is centered about 30°N latitude and extends about 45° east and west in longitude. Similar faults should occur at the antipodes, north of Hellas Planitia. The polar regions should be occupied by roughly north-south trending thrust faults which extend close to the equator south of Tharsis and north of Hellas. The regions between Tharsis and Hellas are subject to compression on a NE trending axis and extension along a NW axis east of Tharsis (west of Tharsis the directions are NW compression and NE extension), thus predicting a zone of NNW and ENE strike slip faults east of Tharsis (NNE and WNW west of Tharsis).

Although these patterns, except for the north-south normal faults north of Tharsis, have not yet been recognized, the discovery of such a tectonic system of the same age as Tharsis would provide strong support for the reorientation idea. Stresses due to reorientation appear to have little to do with Valles Marineris, since the stress normal to the axis of the Valles is predicted to be compressive, whereas geologic evidence suggests extension.

Surface Materials of the Viking Landing Sites - Extended Mission

H. J. Moore, U. S. Geological Survey, Menlo Park, CA 94025.
C. R. Spitzer, NASA LRC, Hampton, VA 23665.
P. M. Cates, Jet Propulsion Laboratory, Pasadena, CA 91103.
K. Z. Bradford, Martin Marietta Aero., Denver, CO 80201.
R. F. Scott, Dept. Engr. Appl. Sci., Cal. Inst. of Technology, Pasadena, CA 91125.
R. E. Hutton, Harbor City, CA 90710.
R. W. Shorthill, Univ. Utah Res. Inst., Salt Lake City, UT 84117.

The surface materials at the Viking landing sites may be grouped into four categories: (1) drift material, (2) crusty to cloddy material, (3) blocky material, and (4) rocks.

Drift material, which occurs at the VL-1 site, is the weakest by all criteria. Footpad 2 of VL-1 penetrated 16.5 cm into drift material during landing. Small forces (25-50N) were exerted by the surface sampler while the collector head was excavating relatively deep trenches. One trench reached 23 cm depth during excavation of a deep hole. Backhoe penetrations during normal de-elevations of the surface sampler collector head to surface were large, near 3-4 cm. Comminution of a sample of drift material did not cause a noticeable increase in comminutor motor currents above the no-load current.

Crusty to cloddy material, which occurs at the VL-2 site, appears to be stronger than drift material. Locally, crusty to cloddy material is covered by a thin veneer of lumpy-to smooth-appearing fine-grained soil. Moderate forces (25-100N) were exerted by the surface sampler while the collector head was excavating trenches. A trench depth of 11-12 cm was reached during excavation of a deep hole. Backhoe penetrations during normal de-elevations of the surface sampler collector head to the surface were 0.9-1.4 cm. Comminution of a sample of this material caused comminutor motor currents to rise about 0.25 to 0.75A above the no-load current.

Blocky material, which occurs at the VL-1 site, appears to be the strongest soil-like material. Footpad 3 of the VL-1 penetrated 3.6 cm into blocky material during landing. Large forces (to 210N) were exerted by the surface sampler while the collector head was excavating trenches, and the sampler frequently failed to achieve the commanded extensions. A trench depth of 13 cm was reached during excavation of a deep hole. Backhoe penetrations during normal de-elevations of the surface sampler collector head to the surface were 0.5-1.4 cm. Comminution of a sample of this material caused comminutor motor currents to rise about 1.5A above the no-load current.

Rocks occur at both VL sites but little is known about them. Footpads 2 and 3 of VL-2 appear to have struck rocks during landing. During attempts to push rocks with the surface sampler collector head, none of them appear to have chipped, scratched, or spalled, although forces up to 210N were exerted on some of them. If any rock was crushed or broken, the best candidate is the one that was struck by footpad 3 of VL-2.

Mars: A Cosmochemical-Geophysical Estimate of Bulk Composition

J. W. Morgan, U. S. Geological Survey, Reston, VA 22092.

E. Anders, Enrico Fermi Inst., Univ. of Chicago, Chicago, IL 60637.

If we assume that protoplanetary material has undergone the limited number of cosmochemical processes recorded in chondrites, the bulk composition of a terrestrial planet may be inferred from the ratios of a few key elements of contrasting volatility; e.g., K (moderately volatile)/U (refractory), Tl (very volatile)/U. Geophysical measurements (density, heat flow, moment of inertia) and experimental petrology provide additional constraints. For Mars, the Soviet Mars 5 orbital γ -ray spectrometric determinations of U, Th, and K ($K/U \approx 2.2 \times 10^3$ by weight) and the Viking rare gas measurements (particularly Ar^{36}/Ar^{40} which suggests $Tl/K \approx 2.3 \times 10^{-6}$) may substitute, to some extent, for the appropriate element analyses of crustal rocks that are now lacking. Accepting a present-day heat production compatible with the Toksoz-Hsui thermal history model, we derive bulk contents of 28 ppb U, 100 ppb Th, and 62 ppm K, using the measured K/U and a chondritic Th/U value of 3.6. The bulk U content determines the abundance of a refractory (Ca-Al rich, Si-poor) component. The density of the martian mantle of 3.55 g.cm^{-3} interdependently constrains the refractory component contribution and FeO/MgO; for 28 ppb U, molar $MgO/(FeO + MgO)$ is 0.77. The mantle of Mars is volatile-poor and is almost identical in composition with the bulk Moon. The martian core makes up 0.19 by weight of the planet and contains 10 weight % of FeS if a cosmic S/K ratio is assumed. Comparison of the inferred composition of Mars with those of other planets (Earth, Venus, Moon, eucrite parent body) strongly suggests that volatile depletion is a function of planetary size and does not depend critically upon radial distance from the Sun.

The Spectral Model of the Atmospheric General Circulation of Mars

S. Moriyama, The Physical Science Laboratories, Nihon Univ. at Narashino, Funabashi, Chiba 274, Japan.

T. Iwashima, Geophysical Institute, Kyoto Univ., Kyoto 606, Japan.

A numerical experiment of the martian atmospheric general circulation was performed using a three-level linear balance model based upon a spectral method. We examined mainly the effects of topography and of dust suspended in the martian atmosphere upon the general circulation. Our results indicate that topography, when it exists in the dusty field, would have a very important influence upon the stage of development of a dust storm through an acceleratively intensified blowing off effect of dust particles from the specified surfaces, such as Hellespontus-Noachis region; that a strong thermal tide which is produced by radiative effect of dust is superposed on the quasi-stationary disturbances induced by topography and, as a result, a large coupling oscillation appears in the atmosphere having the predominant wavenumbers 1 and 2 which are correlated with diurnal and semidiurnal tidal components, respectively.

The equinoctial season for the southern hemisphere is treated in this paper.

Rampart Crater Formation on Mars

P. J. Mougini-Mark, Dept. of Geological Sciences, Brown Univ., Providence, RI 02912.

Mapping of large (>40 km) fresh martian rampart craters indicates that a complex scenario is required to account for the multiple lobate flows, slump features, secondary craters and smooth terrain that surrounds these craters. Morphologic differences between ejecta surrounding small (<30 km) and large rampart craters are attributed to two alternate physical conditions which may exist during the impact event. Secondary craters associated with large craters may be the product of material ejected from depths greater than the thickness of an hypothesized permafrost layer. Alternatively, the transient atmosphere generated around the impact (as a consequence of target volatilization) may be sufficient to entrap secondary crater-forming blocks for small craters, but unable to prevent ejecta associated with big impacts from breaking through the cloud.

Computer models of a basalt meteorite impacting a frozen sand target (taken to be analogous to martian permafrost) at 15 km/s were used to derive residual temperatures and phase changes for the ejecta. Results indicate that atmospheric winnowing of ejecta may not be as significant as previously believed, due to the high atmosphere/cloud density ratio and the "hypervelocity" motion of fine ejecta as a result of hot expanding volatiles within the cloud.

Large volumes of ejecta are believed to be emplaced above martian ambient temperature and will be sufficiently warm to liberate melt water from the underlying terrain. For example, a 100 m thick, isothermal blanket (initially at 400K emplaced upon permafrost at 210K containing 5% by volume of water ice) indicates that over 40 cc of melt water per square centimeter of the interface would be liberated in less than a year. Many of the lobate deposits around rampart craters of all sizes can be related to surface-flow phenomena as a consequence of the impact event. Specific examples of hummocky and smooth terrain, however, are believed to be products of post-depositional remobilization of ejecta by melt water liberation from the underlying permafrost.

Enigmatic Landforms on Mars

T. A. Mutch, Department of Geological Sciences, Brown University, Providence, RI 02912

Distinctive large-scale landforms of Mars, including volcanoes, canyons, channels, layered terrain, and collapsed terrain, are well known and frequently discussed. There are, in addition, a variety of small-scale landforms characterized by unusual -- commonly geometric -- shape and sharp topographic boundary. The presence of these exotic features distinguishes Mars from the Moon and Mercury. On the latter two bodies the topography is dominated by impact-related features that combine to form a randomly irregular surface. Topographically singular elements are few, the best example being lunar rilles.

Because many of the martian features defy persuasive explanation they tend to be neglected in the literature. It is possible they are all related to a few geomorphic processes, most likely eolian erosion and deposition, and near-surface phase change and movement of H₂O. In this talk a sampling of the enigmatic features are presented for your amusement and/or edification.

Martian Ages

G. Neukum, K. Hiller, J. Henkel, J. Bodechtel, Institut Fuer Allgemeine Und Angewandte Geologie Der Ludwigs-Maximilians-Universitaet Luisenstr. 37, 8000 Muenchen 2, West Germany

A brief summary of age dating by crater counting methods is presented. The current three Mars model cratering chronologies (Hartmann, 1973; Soderblom et al., 1974; Neukum and Wise, 1976) are discussed with emphasis on the latter two. Application of those two different chronologies to a number of crater size-frequency data, from our measurements and from the literature, yields drastically different histories of Mars:

1. The oldest crust investigated shows ages in excess of 4.15 aeons, bulk lying between 4.2 and 4.3 aeons. These ages are given by the frequencies of large craters that survived resurfacing processing. Both models coincide for these units.

2. Highland lavas and plain lavas record two major episodes of resurfacing activity. In our model they took place between 4 and 3 aeons and in some few places 1.0 aeons ago, in Soderblom's between 3.9 and 0.3 aeons ago. The resurfacing is clearly due to large scale volcanic activity in most areas (e.g., Elysium/Isidis Planitia, Nili Fossae, N. E. Alba Patera). This volcanic activity is parallel in time to the erosional retreat of the scarp between highlands and northern lowland plains.

3. Piling up the shield volcanoes was the final stage of volcanic activity, starting probably before 3 aeons ago and ending approximately 1 aeon ago in our model. Using Soderblom's model the main activity started 0.5 aeons ago, lasting closely to present times.

4. The main aeolian and/or fluvial activity seems to have taken place between 4 and 3.7 aeons ago in our model. Most of the resurfacing activities in the time less than 3 aeons ago seems to have been volcanic with possibly few exceptions. In the second model we get main aeolian activity lasting for 3.5 aeons until 0.5 aeons ago.

There are a number of plausibility arguments for the validity of either model. Since we do not have the possibility of radiometric dating of martian rocks yet, it is necessary to find other chemical/physical boundary conditions for the models, such as the history of the martian atmosphere and from it the time frame for aeolian or fluvial erosion, or the frequency of occurrence of seismic events to evaluate the likelihood of recent volcanic activity, or the comparison with present-day asteroid impact rates on the Moon versus those on Mars to obtain a better value for the recent impact chronology, and so forth. Currently, such boundary conditions do not support a youthful Mars but support our view that most of the geologic activity of Mars was terminated prior to 1-2 billion years ago.

Cosmic Pollution: Evidence for Recent Major Martian Atmospheric Loss?

M. J. Newman, Theoretical Div., LASL, Los Alamos, NM 87544.

D. M. Butler, Laboratory for Planetary Atmospheres, NASA/GSFC, Greenbelt, MD 20771.

Encounters with interstellar clouds of sufficient density to penetrate the solar system to within the orbit of Mars should have occurred many times during the past 4.7×10^9 years. Depending on the relative velocity of the encounter, many of these events result in the addition of significant amounts of material to the martian atmosphere. While light inert species like He are lost quickly, following an encounter, and reactive species like H, C, and N are not expected to remain in the atmosphere indefinitely, heavy noble gases like Ne and Ar should act as reliable tracers of atmospheric change. It is difficult to make precise statements concerning the times at which major accretion events have occurred on Mars, since encounters with sufficiently dense clouds at low relative velocity are an inherently random process. However, it appears that an encounter sufficient to have added more Ne, ^{36}Ar , and ^{38}Ar to the martian atmosphere from the interstellar medium than is currently observed is likely to have occurred in the last 500 million years. Since continuous loss mechanisms for these relatively heavy species are unlikely, significant atmospheric mass loss in the comparatively recent past may be indicated.

Mechanics of Fluid Release on Mars

D. Nummedal, Dept. of Geology, Louisiana State Univ., Baton Rouge, LA 70803.

Analysis of Viking Orbiter imagery has provided a wealth of additional support for the thesis that many of the large channels on Mars were carved by the action of running water (Baker, 1977). In striking similarity to the controversy surrounding Bretz' hypothesis regarding the Channeled Scabland, the major obstacle to a general recognition of the role of fluid erosion on Mars appears to be the lack of a well-understood mechanism for the sudden release of large quantities of water.

Paleohydraulic estimates suggest, in spite of large error-margins, that the discharges responsible for large channels in the Chryse region, are orders of magnitude larger than that of the flood responsible for the Channeled Scabland (Masursky et al., 1977). Yet, many channels show no evidence of large reservoirs near their source. Other channels display morphologic evidence of a fluid source in terms of large areas of chaotic terrain near their headwaters. The possible mechanisms of water release associated with the formation of the chaotic terrains are examined in this paper. Sharp (1973) suggested that chaotic terrain reflected localized collapse caused by the subsurface withdrawal of ground ice or magma. Carr (1978) proposed it is due to collapse following the catastrophic release of water from a confined aquifer, and Nummedal (1978) suggested that sudden liquefaction of metastable volcano-clastic sediments could also be a responsible mechanism. The latter two mechanisms are capable, not only of explaining the origin of chaotic terrains, but also of providing a detailed sequence of events leading to the sudden release of large volumes of water.

Nummedal (1978) calls for spontaneous liquefaction, a process characterized by the sudden loss of shear strength throughout a sedimentary deposit as the result of a minor vibration or shock. Liquefaction may start at a single point and spread to adjacent deposits possessing metastable packing. Liquefaction waves are known to propagate over large areas (10's of km) at velocities up to 100 km/h and occur both in subaerial and subaqueous environments. Commonly, the scar left behind following a liquefaction flow is a large bowl-shaped depression with a narrow outlet into the downstream channel. Blocks of non-liquefied crust generally litter the floor.

One conclusion which can be drawn at this point is that the physical characteristics of known terrestrial liquefaction flows are consistent with the morphology of the chaotic terrains and associated channels on Mars.

Work currently in progress addresses the question of what specific soil mechanical properties would be conducive to the development of large areas underlain by sediments susceptible to spontaneous liquefaction.

References:

- Baker, V. (1977) Viking-slashing at the Martian scabland problem, NASA TMS-3511, 169-172.
- Carr, M. H. (1978) Formation of Martian flood features by release of water from confined aquifers, NASA TM 79729, 260-262.
- Masursky, H., J. M. Boyce, A. L. Dial, G. G. Schaber and M. E. Strobell (1977) Classification and time of formation of Martian channels based on Viking data, *J. Geophys. Res.* **82**, 4016-4038.
- Nummedal, D. (1978) The role of liquefaction in channel development on Mars, NASA TM 79729, 257-259.
- Sharp, R. O. (1973) Mars: Fretted and chaotic terrains: *J. Geophys. Res.* **78**, 4073-4083.

Origin of Volatiles in the Martian Atmosphere

T. Owen, State University of New York, Stony Brook

The volatiles in the atmospheres of the inner planets appear to have been delivered in the form of a late-accreting veneer that is distinctly different for each object. On Mars and Earth, the composition of the veneer-producing material may well have resembled that of the meteorites we now classify as carbonaceous chondrites of type C3V. But Mars evidently acquired much less of this material than Earth, and experienced a smaller amount of total degassing. The smaller size of Mars may have been the cause of both of these effects, and has also led to the absence of a plate-tectonic system that could recirculate volatiles trapped in sediments. An early atmosphere that was denser than the present one is indicated, with a limited lifetime determined by deposition and escape. This atmosphere may have produced a sufficient greenhouse effect to lead to significant warming of the planet during the low luminosity phase of the young sun, even in the absence of ammonia. Preliminary Pioneer results indicate that Venus shows the same pattern of rare gas abundances exhibited by Mars, Earth, and the meteorites, which tends to support this model. But the high absolute abundance of noble gases relative to carbon and nitrogen suggests that another component of the veneer-forming material must have played a large role on this planet. An out-of-plane source seems suggested, with early comets an attractive possibility. The removal of initial atmospheres by an intense T-Tauri solar wind now seems even more unlikely.

Mars: Crust and Upper Mantle Structure

R. J. Phillips and B. G. Bills, Jet Propulsion Laboratory, California Institute of Technology, Pasadena, California 91103

An understanding of the crust and upper mantle structure of Mars follows mainly from analysis of gravity and topography data acquired by the Mariner 9 and Viking missions. Because of the inherent non-uniqueness in the inversion of gravity data, additional information must be brought forth from seismology, observations of surface tectonics, compositional assumptions, and rheological constraints such as isostasy and maximum shear stress.

The Tharsis region of Mars represents a major physiographic subdivision of the planet. This volcanic/tectonic province, roughly 4000 km square centered about 110°W longitude on the equator, lies eight to ten kilometers above the average global height. Geomorphologically, the topography is dominated by a domal structure, although up to 20% of the elevation could be volcanic-constructive. A long wavelength free-air gravity anomaly of about 500 mgals exists over the Tharsis province, flanked by gravity lows of about -200 mgals in the adjacent lowlands of Chryse and Amazonis.

Gravity data from the Mariner 9 mission, combined with elevation information from this mission and Earth-based radar, have shown that Mars can be divided into two "geophysical" provinces (Phillips and Saunders, 1975). Tharsis and the adjoining low regions of Chryse and Amazonis show a high correlation of gravity to topography, up to at least spherical harmonic degree and order three. The remainder of the planet shows little or no correlation of long wavelength terms (much like the Earth), strongly implying isostatic compensation at shallow depths.

This geophysical dichotomy is the crux of the problem in trying to understand the crust and upper mantle structure for Mars. One must find models which isostatically compensate the non-Tharsis terrain and at the same time provide a large free-air anomaly over Tharsis. Successful models, i.e., those that satisfy a set of observational and rheological constraints, might be a perturbation (of, for instance, density or thickness) on an otherwise horizontally stratified medium, or they might represent a total disparity in structure between the two geophysical provinces.

The simplest interpretation of the gravity data results from the correction for the effects of topography (the "complete Bouguer correction"). The resulting Bouguer anomaly is indicative of lateral density variations in the interior of the planet. Phillips *et al.* (1973) performed a preliminary analysis of the martian equatorial regions using Mariner 9 gravity data and Earth-based radar topography. They found a strongly negative Bouguer anomaly over the Tharsis Plateau, indicative of a density deficiency in the interior. The simplest interpretation of this result is a thickened crust under Tharsis, which Phillips *et al.* (1973) suggested was not in isostatic balance with the plateau uplift. Bills and Ferrari (1978) carried out a more extensive global Bouguer analysis and in addition presented a crustal thickness model. In a two-layer subsurface model of this type, crustal density, mantle density, and mean crustal thickness must be assigned. Bills and Ferrari constrained the mean thickness by using the possible 15 km crustal thickness at the Viking 2 site derived from Viking seismic data (Anderson *et al.*, 1977). Additionally, they sought a minimum value by finding a model with zero crustal thickness in the topographically lowest regions of Mars, the Hellas basin.

Phillips and Saunders (1975) studied isostasy using a simple Airy model of compensation of the topography, supposing that compensation took place by a root/antiroot density interface, presumably the crust-mantle boundary. Because the wavelengths they considered were much greater than the depths of compensation, their analysis is equally valid for simple Pratt models whose depths of compensation are twice that of the Airy models. Isostasy was studied using the ensemble of harmonics through degree and order 8, based on the gravity model of Sjogren *et al.* (1975) and the topography model of Christensen (1975). They found that only partially compensated Airy solutions are possible, taking place on a surface whose mean depth is no greater than 100-150 km. Working with individual harmonics Phillips and Saunders (1975) find a depth of compensation of the 2.2 harmonic of about 1100 km and a depth of compensation of the 3.2 and 3.3 harmonics of about 600 km.

This gross disparity in the depths of compensation argues against a simple Pratt or Airy model. The acceptance of a partially compensated model of the Tharsis region leads to an inquiry regarding the stress regime in the interior. Certain subsurface configurations lead to unacceptably high shear stresses; i.e., that exceed what we understand to be the finite strength of rock materials over an estimated range of temperature and confining pressures. If these configurations are to exist, the implication is that they must be dynamically supported. Phillips *et al.* (1979) considered the stress regime imparted by the partially compensated Tharsis models. They show that the anomaly, with dominant second and third spherical harmonic energy, would tend to be supported in the lower mantle. However, this is inconsistent with the volcanic activity observed and the expectation is that imposed shear stresses would rapidly decay from the deep interior, if indeed they ever existed at great depth. Finite strength support must ultimately be supplied by the lithosphere, and the question of stress levels depends mainly on elastic lithosphere thickness.

Considerations of both thermal model temperature gradients and the location of certain concentric tensional features postulated to result from loading failure due to the Pavonis Mons shield volcano result in a lithospheric thickness estimate of approximately 100 km (Phillips *et al.*, 1979). Thurber and Toks8z (1978) analyzed the flexure and stresses due to the load of the shield volcano Olympus Mons. Their conclusion is that if the lithosphere is much less than 150 km thick, then there should be a pronounced topographic moat surrounding the volcano; such a depression is not observed. Further, Thurber and Toks8z (1978) show that lithospheres thinner than 150 km will generate tensional stresses in excess of a kbar, leading to the presence of concentric tensional features such as the type associated with Pavonis Mons. No clear cut evidence exists for such features associated with Olympus Mons and we would argue, in fact, that such tectonics should develop at the 100 bar stress level.

Phillips and Sjogren (1978) analyzed high resolution Viking gravity data for Olympus Mons and could not find a flexural component in the Bouguer anomaly; the surrounding negative anomalies are too large in magnitude. They further conclude that there is a substantial subsurface contribution to the Olympus Mons anomaly and that this mass extends to the northwest and is contiguous with the main and apparently youngest lobe of the grooved terrain. Such a model is consistent with Karl Blumius' (personal communication) hypothesis that there is a continuous crustal igneous intrusion from Olympus Mons to the grooved terrain, with the latter feature a partial unroofing of the intrusive or the overlying caprock. The general character of the high resolution gravity data in the Tharsis region (Sjogren *et al.*, 1979) suggests the importance of crustal intrusion as a late stage process associated with shield volcanism.

The lack of identification of a flexural component in the gravity data does not eliminate the fact that the martian lithosphere must be relatively thick to support Olympus Mons. It is clear that even if an isostatic model is found for the Tharsis province, there are constraints on lithospheric thickness in terms of passive support over long periods of geologic time. Lithospheres that are 100 km or less in thickness will support neither Olympus Mons nor the regional Tharsis uplift. Lithospheres that are on the order of 200 km may be consistent with a finite strength support of Olympus Mons, but still lead to maximum shear stresses that are at least several kbars for the partially compensated long wavelength anomalies.

As an alternative to dynamic support of the Tharsis region, we might investigate isostatic configurations more complex than those previously considered. In Pratt or Airy isostasy the free-air gravity anomaly is directly proportional, on a harmonic basis, to the height of the compensated topography. Sleep and Phillips (1979) proceeded in a heuristic fashion by assuming that the Tharsis gravity anomaly arises from an upper mantle complete Pratt compensation of the plateau, and then derived what the compensated topographic elevation ought to be. For reasonable depths of compensation, the derived height exceeds the actual height; the difference is assumed to be taken up at the crust-mantle boundary with an appropriate correction for density contrast. The model that results is thus that of a low density upper mantle compensating loads at both the surface and the crust-mantle boundary. If the depth of compensation is on the order of 200 km or greater,

then reasonable values of crustal thinning, upper mantle density contrast, and maximum shear stress result. This model for Tharsis is similar to the compensation mechanism under the Basin and Range province of the western United States (Garland, 1971). These provinces also compare favorably in the sense that they are both elevated regions of extensional tectonics and extensive volcanism.

Given any model for the present crust and upper mantle structure for Tharsis, the origin of the uplift and volcanism remains enigmatic, while certain aspects of the tectonic pattern seem somewhat more understandable. The radial fracture system associated with Tharsis appears to be a natural consequence of the stresses associated with the existence of the elevated region (Phillips *et al.*, 1979; Wise *et al.*, 1979). It has been shown (Phillips *et al.*, 1979) that the stresses resulting from the present-day gravity field and topography adequately predict the regional tectonic patterns of Tharsis, implying an overall tectonic quiescence over a long period of martian history, since the major fracturing may be at least 3 billion years old. During this extended period, growth of the shield volcanoes and associated local tectonism took place (Wise *et al.*, 1979).

References:

- Anderson, D. L., W. F. Miller, G. V. Latham, Y. Nakamura, M. N. Toksoz, A. Dainty, F. K. Duennebier, A. R. Lazarewicz, R. L. Kovach and T. C. D. Knight, (1977) Seismology on Mars, *J. Geophys. Res.* 82, 4524-4546.
- Bills, B. G. and A. J. Ferrari (1978) Mars topography harmonics and geophysical implications, *J. Geophys. Res.* 83, 3497-3508.
- Christensen, E. J. (1975) Martian topography derived from occultation, radar, spectral, and optical measurements, *J. Geophys. Res.*, 80, 2909-2913.
- Garland, G. D. (1971) *Introduction to Geophysics, Mantle Core and Crust*, W. B. Saunders Co., Philadelphia, 420 pp.
- Phillips, R. J. and R. S. Saunders (1975) The isostatic state of martian topography, *J. Geophys. Res.* 80, 2893-2897.
- Phillips, R. J. and W. L. Sjogren (1978) Gravity constraints on martian lithospheric thickness, (abs.) EOS 59.
- Phillips, R. J., R. S. Saunders and J. E. Conel (1973) Mars: Crustal structure inferred from Bouguer gravity anomalies, *J. Geophys. Res.* 78, 4815-4820.
- Phillips, R. J., W. B. Banerdt, N. H. Sleep and R. S. Saunders (1979) Martian stress distributions: Arguments about finite strength support of Tharsis, in press, *J. Geophys. Res.*
- Sjogren, W. L. (1979) Mars gravity: High resolution results from Viking Orbiter II, in press, *Science*.
- Sjogren, W. L., J. Lorell, L. Wong and W. Downs (1975) Mars gravity field based on a short arc technique, *J. Geophys. Res.* 80, 2899-2908.
- Sleep, N. H. and R. J. Phillips (1979) An isostatic model for the Tharsis province, Mars, submitted to *Geophys. Res. Lett.*
- Thurber, C. H. and M. N. Toksoz (1978) Martian lithospheric thickness from elastic flexure theory, *Geophys. Res. Lett.* 5, 977-980.
- Wise, D. U., M. P. Colombeck and G. E. McGill (1978) Tharsis province of Mars: Geologic sequence, geometry and a deformation mechanism, submitted to *Icarus*.

On The Formation of Martian Lee Waves

A. O. Pickersgill and G. E. Hunt, Laboratory for Planetary Atmospheres, Department of Physics and Astronomy, University College London, London WC1E 6BT.

Mars is a planet with a thin atmosphere whose pressure is less than one hundredth of the Earth's atmospheric pressure at the same altitude. The topography consists of high mountains and deep basins, together with numerous smaller craters. These features produce wave patterns downstream of craters which have been observed by Mariner 9 and more recently in the Viking project.

An investigation into the Mariner 9 data and pictures by Briggs and Leovy (1974) determined that several wave patterns observed were atmospheric lee waves. These waves produced clouds which were estimated to lie between 6 kilometres above ground level, and 20-30 kilometres in altitude, which represents a considerable spread of altitudes in an atmosphere of depth about 50 kilometres.

The orbital imaging observations of dynamical phenomena on Mars was recorded for a range of aerocentric longitudes of the sun, L_s , from 87° to 145° , corresponding to the last days of northern spring through late summer by Briggs et al. (1977). Several different types of wave clouds have been observed, the 'ship wake' pattern produced in the lee of craters which was reported by Briggs and Leovy (1974), together with wave patterns of a less well known type. A bore was observed between Pavonis Mons and Arsia Mons near the dawn terminator on revolution 62 (V_{01} , $L_s = 112^\circ$) which stretched for several hundred kilometres. Also a plumelike cloud to the west of Ascræus Mons acquired by V_{01} on revolution 58 ($L_s = 110^\circ$) was observed, bearing some resemblance to the Mariner 9 image of lee waves produced by crater Milankovic $55^\circ N$ $145^\circ W$ for $L_s \approx 344^\circ$.

Pirraglia (1976) has investigated the theory of trapped martian lee waves produced by an isolated crater of diameter 100km. in the northern winter. He used a modified version of a model proposed by Scorer (1949), and extended in Scorer and Wilkinson (1956), to predict Mariner 9 results for crater Milankovic, including the example of $L_s \approx 344^\circ$ mentioned above. The author deduced that the 'ship wake' pattern could be obtained from a theoretical consideration of matching the angle of the pattern and transverse wavelength. However, the wind speeds deduced are extremely dubious, as any set of wind speeds, with the same ratio of upper layer to lower layer produce the same result. Pirraglia's result also has a serious drawback in that untrapped lee wave modes, of importance at higher altitudes, were ignored in his paper.

This paper investigates flow over a crater for the 'ship wake' pattern. A 100km. diameter crater is considered, and the flow pattern obtained is compared with those obtained for crater Milankovic for the Mariner 9 results. This crater was seen to produce a wave pattern by Viking Orbiter 2 on revolution 171. Two approaches are adopted, the method of Pirraglia which introduces a velocity discontinuity at an interface in the atmosphere, and Scorer's 1949 approach which introduces a static stability discontinuity, while maintaining a velocity profile which is continuous throughout the atmosphere.

The models are investigated at different elevations to observe whether the role of trapped waves has a significant effect at certain altitudes on the displacement of streamlines. The behaviour of streamlines near the ground is used to indicate where erosion occurs in the lee of craters in this model. This interaction may be a mechanism for the formation of local dust storms in areas of large topographical variation. Wind associated crater streaks have been discussed by Veverka (1975); while Briggs et al. (1977) comment that waves are set up in the Hellas basin, an area where dust storm activity is known to occur.

References:

- Briggs, G. A. and C. B. Leovy (1974) Mariner 9 observations of the Mars north polar hood; *Bull. Amer. Meteor. Soc.* 55, pp. 278-296.
Briggs, G. A., K. Klaassen, T. Thorpe, J. Wellman, and W. Baum (1977) Martian Dynamical Phenomena during June - November 1976; Viking Orbiter Imaging Results; Sci. Results of the Viking Project pp. 4121-4150.

A. O. Pickersgill and G. E. Hunt...2

Pirraglia, J. A. (1976) Martian Atmospheric Lee Waves, Icarus 27, pp. 517-530.

Scorer, R. S. (1949) Theory of waves in the lee of mountains; Quart. J. R. Met. Soc. 82, pp. 419-427.

Veverka, J. (1975) Variable features on Mars V: Evidence for crater streaks produced by wind erosion, Icarus 25, pp. 595-601.

Evaporites from the Southwestern Desert, Egypt: Possible Martian Analogues for the Production of Duricrust

D. J. Prestel, Lockheed Electronics Co., Inc., Houston, TX 77058.

D. S. McKay, NASA Johnson Space Center, Houston, TX 77058.

C. V. Haynes, Depts. of Anthropology and Geosciences, Univ. of Arizona, Tucson, AZ 85721.

Although it is likely that water-regolith interaction played an earlier role in modifying the martian surface^{1,2,3}, there is considerable evidence that the surface of Mars is now dominated by eolian processes⁴.

The successful Viking landers have provided information about the surface morphology of Mars. The fines appear to be composed of silicate particles, with some oxides and possibly carbonates⁵. Both landing sites show the presence of a crustified layer, interpreted by Toulmin et al.⁶ as a caliche-like duricrust consisting of fine-grained material cemented by sulfate and chloride minerals. Sulfur-rich pebbles on the surface are interpreted to be fragmented duricrust. These investigators suggest that the cement may have formed by leaching of soluble ions from rock particles into a thin intergranular film of moisture, with subsequent evaporation and deposition at the martian surface.

On the basis of these Viking results it appears that, although eolian processes may now be the dominant agents for erosion and transportation on the surface of Mars, it is still possible that chemical weathering processes are active, particularly those associated with leaching and deposition of evaporite-related species. Consequently, we have undertaken a study of potential analogue processes in a terrestrial environment which most closely approaches the martian surface in several respects. In particular, we consider the Southwestern Desert of Egypt (Darb El Arbain region) to provide the necessary conditions: the extreme dryness, near or total lack of liquid surface water, and the predominance of eolian features^{6,7,8}.

We are studying evaporites and associated sands and clays from birs (wells) and playas. The samples include efflorescent crusts of complex mineralogy, salts, sands, clays and the underlying bedrock. As an example, the mineralogy of one set of samples forming a surface salt crust was determined to be tamarugite, $\text{NaAl}(\text{SO}_4) \cdot 6\text{H}_2\text{O}$, bloedite, $\text{Na}_2\text{Mg}(\text{SO}_4)_2 \cdot 4\text{H}_2\text{O}$, gypsum, halite and quartz by x-ray diffraction studies. We are characterizing the morphology and chemistry of tamarugite and bloedite by scanning electron microscopy with attached energy dispersive x-ray analysis. Our initial interpretation is that these sulfate minerals were formed by leaching of the underlying rocks and sediments with capillary transport to the surface along grain boundaries followed by evaporation in the extremely arid climate. The result of this process is that a sulfate-rich crust forms near the desert surface. We are investigating the applicability of this process to the martian atmosphere.

Additionally, we are attempting to establish mineralogical, textural and chemical criteria for distinguishing playa deposits from evaporate deposits originating from sub-surface moisture.

Since upward-migrating water would react with surface rocks and evaporate in the martian atmosphere, we are studying the precipitation of minerals of different solubilities on sand grains. The combination of observational and experimental studies may lead to the determination of the solubility of the available ions under martian conditions and the evaporite mineralogy to be expected.

References:

- ¹Fuller, A. O. and R. B. Hargraves (1978) *Icarus* 34(3), 614.
- ²Soderblom, L. A. and D. B. Wenner (1978) *Icarus* 34(3), 622.
- ³Clark, B. A. (1978) *Icarus* 34(3), 645.
- ⁴Match, T. A. et al. (1976) *The Geology of Mars*, Princeton Univ. Press, Chapter 7.
- ⁵Toulmin et al. (1977) *J. Geophys. Res.* 82(28), 4625.
- ⁶Li-Baz, F. (1978) Mars and Comparative Studies in the Inner Solar System Symp. COSPAR, Innsbruck, Austria.
- ⁷Wendorf et al. (1976) *Science* 193(4248), 103.
- ⁸Haynes, C. V. (1978) In Greeley, R. and D. Black, eds., *Planetary Geology Field Conf. on Aeolian Processes*, NASA TN-78, 455, p. 22.

Radar Morphometry of Craters, Basins and Volcanic Landforms on Mars

L. E. Roth, G. S. Downs, R. S. Saunders, Jet Propulsion Laboratory, California Inst. of Technology, Pasadena, CA 91103.
G. Schubert, Dept. of Earth and Space Sciences, Univ. of California, Pasadena, CA 90024.

Goldstone radar ranging of Mars over the past few oppositions has yielded altitude profiles along arcs of nearly constant latitude in the planet's equatorial belt. The radar profiles confirm the overall shallowness of the large martian craters, permit accurate determination of the regional topographic gradients, and verify the existence of a degraded impact basin in Margaritifer Sinus and a secondary volcanic shield in the Arsia Mons massif. The radar depths of a mixed-population sample of the large craters ($D \geq 20$ km), all located within the strip around the planet bounded by latitudes -14° and -22° , are a weak function of diameter. Beyond a certain diameter range the radar depths are virtually independent of the crater size and cluster around the value of 2000 m. The basin in Margaritifer Sinus, circumscribed by an incomplete ring of mountainous topography, occupies the region between -14° and -22° in latitude, and between 25° and 33° in longitude. It is about 2000 m deep and has a diameter of about 500 km. The radiating pattern of a likely drainage system discharging into the basin hints at the presence of an extensive watershed. The secondary volcanic shield is located SSW of the Arsia Mons summit. The diameter of the shield at its base is at least 400 km and the volume is comparable to that of the Arsia Mons main shield. The source region of the Arsia flow fields identified previously, coincides with the approximate location of the center of the secondary shield. Along its south flanks the secondary shield displays a simple conical shape, and the lava flows in the same area are oriented in the directions of the maximum radar topographic gradients.

Mars, the Neglected Planet: A Summary of Past Deeds and Future Needs for Magnetic and Solar Wind Interaction Studies

C. T. Russell, Inst. of Geophysics and Planetary Physics, Univ. of California, Los Angeles, CA 90024.
F. L. Scarf, TRW Defense and Space Systems Group, Redondo Beach, CA 90278.

The natural course of a program of planetary exploration is to proceed in stages of increasing sophistication: first reconnaissance, then exploration and then intensive study. Often there is pressure to jump ahead and skip parts of the exploratory phase and initiate intensive study. Such skipping ahead occurred on the Apollo program in which samples were returned before geochemical and geophysical surveys of the surface were undertaken. It is again occurring on Mars. In the field of comparative planetology Mars, Venus, and the Earth form an important triad. However, the lack of many first-order measurements at Mars prevents us from making comparisons. For example, we do not know whether Mars has any intrinsic magnetic field, nor the rate at which the upper atmosphere is accreting or being lost in its interaction with the solar wind. In this area compared to the Earth and Venus, Mars is truly a neglected planet.

The only American spacecraft to carry magnetic or solar wind instrumentation to Mars was Mariner 4 almost 14 years ago. Mariner 4 passed too far from the planet to detect anything but the planetary bow shock. Three Russian spacecraft have carried such instruments into orbit. However, no data have been acquired in the very important wake region behind the planet. Furthermore, no data have been acquired anywhere below 1100 km altitude. The interaction region with the ionosphere and upper atmosphere is well below this level.

The data that have been obtained are ambiguous and controversial. Dolginov and co-workers claim to have measured a planetary field. Wallis and Russell independently claim otherwise. Vaisberg and colleagues claim they observe erosion of oxygen from the martian upper atmosphere by the solar wind. Gringauz and co-workers claim that Vaisberg et al. are simply measuring magnetosheath protons.

If we can resolve these issues, then we can answer such questions as whether Mars has an active dynamo and how the martian atmosphere has evolved over the aeons since formation. The answers to these controversies lie in acquiring new data with orbiting spacecraft.

Martian Impact Crater Ejecta Emplacement

P. H. Schultz, Lunar and Planetary Inst., Houston, TX 77058.

D. E. Gault, Murphys Center of Planetology, Murphys, CA 95247.

Martian impact craters exhibit considerable variety in the morphology of their ejecta deposits. Although the possible presence of ground ice may complicate the cratering process and ejecta emplacement, its presence cannot solely account for the observed absence of secondary crater fields beyond the ejecta flow termini of many craters between 5 km-50 km in diameter. It is proposed that fine-grained in situ target materials and extensive comminution enhanced by the presence of ground ice result in small-size ejecta that undergo appreciable decelerations. Sufficiently small ejecta selectively arrive near the rim and become entrapped in a complex near-rim ejecta flow. Numerical models of ballistic ejecta in the present martian atmosphere suggest that ejecta fractions smaller than 4 cm from 5 km-diameter craters and 15 cm from 20 km-craters will exhibit pronounced reductions in range and alteration of the ejecta emplacement sequence. Complexly bedded/jointed near-surface stratigraphies result in larger fractions of large-size ejecta that are not affected by drag and may produce a component of the ejecta facies resembling facies around lunar and mercurian craters.

Genesis of Martian Outflow Channels by Crater-Controlled Intrusions

P. H. Schultz, H. Glicken, T. R. McGetchin, Lunar and Planetary Inst., Houston, Tx 77058.

On the Moon, floor-fractured and basalt-filled craters reflect intrusions/extrusions localized by impact-induced crustal weaknesses on the margins of the maria. On Mars, similar endogenically modified craters also occur adjacent to vast lava plains. These craters are observed within or adjacent to chaotic terrains, fretted terrains, plateau plains, and outflow channels. Consequently, crater-controlled volcanism evident on the Moon also may have occurred on Mars with the important complication of a ground ice layer. Previous workers have suggested that emplacement of intrusive bodies may have melted the ground ice, resulting in ponded water and a subsequent catastrophic flood capable of producing outflow channels. Approximate solutions to the cooling history of sill-type intrusive bodies suggest that intrusion-related melting beneath relatively small craters ($D < 100$ km) extends to very near the surface for a thick (1 km) intrusive at relatively shallow depths ($d/D < 0.1$). Thin (0.1 km) intrusive bodies beneath small craters may result in melting at depths greater than approximately 0.5 km. Intrusions beneath larger craters generate sufficient heat for melting to the surface only for thick (> 1 km) and relatively shallow (< 8 km) bodies. Consequently, massive intrusions beneath small martian craters comparable to some lunar floor-fractured craters could induce a loss of strength in the overburden and a subsequent catastrophic release of the contained slurry. Intrusion-induced ring fractures, features common to volcanically-modified lunar craters, could conceivably be pathways for the escape of liquid or gas H_2O resulting from the deterioration of ground ice by thin and/or deep intrusions.

Mars: Viking Appraisal of Mariner Geologic Mapping

D. H. Scott, U. S. Geological Survey, Flagstaff, AZ 86001.

The systematic geologic mapping of Mars using Mariner-9 images was completed in 1978 and produced 30 geologic quadrangle maps of the entire planet and a smaller scale geologic map representing a compilation in part of the larger scale map series. The quality of many of the Mariner-9 photos was degraded by atmospheric haze and high-sun angles producing strong albedo contrasts, particularly in the high northern and southern latitude belts. Geologic maps of these regions reflect these deficiencies but at present are the only ones available that cover the entire planet.

Geologic mapping using Viking images has allowed comparisons to be made with the previous work. Most of the initial studies are in the northern hemisphere and involve rock units of the subpolar region, lowland plains, and the border land between plains and the highland plateau. On a broad scale, the Mariner mapping delineated geologic boundaries between and within these physiographic provinces reasonably well. Important rock units and subdivision of units, however, were not recognized because of the quality and resolution of the Mariner pictures. This discussion describes these rocks and their relations to the time stratigraphy of Mars.

The most extensive geologic units appearing on the Mariner pictures in the northern hemisphere are mottled plains, cratered plains, and smooth plains. They occupy vast areas of the lowlands and extend to the boreal region (Scott and Carr, 1978). These rocks, as their names imply, are characterized by light and dark patches, common superimposed craters and broad featureless expanses. The cratered and smooth plains were interpreted as lava plains covered by a veneer of eolian deposits of varying thickness; where the eolian mantle was relatively thin, craters in the underlying lava flows were more visible, thus giving the appearance of older age to these regions. The mottled plains are easily recognized on Mariner images but difficult to interpret both as to lithology and probable origin. They were variously considered to represent sediments with pore spaces filled by permafrost (Elston, 1978), ancient terrain exhumed by wind erosion (Underwood and Trask, 1978), or having a surface texture produced by frost heaving or other frost phenomena (Greeley and Guest, 1978).

Viking pictures clearly show that the previously mapped cratered plains and smooth plains units occupying the Vastitas Borealis region of Mars have many differences in texture, topographic expression, color, and other physical characteristics that require their further subdivision. Some 10 different types of plains materials presently comprise the two originally mapped rock units. The mottled plains, however, are not yet capable of similar differentiation. Viking photos in these regions show numerous bright haloed craters and relatively small hills and knobs which provide a hummocky texture to the terrain but their relationship to the dark patches is not clear nor are stratigraphic relations at their boundary with both the smooth and cratered plains materials.

References:

- Elston, W. E. (1978) Geologic map of the Cebrenia quadrangle of Mars, U. S. G. S. Misc. Geol. Inv. Map (in press).
- Greeley, R. and J. E. Guest (1978) Geologic map of the Casius quadrangle of Mars, U. S. G. S. Misc. Geol. Inv. Map I-1038.
- Scott, D. H. and M. H. Carr (1978) Geologic map of Mars, U. S. G. S. Misc. Geol. Inv. Map I-1081.
- Underwood, J. R., Jr. and N. J. Trask (1978) Geologic map of the Mare Acidaliæ quadrangle of Mars, U. S. G. S. Misc. Geol. Inv. Map I-1048.

Terrestrial Debris Flow Deposits as Analogs of Martian Strewn Fields

A. Shultz, L. J. Suttner, A. Basu, Dept. of Geology, Indiana Univ., Bloomington, IN 47405.

Martian sediments near the Viking Lander sites are characterized by a remarkable bimodal size distribution with a lack of 0.01 cm to 4.0 cm sized particles. If the parent rocks of these sediments were exclusively basalt and if they were exposed for a long period of time (e.g. >1 b.y.), they could have weathered primarily into clay minerals in the presence of H₂O and CO₂; hardly any resistate, such as quartz, would have been produced. However, quartz or quartz-bearing lithic fragments usually make up most of the >0.01 cm size fraction in terrestrial sand bodies. Thus, there is a possibility that the bimodality in martian sediments is due to weathering of quartz-free parent rocks. Alternatively, or perhaps additionally, a mechanism of transport, such as debris flows, may be responsible for the bimodal size-distribution. The general paucity of very small craters and the presence of lobate megascopic flow patterns originating from impact craters (e.g., Mie near the VL2 site) are circumstantial evidence of possible debris flows.

We are currently investigating 16 ancient debris flow deposits, all from the ~250 m.y. old Cutler Formation in Colorado, and our preliminary data provide a basis for comparison with VL imaging data.

Seven of the sixteen debris flows show reverse grading in sizes >5 cm, whereas three others show normal grading and the rest show no obvious size grading. Our tentative hypothesis is that reverse grading is more likely to occur in flows with relatively high viscosity where the internal dispersive force can be transmitted more easily and the strength of the flow unit is also greater. Regardless of the phenomenon of grading, there is a general dearth of 0.4-3.2 cm sized particles, a bimodal size distribution, and the matrix is <0.07 cm in all the debris flow deposits. It is not known at this time if there is any size grading in the <0.2 cm sized material. However, if all the clasts respond similarly to the internal dispersive pressure, then in reverse graded units the smaller clasts would tend to be concentrated at the bottom of the flow. This would enhance the bimodality of grain sizes near the top of the flow. Reworking of tops of previous debris flow deposits by younger flows and recycling of bimodal loads would greatly increase the bimodality of the final deposit. Such a situation could explain the bimodality of martian strewn fields. A good correlation exists between the thickness of flow units and the maximum clast size in our debris flows ($r = 0.89$). If some of the martian sediments were indeed laid down by debris flows comparable to the ones that we are investigating on Earth, then the thickness of the topmost flow near/around VL2 can be estimated to be ~1 m judging from the largest block (~0.8 m) in the vicinity.

Our studies of terrestrial debris flows are still in progress and cannot yet be compared directly with martian data. Nevertheless, it appears that flow of high viscosity mud carrying weathered basaltic debris and blocky ejecta from impact craters is a reasonable process by which the materials of the martian strewn fields could have been deposited. It will be interesting to study debris flow deposits in an old terrestrial province as a martian analog.

Hellas Planitia Gravity Anomaly

W. L. Sjogren, R. N. Wimberly, Jet Propulsion Laboratory, California Inst. of Technology,
Pasadena, CA 91103.

Doppler radio tracking data, obtained from Viking Orbiter I during the latter part of 1978, have provided the first high resolution gravity observations of the Hellas basin. Spacecraft altitudes were approximately 300 km when the orbiter passed over the northern portion of the basin. Initial results show the basin has a significant mass deficiency, however definite signatures remaining in the data residuals imply that additional information exists. Results of more detailed modeling to remove the residual signatures will be presented.

Viking Bistatic Radar: Preliminary Results from the North Polar Region

R. A. Simpson, G. L. Taylor, Center for Radar Astronomy, Stanford, CA 94305.

Radio waves from the Viking orbiters were scattered from Mars' surface during the 1978 opposition. Preliminary results from a track across Hellas recently appeared in Science. This paper represents a progress report; we will discuss our tentative estimates of surface roughness and dielectric constant, providing illustrations from data acquired north of 60°N latitude.

Mars in the Solar Wind: Implications of an Earth-like Interaction

E. J. Smith, Jet Propulsion Laboratory, California Institute of Technology, Pasadena,
California 91103

Observations by magnetometers and plasma analyzers on board one American and several Russian spacecraft indicate that Mars is weakly magnetized. The generally accepted upper limit to the martian dipole moment shows that, compared to the other planets, Mars is an anomaly and is deserving of further study. The absence of a reasonably strong field has generally been interpreted as evidence that Mars has a core that is either small or solid. The constraints imposed by various magnetic field limits, including the absence of a field, on models of the martian interior and on its thermal evolution will be discussed. It is important to note that the available observations can be considered consistent with a planetary field strong enough to hold off the incident solar wind. Therefore, as a complement to the presentation by D. Intriligator, I will discuss the implications associated with an Earth-like interaction of the solar wind with Mars. Scaling laws will be used to compare the hypothetical magnetosphere of Mars with the magnetospheres of Mercury, Earth and Jupiter. The controversy stimulated by the Russian claim to have detected a planetary field will be reviewed and our current understanding of Mars' field will be assessed. The presentation will conclude with a brief statement of the requirements to be imposed on future missions, if these issues associated with the planetary field are finally to be resolved.

Viking Scientific Results, September 1977 to September 1978

C. W. Snyder, Jet Propulsion Laboratory, Pasadena, California 91103

Although two of the Viking Lander investigations - organic analysis and biology - had made essentially all the observations of which they were capable and had been turned off prior to the period covered in this report, the other experiments, both on the landers and on the orbiters, were very active. One quantitative measure of this activity is the number of pictures acquired. Between 1 September 1977 and 1 September 1978, the orbiters successfully acquired 18,624 pictures and the landers took 1641 pictures. Comparison with the figures for the primary mission - 7600 and 1036, respectively - shows what a tremendous bonus the extended mission of the four spacecraft has been.

Of greater significance than the numbers are the scientific findings that have increased our understanding of the planet Mars. These are principally in the fields of the geology of the martian surface and the meteorology of the martian atmosphere.

The Geology of Mars

The geologic observations have been made by the orbiter cameras. Many of the results are complex and very technical in nature. They are being published in the open literature, but they do not lend themselves to simple summarization. Some specific items are the following:

During this year more than 80 percent of the surface has been mapped at resolutions between 150 and 250 meters per pixel. This is an activity of very great potential importance that had not even been considered as an objective of the original Viking mission because of the long period of time and large quantity of pictures required. It means that we can now produce maps of nearly all of Mars that will surpass by an order of magnitude those that were derived from Mariner-9 observations. These maps will be a major tool of geologists for years to come, and they are just beginning to be produced.

We have mapped completely the circumpolar dune fields that surround the north polar cap, determining their boundaries and extent. They are by far the largest collection of sand dunes that are known.

The plains in the southern hemisphere, which appeared to be smooth and nearly featureless in the Mariner 9 pictures, are found to contain a large amount of structure, which is just beginning to be studied.

On the other hand, the polar layered terrain in the north is found to be nearly craterless; hence it is apparently the youngest region on the planet.

It is found that the great volcanoes on the Tharsis Ridge and Olympus Mons have all produced very much more lava than had been recognized from the earlier photography, with some flows extending for hundreds of kilometers. Accurate crater counts can now be made, which are starting to provide information on the ages and history of this volcanic activity.

It has been possible to trace some of the layered deposits in Valles Marineris over considerable distances. Only the vaguest hint of these layers had been seen previously. It has also been found that the canyon bottom is not rock-covered as expected, but is covered with fine-grained material. This information was derived from IRTM, not from the VIS pictures.

From a study of the thickness of lava flows and of the width and depth of lava channels, it has been possible to deduce the viscosity of the lava in some areas. The flows from Olympus Mons and those from Arsia Mons, only a little more than 1800 km apart on the same side of the planet, differ by a factor of a hundred in yield strength.

Many very high resolution pictures have been taken of small regions scattered over the planet from ranges between 300 and 500 km. The best of these have resolutions of 8 meters per pixel. Quite often the features revealed are strange and incomprehensible. As the quantity of these very high resolution pictures increases, it is becoming possible to study the ages and flow parameters of the great floods, which still constitute one of the major mysteries of Mars.

Some of the very high resolution pictures show places where the surface is saturated with craters as small as can be detected. These observations contradict the pre-Viking assumption that the atmosphere would inhibit the production of craters smaller than about 40 meters.

Analysis during this period of the very high resolution pictures that were taken of Phobos somewhat earlier in the extended mission have provided some surprises. (1) The several families of nearly straight parallel grooves on the surface of Phobos radiate from Stickney, the largest impact crater on the satellite, and converge on its antipode. This configuration indicates that the grooves were caused by the fracturing of Phobos by the impact that produced the crater. (2) Many of the grooves on Phobos are dotted with circular craters that have raised rims, indicating some kind of gas evolution. That such very small astronomical bodies can exhibit degassing activity is a new thought having profound consequences.

In October 1977 a propulsive maneuver was performed with Orbiter 2 to provide five close encounters with Mars' outer satellite, Deimos. The closest pass, 28 km from the surface, was the closest fly-by of any astronomical body that has yet been achieved. The pictures obtained in this series of observations have revealed several interesting and puzzling facts about the satellite. It is found that bright patches on the surface (which had been observed earlier) are deposits of fine-grained material that partially fills in impact craters and makes Deimos appear smoother than Phobos. The material is presumed to be the ejecta from impact craters, and the puzzle is how such a small body can hold on to so much of the ejecta and why Phobos does not do the same. Some of the craters on Deimos have tails that look like those that emerge from martian craters and are ascribed to the action of wind. Obviously there was never any wind on Deimos, so the streaks must be base surge deposits, material ejected by the impact and flowing along the surface. This constitutes another novel idea about the physical processes that occur on tiny bodies, as it had always been assumed that the debris would fly away from the surface instead of hugging close to it.

The Meteorology of Mars

The second major thrust of the Viking extended mission has been the study of the climate on Mars. Contributions to this coordinated study are being made by the lander meteorology instruments, the lander cameras, the orbiter cameras, the infrared thermal mapper, and the Mars atmospheric water detector. During the period reported here, we completed one full Mars year (687 Earth days) of monitoring the martian weather and have commenced on the second year. The single issue of greatest interest now is the degree to which the climatic conditions repeat themselves in successive years.

It has been found that a predominant factor in the martian climate is the global dust storms that usually, if not invariably, occur during the southern summer. In the Viking year there were two of them, the later of which had just cleared shortly before the period reported here (Sept. '77). Analysis of the dust storm effects has been intense in recent months, with more than a dozen papers having been written which will appear in a winter issue of the Journal of Geophysical Research. The most interesting conclusions from the data obtained in the summer of 1977 have come from these analyses.

The lander cameras discovered that, at some time near the middle of winter, the surface around Lander 2 was covered with a thin layer of white frost, which is probably water ice. With the approach of spring, it gradually disappeared, persisting longest in the shadow of larger rocks.

In the spring season many pictures were taken of the surroundings with the positions of the sun matching precisely those of pictures that had been taken the previous autumn. This technique made it possible to search for very subtle changes that might otherwise have been masked by differences in illumination. It was found that a very thin layer of light-colored dust had settled on the surface around Lander 2 during the winter. It is believed that the frost was transported from the southern hemisphere, condensed on the dust particles that settled out from the global storms.

The continued monitoring of the atmospheric pressure at both landers has now shown that this one meteorological parameter repeats the values that it had one year before. This pressure is in reality a measure of the amount of carbon dioxide that is frozen into and released from the polar caps as the seasons change. From the change in pressure from northern summer to winter it can be calculated that the quantity frozen in the southern

cap is sufficient to cover uniformly the maximum extent of the cap to a depth of more than 23 centimeters. Since the dry-ice cover is certainly not uniform, its depth is probably at least several feet in some places.

The rate of retreat of the southern polar cap during the past summer has been found to be quite anomalous. Observations from earth over many decades have shown great reproducibility in the rate and pattern of this retreat, but the Viking photographs show that the disappearance of the cap lagged more than 30 days behind schedule at times. This behavior is attributed to the very early occurrence of the first major dust storm and emphasizes the unusual nature of this event.

The extent of ice cover at the north pole this summer has been appreciably less than last summer.

Analysis of the local dust storms that preceded and presumably triggered the large storms reveals that about half of them occurred near the edge of the south polar cap (between 54 and 71 degrees south latitude), where surface winds are presumably enhanced by strong temperature gradients. About half were observed to be in regions where the topography is such as to produce large upward components in wind velocity; most of these are in the southern hemisphere also. The early storm appears to have been triggered by the polar family of little storms, and the mid-summer storm, by the topographically controlled family.

The water vapor in the atmosphere has been found to be distributed fairly uniformly through the lower 10 kilometers or so. This is an important discovery, as it had generally been assumed that the vapor was near the surface and hence might easily be condensed during the night to form frost or ground fog. The entire planet appeared very dry during the southern summer because vapor was both hidden from the view of the orbiters and precipitated out of the atmosphere by the dust storm. The total water vapor visible in the entire atmosphere dropped to less than one-quarter of the amount measured at the start of the Viking mission.

One of the most significant of all the discoveries about the meteorology of Mars was the detection by the meteorology experiment on Lander 2 of evidence for the regular eastward passage of a sequence of cyclones and anticyclones with centers somewhat north of the landing site. Recent analysis of pressure and wind records has shown this phenomenon to be present throughout the northern autumn season. It disappeared during the winter and has returned again with the coming of spring. Some of these circulating systems are clearly associated with fronts. No similar phenomena have been observed at Lander 1.

Miscellaneous Observations and Events

A cooperative effort between the lander imaging and orbiter imaging teams provided a precise location of Lander 1. A swath of orbiter pictures taken from 300-km altitude showed a number of small craters in the general vicinity of the lander. Comparison of these with computer-processed Lander 1 pictures made it possible to identify features near the horizon with several of these craters. The position of Lander 1 relative to observed surface features is now known to be better than 40 meters. The lander itself is about 5 times too small to show up in any orbiter picture.

Another significant event for the lander cameras during this period was the acquisition of a picture of Phobos in the night sky - a difficult feat because of the small size and rapid motion of the little moon.

Continued operation of the x-ray fluorescence spectrometers and analysis of the data from them has progressively improved the precision of our knowledge of the elemental composition of soil at the landing sites. A significant result was the detection of bromine at a level of nearly 100 parts per million - about ten times higher than had been expected. The high abundance of this element correlates with that of chlorine, both indicating a high salt content in the surface material. Contrary to the case on the moon, martian "soil" would be too salty to support agriculture.

In addition to the continuing acquisition of tracking data (doppler and ranging) for landers and orbiters and the occultation data from Orbiter 1, the Radio Science Team has conducted two special experiments of opportunity during the past year. From November 1977 to March 1978, when the Earth passed close to Mars, approximately thirty bistatic radar observations were carried out, involving pointing the high-gain antenna on one of the orbiters

toward the planet so that radio waves reflected from the surface could be recorded on Earth. These data contain information on the roughness and physical properties of the surface, similar to that provided by Earth-based radar, but the advantages are a considerable increase in surface resolution and the ability to probe areas (e.g., the polar regions) that are never observable from Earth. Analysis of the results of this experiment has been postponed until 1979.

The other special radio science experiment took advantage of a particularly favorable orbital geometry and the very low periapsis of Orbiter 2 to measure orbiter accelerations near periapsis and obtain high-resolution data on local gravity anomalies. Data from this experiment are still being analyzed. The largest detected anomaly was produced by Olympus Mons, and it appears that this enormous mountain is simply sitting on the topography with little or no bistatic adjustment.

Shortly before the final shutdown of the surface samplers, a magnet cleaning operation was successfully executed on Lander 2. This difficult maneuver had not been attempted earlier in the mission because of the danger of incapacitating the sampler. Subsequently the magnets were inserted three times into the soil and pictures were taken of them, providing data for the magnetic properties experiment of greatly superior quality than any acquired earlier. The results confirmed earlier tentative conclusions that the soil contains a few percent of a highly magnetic mineral homogeneously distributed in the fine-grained material.

Correlation of large quantities of IRTM data have shown that both landing sites are unusual in that they are brighter in the infrared and have higher thermal inertia than most of the planet surface. Hence lander data on site characteristics can only be extrapolated to the whole planet with appropriate caution.

Pictures were taken by each lander of the surface under the spacecraft that had been eroded by the exhaust of the descent engines. Analysis of these pictures (not yet begun) will provide additional information about surface properties.

From December 1977 to February 1978 an intensive set of observations of the surface of Mars was made by the Infrared Thermal Mapper of the brightness of the planet in the infrared at small phase angles. In a cooperative program simultaneous observations were made by 13 Earth-based observatories. The importance of this program stems from the fact that Mars is customarily used as a standard source for infrared observations even though the constancy of its brightness has not been known. It was found that the brightness temperature varied by as much as 7 degrees as a function of the central longitude of the planet. These results will contribute to the accuracy of many past and future astronomical observations.

Evolution of the Topography of the Martian Polar Laminated Deposits

S. Squyres, Geological Sciences Dept., Cornell Univ., Ithaca, NY 14853.

Detailed observations of Viking images of the martian polar regions show that the dark spiral markings in the perennial ice caps are associated with grooves in the laminated deposits. The poleward-facing slopes and the flats separating the grooves are covered with perennial H₂O ice, while the equatorward-facing slopes are ice-free due to high insolation. Adhesion to this ice is probably necessary for retention of deposition dust. While ongoing dust deposition in the polar regions is likely and a uniformitarian approach is favored because of the young age of the features, a purely depositional origin for the grooves, such as that of Cutts et al. (1979), is unlikely for several reasons: 1) Minor escarpments necessary to begin groove development would probably not form a spiral pattern. 2) Equatorward-facing escarpments subjected to deposition at their heads and feet should gradually migrate headward rather than develop into a groove. 3) A depositional origin requires that both slopes of a groove be stabilized against deposition, but there is good evidence for recent deposition on poleward-facing slopes. The following alternative model is proposed: Cyclic fluctuations of the perennial ice margin related to equinoctal precession repeatedly cover and expose the laminated deposits. When ice-covered, deposited dust is retained on the surface. When exposed, the grooves are elongated by deflation. They may begin at a minor irregularity such as an impact crater and grow gradually over many cycles. Deposition on the poleward-facing slopes and the adjacent flats should cause poleward migration of a stable groove form. This migration may over time accentuate the spiral pattern.

Reference:

Cutts, J. A., K. R. Blasius and W. J. Roberts (1979) Polar layered deposits: The geological consequences of Martian dust storms, in press.

Crustal TRM and the Magnetic Field of Mars

L. J. Srnka, Lunar and Planetary Inst., Houston, TX 77058.

The upper limit of 2×10^{21} - 2.5×10^{21} G-cm³ for the magnetic dipole moment of Mars set by the Soviet Mars 3 and Mars 5 spacecraft data is examined in terms of the possible magnetic properties and thermal history of the planet. Assuming a present Curie isotherm depth of 100 km and a crustal Fe₂O₃ content of 1 - 10 vol.%, it is shown that a remanent dipole moment may exist which is comparable to the upper limit, if the ancient martian dynamo field presumed to be the source of the TRM was non-reversing and had a surface equatorial value of ~ 1 G. However, if the ancient dynamo self-reversed as does the geodynamo, then it is difficult to account for global dipole moments larger than 10^{20} G-cm³ using crustal thermoremanence. In this second case the present martian field should be dominated by large magnetic anomalies associated with rapidly emplaced volcanic and sedimentary structures.

Color Enhanced Viking Lander Images of Mars

E. L. Strickland III, Department of Earth and Planetary Sciences, Washington University,
St. Louis, Missouri 63130.

Subtle color variations of the generally reddish martian surface materials, imaged by the Viking Lander cameras during the primary mission, were enhanced at the U.S.G.S. Flagstaff Facility. Ratioed images (e.g. Blue/(G&R), etc.) were contrast stretched and recombined with brightness information to yield color enhanced images. These images show that diffuse skylight is redder than sunlit grey lander surfaces, and bluer than sunlit soils. As a consequence, shadowed (i.e. skylit) surfaces appear redder than sunlit ones in the enhanced images.

At VL-1, five distinct soil colors can be discerned. A bright, relatively "Red"* soil forms a thin, discontinuous layer that covers most other soils. This unit is at most a few centimeters thick near the lander, and may be only microns thick. A darker "Blue" soil is exposed: (a) Where the bright "Red" soil was eroded by lander engine exhaust, (b) In the "Sandy Flats" trench (which sampled drift material), and (c) In irregular patches between rocks. Under the engine, as seen by camera 2, the dark "Blue" soil was eroded and a unique patch of bright "Orange-Red" duricrust is exposed. The "Rocky Flats" sample site, and other patches between rocks and on drifts, show a distinctive "Green-blue" color. The soil that caps the "BIG JOE" boulder, and surrounds several groups of boulders, is a dark soil that is "Redder" than the bright "Red" soil.

At VL-2 relative soil colors are similar to those at VL-1 and the interpreted stratigraphy is also similar. Widespread duricrust-textured surfaces are all "Redder" than the scene average. A darker "Blue" soil is exposed in two sample trenches and under the engine. A thin layer of intermediate-brightness, "Green-blue" soil is present as smooth patches filling dips and hollows in the duricrust. It also forms small drifts in the linear trough several meters from the lander. Beyond the trough are scattered smooth-surfaced, bright drifts of "Red" soil that are identical in color to the duricrust. The similarity between the soils at both sites suggests that globally distributed soil units may be present on Mars.

High albedo surfaces on many rocks at both sites have a green/(B&G) ratio greater than any other surface material, indicating a spectral reflectance distinct from soil surfaces. These surfaces may be a coating of weathering products formed in situ. A field of dark "Blue" rocks at the VL-1 site may be relatively young and may not have optically significant weathering rinds. At VL-2, surfaces on the sides of many rocks are identical in color to the duricrust and the "Red" drifts, and may be soil coatings. The distribution of surface colors on most rocks at both sites suggests control by environmental processes, rather than mineralogical variation within the underlying rock.

* Colors named are relative to scene averages as seen in the enhanced images.

Seasonal and Secular Behavior of Crater-Related Streaks on Mars: A Study of Mariner 9 and Viking Orbiter Data

P. Thomas, Laboratory for Planetary Studies, Cornell Univ., Ithaca, NY. 14853.

The pattern of near surface wind directions in 1976-1978 inferred from crater-related streaks visible in Viking Orbiter images is essentially identical to that observed by Mariner 9, 3 martian years earlier. The great majority of streaks at all latitudes reflect the global wind flow of late southern spring, summer, and early fall, with significant topographic influence being evident. However, some material can apparently be moved at all seasons, but with only small effects on global streak pattern.

Viking observations over 1 martian year document the following classes of behavior: (1) Bright streaks that are essentially unchanged during 4 martian years, e.g., Mesogaea, Hesperia. (2) Bright streaks that change rapidly, especially during southern spring and summer, but which retain consistent directions, e.g., Syria Planum. (3) Dark erosional streaks that form annually after global dust storms, with repetition of form and direction, e.g., Hesperia. (4) Dark erosional streaks that form in approximately the same areas as during Mariner 9, but which display forms and directions different from those in 1972, and which vary during Viking observations of southern summer and fall, e.g., Daedalia, Noachis. (5) Secular lengthening of mixed tone streaks in Oxia Palus and Cerberus between 1972 and 1978, and of bright streaks in Cerberus. The directions of elongation of these streaks are consistent with wind directions in southern summer.

High resolution images (~20 m/pixel) complement the global coverage by showing details of the streak forms. Dark erosional streaks develop by formation of a series of parallel or anastomosing dark filaments. Bright streaks are formed by deposition of very thin dust layers in streamlined zones with very diffuse boundaries and almost no internal structure.

Observations and Analysis of Frontal Systems and Periodic Processes in the Martian Atmospheric Surface Layer.

J. E. Tillman, Department of Atmospheric Science, University of Washington

Observations in the Martian atmospheric surface layer during the first autumn at the Viking Lander 2 site, 48 N, have clearly demonstrated the existence of synoptic systems that exhibit a time history very similar to terrestrial systems. The time evolution of wind, temperature and pressure during the autumn, implies that low and high pressure systems travel from west to east, north of the landing site, with a high degree of regularity. The major differences are that the diurnal and semi-diurnal tidal components are much stronger than on earth and that the passage of the systems is more regular. This periodic passage is readily observed by a time varying spectral analysis of pressure and other variables and is compared with the results of rotating "dishpan" and numerical general circulation models. An analysis of a strong system is presented along with details of the convective structure during the unstable daytime periods.

Internal Structure and Evolution of Mars

M. N. Toksöz and A. T. Hsui, Department of Earth and Planetary Sciences, Massachusetts Institute of Technology, Cambridge, MA 02139

Models of the structure and evolution of the interior of Mars have been constructed in the light of data from Viking and other missions. In addition to quantitative constraints, comparative knowledge from the earth and the Moon is incorporated into the modeling. The mean density ($\rho = 3.96 \text{ g/cm}^3$) and the moment of inertia factor ($C/Ma^2 = 0.365$) are still the primary geophysical data for the internal properties. Combining this information with a temperature profile obtained from thermal evolution modeling, a mantle composition similar to that of the earth, and an appropriate equation of state, the resultant density models favor a relatively homogeneous olivine rich mantle and a molten Fe-FeS core. The core radius is about 1500-2000 km, depending on composition. The mantle is enriched in FeO relative to the earth's mantle. An olivine-spinel phase transition occurs at a depth of 1200 to 1500 km depending on the temperature.

The temperatures inside the planet and its evolution history are calculated utilizing both geological and geophysical data as constraints. The Martian evolution can be characterized by four stages. (1) Core formation and early crust differentiation: this stage starts from the planet formation to about 1 b.y. thereafter. (2) Heating, expansion and mantle differentiation: this stage spans about 2 b.y. after the Martian core is formed, and is characterized by a gradual temperature rise in the interior. Towards the end of this period, extensive differentiation and outgassing occur. Extensional features observed at the Martian surface most likely were generated at this stage as a result of planet-wide expansion. (3) Mature phase: this stage covers the period between 3 and 4 b.y. after the planet formation, and it is characterized by the thickening of the lithosphere and the deepening of the partial melt zone. (4) Cooling phase: this is the period from 4 b.y. to present, when the planet is cooling slowly. The partial melting zone shrinks and volcanic activities taper off. Our thermal model indicates that the Martian lithosphere is about 200 km thick.

The Viking Seismic Experiment provided information about the level of seismic activity, but not about internal structure. The lower seismicity of Mars relative to the earth is consistent with the models of a cooling planet with a relatively thick lithosphere.

History of the Martian Climate

O. B. Toon, Space Science Division, NASA-Ames Research Center, Moffett Field, CA 94035

Three time scales of possible climatic change have been discovered on Mars. Interannual variations in dust storm activity, as well as CO_2 and H_2O cycles have been observed directly. Climate changes over $10^5 - 10^6$ years are suggested by theoretical studies of orbital element variations and by observations of polar sedimentary deposits. Fluvial features, and isotopic evidence for long term atmospheric composition changes may imply climatic alteration over 10^9 year time scales. The 10^5 year climatic changes can be understood by extrapolating from our current knowledge of seasonal dust, CO_2 , and H_2O cycles and their variation. We presently observe an annual CO_2 pressure oscillation as CO_2 is transferred from the annual polar caps, and perhaps the regolith, to the atmosphere. As the martian axial tilt, or obliquity changes, this same process is amplified so that less CO_2 is in the atmosphere at low obliquity and more CO_2 is in the atmosphere at high obliquity. Dust storm activity now occurs near perihelion and wind tunnel studies show that the martian atmospheric pressure is so low that only freak winds can lift dust. At the 10^5 year time scale these observations imply that no dust will be raised at low obliquity, dust will only be raised at current obliquity when the eccentricity is large, while at high obliquity, dust may be lifted at all eccentricities. Presently, H_2O vapor is transferred to the atmosphere from the permanent polar cap during summer and is returned over the area of the annual polar cap during winter. On the 10^5 year time scale we expect water will be preferentially deposited with polar dust at low obliquity and preferentially removed from polar ground at high obliquity. The polar laminae probably reflect an alteration of the water ice to dust ratio caused by increased water deposition at low obliquity and increased dust deposition at high obliquity. Numerous complications to this simple picture arise because of feedbacks between the CO_2 , dust and H_2O cycles and because the cycles are also modified by the eccentricity. Long time scale climate changes are probably driven by the geologic and chemical evolution of the martian atmosphere. These climatic changes represent significant deviations from the present day martian climate, but they can be understood within the framework of the evolution of the Earth's climate and in comparison with the present climates of the terrestrial planets. Prior to the formation of a carbonate and clay containing polar regolith, the martian atmosphere could have contained several hundred mbars of CO_2 . Such an atmosphere might not have maintained global average temperature above the freezing point of water, but equatorial regions and summer polar areas might have had above freezing temperatures due to the CO_2 , H_2O greenhouse. It is also possible that prior to this massive CO_2 atmosphere a few hundred mbar reduced atmosphere, of for example CH_4 and NH_3 might have maintained global average temperatures above freezing. Photodissociation would have allowed the hydrogen to escape, eventually producing the oxidized atmosphere we observe today.

Phobos and Deimos: A Review of Major Viking Results

J. Veverka, Laboratory for Planetary Studies, Cornell University, Ithaca, NY 14853

Comprehensive maps of the surface features on Phobos and Deimos based on high resolution Viking Orbiter coverage and making it possible for the first time to study the nature and evolution of the two surfaces in a comparative way. Both objects are covered with dark, grey, heavily-cratered regoliths, but many characteristic differences in surface morphology do occur. For example, while Phobos is criss-crossed by families of trough-like, pitted grooves, such features are entirely absent on Deimos. On the other hand, the surface of Deimos is covered with elongated deposits of relatively bright material which do not occur on the inner satellite. Available information on the morphology, distribution and probable origin of interesting surface features, such as the grooves of Phobos and the bright deposits on Deimos will be summarized, as will inferences about the composition of the satellites based on mean density and spectrophotometric measurements. Finally, current views on a number of important questions will be summarized: Why are there no grooves on Deimos? Why are older surface features on Deimos (but apparently not on Phobos) blanketed by meters of fine material? Are the two satellites made of the same material? What is the origin of the two objects?

Snow on Mars? Quantitative Evidence of Condensates Formed at the Viking Lander 2 Site During the Martian Winter

S. D. Wall, Jet Propulsion Laboratory, Pasadena, CA 91103
K. L. Jones, Planetary Research, Inc.,

One of the most striking observations made by the Viking Lander 2 during its first winter on Mars was the accumulation of a white surface condensate. Jones et al. believe that the condensate was composed of water ice, transported to the site not in the vapor phase but condensed on the surfaces of dust grains. Subsequent condensation of CO_2 ice accelerated the precipitation of both water and dust to the surface. The evidence for water ice is the extremely long time span required for the condensate to disappear; evidence for CO_2 ice is the correlation of condensate formation with the arrival of temperatures near the condensation point of CO_2 . Unfortunately, photographic support for these conclusions is obscured by constant changes in both intensity and coloration of the surface irradiance as two major dust storms passed over the landing site during the same time period.

"Pseudo-chromaticity" coordinates, similar to CIE chromaticity coordinates but with spectral bandpasses defined by the lander camera channel responsivities, have been calculated for surface patches around the lander and for a dust-free portion of the lander body. Ratios of these two sets of coordinates are relatively independent of sky color variations. These ratios provide a sensitive and quantitative measure of relative surface color and albedo changes. Plots of these quantities show that condensate accumulation began as early as VL-2 sol 200 and continued for approximately 80 sols. Relative to a condensate free surface, the albedo of selected patches increased by a factor of at most 3.5 with an accompanying color change from yellow-red to approximately neutral.

References

Jones et al, submitted to Science, 1978.

Oxidation State of Martian Basalts

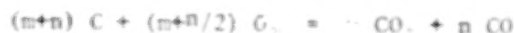
J. Warner, SL-4, NASA Headquarters, Washington D.C. 20546.

Igneous-looking rocks in the nearfield of the Viking landers have been poked and scraped utilizing teeth on the Viking surface sampler (Moore et al., 1977). Neither scratch marks nor flakes of a weathering coat were observed indicating that a weak weathering rind is not present. These observations suggest that the red color of martian rocks (presumably basalts) may be a primary feature because strong weathering rinds are not common on terrestrial rocks. This in turn implies that martian basalts were erupted at an elevated oxidation state relative to terrestrial basalts. Unweathered terrestrial basalts approximate the quartz-fayalite-magnetite (QFM) buffer, contain magnetite, and are dark grey. Unweathered martian basalts may approximate the hematite-magnetite (H-M) buffer, contain magnetite and hematite, and be red.

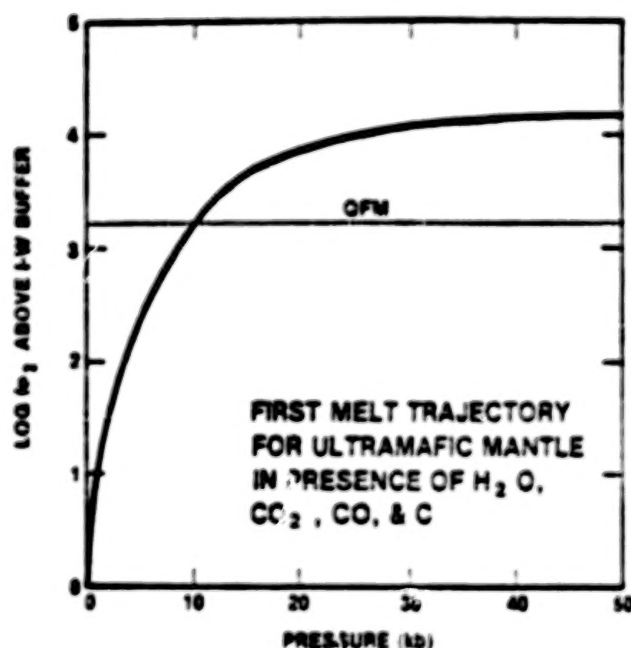
This contribution presents a mechanism whereby gas reactions in the system H-C-O may constrain martian magmas to be extruded at relatively high oxidation states, such that hematite is stable and the resultant rocks are red.

Because carbon is an abundant element and it condenses to diamond or graphite at high temperatures from solar compositions, it is assumed present in the martian mantle. This assumption is supported by terrestrial occurrence of diamond in kimberlites and graphite (or unidentified black material) as an accessory mineral in some basalts.

Sato (1977) has shown that the f_{O_2} in a magma is fixed at any given P and T by the reaction:



The Figure shows f_{O_2} (relative to the iron-wustite buffer) vs P where T at each P is appropriate for onset of melting of an ultramafic mantle in the presence of water.



The f_{O_2} of a magma formed at depth is indicated by the curve if the magma contains excess C, CO_2 , CO, and H_2O . On its trajectory to the surface, the magma's f_{O_2} changes as indicated on the curve as long as the magma contains all four phases (C, CO_2 , CO, and H_2O) in excess. However, if one of those phases is consumed by reaction, the magma's f_{O_2} will depart from the indicated curve. In water-bearing planets C may be consumed by the reaction:



and the f_{O_2} of the rising magma will rise above the indicated curve. The rate of consumption of C is approximately determined by the abundance of water in a planet. The more water in a planet, the more rapidly C will be consumed and the magma will depart from the curve at a higher P and f_{O_2} .

When a magma departs from the indicated curve, its f_{O_2} will be controlled by mineral equilibria. Because the relative f_{O_2} between mineral equilibria is almost constant

over a wide range of P and T, a magma's f_{O_2} relative to the iron-wustite buffer is not expected to change significantly beyond the magma's point of departure from the curve. Magmas that depart the curve at high P will therefore be erupted onto the surface at an elevated oxidation state.

The abundance of chemically-bound water in a planet's mantle determines the concentration of water in basaltic magmas generated by partial melting of that mantle. Those abundances for the Earth must be such that rising basaltic magmas depart from the indicated curve at approximately the f_{O_2} of the QFM buffer. Those abundances for the Moon are so low that rising

basaltic magmas remain on the curve all the way to the surface and are erupted at approximately the f_{O_2} of the iron-wustite buffer.

Based on solar nebula condensation models (e.g., Lewis, 1972), Mars is expected to contain a greater relative abundance of water in its mantle than does the Earth. If that is the case, then rising martian magmas are expected to depart from the indicated curve at a greater P and be extruded onto the surface at a higher oxidation state compared to the terrestrial case. Although this model predicts that martian basalts have a higher oxidation state than terrestrial basalts, it falls short of the goal of accounting for a f_{O_2} that approximates the (H-M) buffer by about 2 log units. Refinements are in progress.

References:

- Lewis, J. S. (1977) *Earth Planet. Sci. Lett.* 15, 286-290.
Moore, H. J. et al. (1977) *J. Geophys. Res.* 82, 4497-4523.
Sato, M. (1978) *Lunar Planetary Sci. IX*, 990-992.

Solar Wind Sputtering of the Atmosphere of Mars

C. C. Watson and P. K. Haff, A. W. Wright Nuclear Structure Laboratory, Yale University, New Haven, Connecticut 06520⁺, and W. K. Kellogg Radiation Laboratory, Caltech, Pasadena, California 91125.

We have investigated the mass loss and the chemical and isotopic fractionation implied by solar wind sputtering (SWS) of the martian atmosphere. A Monte Carlo calculation of proton and alpha particle impact and of the subsequent recoil collisions were performed. Primary proton and alpha collisions resulting in sputtering occur near or above the critical layer. Most sputtered particles are molecular rather than atomic. Proton and alpha particles are about equally effective in sputtering. Because all relevant collision processes occur at very high altitudes or because the sputtering yield is proportional to the path length in this region, ionospheric deflection of the SW may tend to increase the sputtering effects reported below.

Approximate equations were used to tie the Monte Carlo results for a CO₂ atmosphere to sputtering of nitrogen and its isotopes. Over a period of 4.5×10^9 y, SWS may have ejected a total mass roughly equal to that in the modern atmosphere. As much as 97% of the initial nitrogen content can be removed by SWS alone. This large number suggests that significant isotopic fractionation may have occurred. Preferential ejection of lighter elements and isotopes is due mainly to ordinary diffusive separation in the atmosphere and to the fact that the sputtering yield is inversely proportional to the mass of the sputtered particle. The relative enrichment factor for the ¹⁵N/¹⁴N ratio is calculated to be 2.2, assuming an initial ratio equal to the terrestrial value, while the value derived from Viking data is 1.75. These results imply that SWS has played an important role in the chemical and isotopic evolution of the atmosphere of Mars.

⁺Permanent address

TABLE OF CONTENTS

Allen, C. C., Volcano/ice interactions on Mars	1	1/A12
Arvidson, R. E. and Guinness, E. A., Rates of resurfacing of Mars - Constraints on thermal evolution	2	1/A13
Arvidson, R. E. and Jones, K., A year at Mars - Viking Lander imaging results	3	1/A14
Baker, V. R., Morphology of channels on Mars.....	4	1/B1
Balmino, G., Moynet, Reucher, P. and Vales, N., Mars gravity field to degree and order 18: First interpretation	6	1/B3
Baum, W. A., Martin, L. J., Briggs, G. A., and Barnes, J., A review of martian dust clouds and storms	6	1/B3
Bienemann, K., The search for organic compounds in the surface layer and the implications and limitations of the results	7	1/B4
Blasius, K. R., Roberts, W. J. and Glackin, D. L., Topography of martian shield volcanoes: comparison of Tharsis and Elysium structures	7	1/B4
Borderies, N., Balmino, G., Castel, L., and Moynet, B., Study and determination of Mars nutations	7	1/B4
Boyce, J. M., Martian subsurface permafrost: evidence from impact craters	8	1/B5
Breed, C. S., and Ward, A. W., Longitudinal dunes on Mars	10	1/B7
Burke, J. D., Naga - A Mars aeroscience-geoscience orbiter	11	1/B8
Carr, M. R., Formation of martian flood features by release of water from confined aquifers	11	1/B8
Casadevall, T., Stoiber, R. and Dzurisin, D., Terrestrial volcanic degassing: a review of mechanisms and magnitudes.....	12	1/B9
Chen, Z. M., The earliest-stage primitive atmospheres of the Mars and the Earth ..	14	1/B11
Chen, Z. M., The structure and oscillation of the martian upper atmosphere.....	14	1/B11
Christensen, E. J. and Balmino, G., Analysis of a twelfth degree and order gravity model for Mars.....	14	1/B11
Chun, S. F.-S., Pang, K. D. and Ajello, J. M., Photocatalytic oxidation of organic compounds in Marchison meteorite under simulated martian conditions	15	1/B12
Cintala, M. J., The effects of subsurface volatiles on martian impact cratering events	16	1/B13
Clair, B. G., Regolith uptake and recycling of volatiles on Mars	16	1/B13
Cornath, B. J., Planetary-scale wave structure in the martian atmosphere	17	1/B14
Coradini, M., A Thermodynamical approach to the study of the martian permafrost...	17	1/B14
Croft, S. K., Kietter, S. W. and Ahrens, T. J., Low velocity impact craters in ice and permafrost with implications for martian crater-count ages	18	1/C1
Cutts, J. A., Blasius, K. R. and Roberts, W. J., Polar geology on Mars: a climatic archive	18	1/C1
Darrell, J. F., Environment-organism relations and the interpretation of life-search on Mars.....	19	1/C2
Davis, G. S., Goldstone radar probes of Mars (1971-1978): A review.....	19	1/C2
Ducanbier, F. K., Lazarewicz, A. R., Toksoz, M. V., Coins, K., Miller, W. F., Andersen, D. L., Latham, G. V. and Nakamura, Y., A review of the Viking seismology experiment.....	19	1/C2
Dallus, A., Deschamps, M., Gueaux, M., Scamioniti, L. V. and Moroz, V. I., Radiometric analysis of Mars from a Sovietic spacecraft.....	20	1/C3
Durand, V. P., Lamy, Y. and Maurette, M., The Viking imagery, the early history of the martian satellites, and the accretionary tail.....	23	1/C6
Durbury, T. E., Phobos, Deimos and Mars.....	24	1/C7
Durbin, D., Casadevall, T. and Stoiber, R., Terrestrial volcanic outgassing: implications for martian atmospheric evolution and surface geology.....	25	1/C8
El Baz, F., Wind erosion in Egypt's Oweinat Mountain and implications to eolian on Mars.....	26	1/C9
El Baz, F., Clones of martian light-and dark-colored streaks in the southwestern desert of Egypt.....	26	1/C9

Fanale, F. P. and Cannon, W. A., Mars, implications of capillary condensation and adsorption of CO ₂ on clays for volatile storage and climate change.....	271/C10
Flasar, F. M., Dynamics of thermally driven winds controlled by local topography..	271/C10
Frey, H., Martian rift tectonics.....	281/C1
Friedmann, E. I., Endolithic microbial life in the Antarctic dry valleys: a terrestrial model of martian environment.....	281/C1
Gault, D. D. and Wedekind, J. A., Experimental results for effects of gravity on impact crater morphology.....	291/C12
Gibson, E. K., Andrews, P. F. and Urbancic, M. A., Volatile elements and phase determinations in planetary samples: a proven approach for consideration in future Mars studies.....	301/C13
Gottel, K. A. and Davies, G. F., Present constraints on the bulk composition of Mars and the composition of the martian mantle.....	311/C14
Gooding, J. L. and Keil, K., Relative efficiencies of volatile consumption by chemical weathering reactions on Mars.....	311/C14
Greeley, R., A model for the formation of windblown sand-size particles and related structures on Mars.....	321/D1
Guinness, E. A., Arvidson, R. E. and Lee, S. W., Differential aeolian redistribution rates on Mars.....	331/D2
Rapke, B., The photometric function of martian soil in the vicinity of Viking Lander 1.....	341/D3
Hargraves, R. B., Collinsen, D. W., Arvidson, R. E. and Cates, P. M., Viking magnetic properties experiment - results and conclusions.....	341/D3
Hori, Ki-iti, Loose and compacted soils: two basic units composing the martian surface.....	351/D4
Hosen, K. E., Davis, D. E. and Greenberg, R., Unusual ejecta dynamics on the martian satellites.....	361/D5
Bugaciu, R. L., Beal, J. W. and Setchell, T. R., Petrologic units on Mars.....	371/D6
Bugaciu, R. L., Miller, K. J., and Barwood, W. S., Mars: chemical reduction of the regolith by frost.....	381/D9
Hunt, G. E., Dust storms and condensation.....	391/D11
Hunt, D. E., Possible oxidant sources in the atmosphere and surface.....	391/D11
Intrilligator, D. S., Mars in the solar wind: implications of a Venus-like interaction.....	401/D12
Iwasaki, E., Saito, Y. and Akabane, T., Formation and regression of the martian north polar cap in 1975-78.....	411/D12
Jones, P. B., Seasonal behavior of martian polar caps.....	421/D13
Johansen, L. A., Martian splash cratering and its relation to water.....	431/D13
Kietler, B. H. and Palluconi, F. D., The climate of the martian polar cap.....	441/D14
Kietler, B. H. and Soderblom, L. A., Global variations of martian surface materials.....	451/E1
Kietler, S. W. and Sisson, C. H., The role of volatiles in the cratering process: implications for martian surface.....	461/E2
Klein, B. P., The Viking biology experiment: epilogue and prologue.....	471/E3
Komar, P. D., Modes of sediment transport in channelized water flows with ramifications to the erosion of the martian outflow channels.....	481/E3
Krinsley, D., Greeley, R. and McKee, T. B., Simulated aeolian abrasion of quartz and basalt under martian conditions.....	491/E4
Kuhn, W. R., Atreya, S. K. and Postawko, S. E., Influence of ozone on the thermal structure of the martian atmosphere.....	501/E4
Langevin, Y., An analytical model for the regolith evolution of small bodies in the solar system.....	511/E5
Leach, J. B. J., Dune forms and patterns of wind circulation in the north polar regions of Mars.....	521/E7

Leach, S., CO ₂ excitation and emission processes in Mars dayglow	52	1/E7
Levin, G. V. and Straat, P. A., Status of interpretation of Viking labeled release experiment.....	52	1/E7
Levinthal, E. C., Mars in 3-D.....	53	1/E8
Lytleton, R. A., Internal structure of Mars.....	53	1/E8
Macris, C. and Petropoulos, B., The martian atmosphere.....	53	1/E8
Malin, M. C., Mars: evidence of indurated deposits of fine materials.....	54	1/E9
Maxwell, T. A., Field investigation of martian canyonlands in southwestern Egypt..	54	1/E9
McCauley, J. F., Breed, C. S., Crolier, M. J. and Collins, F., The collian features of the north polar region of Mars.....	55	1/E10
McCord, T. B., Singer, R. B. and Clark, R. N., Mars surface composition from reflectance spectroscopy: a summary.....	56	1/E11
Moresh, B. J., Fracture systems on a reoriented planet.....	58	1/E13
Moore, B. J., Spitzer, C.R., Cates, P. M., Bradford, K. Z., Scott, R. F., Hutton, K. E., Shorthill, R. W., Surface materials of the Viking Landing sites	59	1/E14
Morgan, J. W. and Anders, E., Mars: a cosmochemical-geophysical estimate of bulk composition.....	60	1/F1
Moriyama, S. and Iwashima, T., The spectral model of the atmospheric general circulation of Mars.....	60	1/F1
Mouginis-Mark, P. J., Rampart crater formation on Mars.....	61	1/F2
Mutch, T. A., Enigmatic landforms on Mars.....	61	1/F2
Newkum, G., Hiller, K., Henkel, J. and Bodechtel, J., Martian ages.....	62	1/F2
Newman, M. J. and Butler, D. M., Cosmic pollution: evidence for recent major martian atmospheric loss.....	62	1/F2
Nunmedal, D., Mechanics of fluid release on Mars.....	63	1/F4
Owen, T., Origin of volatiles in the martian atmosphere.....	64	1/F5
Phillips, R. J. and Bills, B. G., Mars: crust and upper mantle structure.....	65	1/F6
Pickersgill, A. O. and Hunt, G. E., On the formation of martian lee waves.....	68	1/F9
Prestel, D. J., McKay, D. S., and Haynes, C. V., Evaporates from the South- western Desert, Egypt: possible martian analogues for the production of duricrust.....	70	1/F11
Roth, L. L., Downs, G. S., Saunders, R. S. and Schubert, G., Radar morphometry of craters, basins and volcanic landforms on Mars.....	71	1/F12
Russell, C. T. and Scarr, F. L., Mars, the neglected planet: a summary of past deeds and future needs for magnetic and solar wind interaction studies,	71	1/F12
Schultz, P. B. and Gault, D. E., Martian impact crater ejecta emplacement.....	72	1/F13
Schultz, P. B., Clieken, H., and McGetchin, T. R., Genesis of martian outflow channels by crater-controlled intrusions.....	72	1/F13
Scott, D. B., Mars: Viking Appraisal of mariner geologic mapping.....	73	1/F14
Shultz, A., Suttner, L. J., and Basu, A., Terrestrial debris flow deposits an analogs of martian stream fields.....	74	1/F14
Shoren, K. I. and Wimberly, W. N., Hellas Planitia gravity anomaly.....	75	1/G2
Slingson, S. A. and Taylor, G. L., Viking bistatic radar: preliminary results from the north polar region.....	75	1/G2
Smith, E. S., Mars in the solar wind: implications of an earth-like interaction.	75	1/G2
Snyder, L. W., Viking scientific results, September 1977 to September 1978.....	76	1/G3
Squyres, S., Evolution of the topography of the martian polar laminated deposits.	80	1/G7
Srinka, C. J., Crustal DEM and the magnetic field of Mars.....	80	1/G7
Strickland, E. L., Color enhanced Viking lander images of Mars.....	81	1/G8
Thomas, P., Seasonal and secular behavior of crater-related streaks on Mars: a study of Mariner 9 and Viking Orbiter data.....	82	1/G9

Tillman, J. E., Observations and analysis of frontal systems and periodic processes in the martian atmospheric surface layer.....	92	1/G9
Toksub, M. N and Hsui, A. T., Internal structure and evolution of Mars.....	83	1/G10
Toon, O. B., History of the martian climate.....	84	1/G11
Veverka, J., Phobos and Deimos: A review of major Viking results.....	85	1/G12
Wall, S. D. and Jones, K. L., Snow on Mars? Quantitative evidence of condensates formed at the Viking Lander 2 site during the martian winter.....	85	1/G12
Warner, J., Oxidation state of martian basalts.....	86	1/G13
Watson, C. C. and Haff, P. K., Solar wind sputtering of the atmosphere of Mars....	87	1/G14
Wells, R. A., Mantle flow and crustal structure inferred from the low degree harmonics of the martian geopotential.....	88	2/A5
Wise, D. U., Golembek, M. P. and McGill, G. E., Structural sequence, timing and a model for the evolution of the Tharsis province of Mars.....	89	2/A6
Wu, S. S. C., Topographic mapping of Mars.....	90	2/A7

Mantle Flow and Crustal Structure Inferred From the Low Degree Harmonics of the Martian Geopotential

R. A. Wells*, 145 Posen Avenue, CA 94706

The 9th order and degree harmonic coefficients of the Martian gravity model by Sjogren et al. (1975, *JGR*, 80:2899) were utilized in Runcorn's (1967, *G. J. Roy. Astron. Soc.*, 14:375) equations to generate the horizontal stress field in the crust of Mars. Runcorn's theory as applied to the Earth presumed that lateral density differences were deep-seated, owed their origin to mantle-wide convection, and were responsible for the major features of the geoid. The resulting compression/tension patterns were found to be strongly correlated with the world-wide trench-mountain and ridge-rift tectonic systems. The purpose of applying this theory to Mars was to establish epochal stress maps which could be compared with the photographed surface to shed light on the development of lithospheric plates both with regards to Mars itself and the earlier geologic history of the Earth. Since the dominant harmonics of both the solid surface and the geopotential of Mars are the 2nd and 3rd with contributions from higher harmonics being much smaller, it was possible to vary J_2 of the geopotential from its present value to zero so that the transition in the crustal stress field from the 2nd to 3rd harmonics, respectively, could be observed.

The following results were obtained. The dominant 2nd harmonic stress pattern indicated rising convection currents at the equator and descending currents at the poles. The currents ascended and spread out from the region of Valles Marineris and from an antipodal location. A major escarpment and series of related fractures, heavily flooded by lava, were found in the latter position suggesting that a rift valley like Valles Marineris once existed on the opposite side of the planet. At the south pole, the currents did not simply descend into the interior, but rather swirled around the pole to form a massive compression in a direction towards the pole between the 250° and 270°W meridians at latitudes $\approx 85^\circ$ S. A curving system of trenches is located in this region of compression. Horizontal stresses in the north polar region indicated a more uniform approach of convection currents towards a point off-centered from the pole and located near the center of the unusual 'stacked-plate' or terraced highland. Given that the 2nd harmonic convection pattern operated episodically, then the stacked-plate units discovered at both poles are explicable as crustal rebounds during convective cessation following downwarping during the active cycle. The appearance of the steps as either escarpment terraces or v-shaped troughs depends on the completeness of the rebound so that both types may be present as is observed. (In this model, deposition of dust/ice laminae is strictly limited only to the smaller banding seen in the exposed terrace faces rather than as the origin of the stacked-plate units as a whole. That is, dust/ice layers were apparently periodically laid down over all of each unit during the entire course of the downwarp/rebound cycles.) The asymmetry of the terraced units with respect to the poles and with respect to each other is due to the different manner in which the convection currents approached the site of zero stress- e.g., the compressive swirl in the south which formed trenches that cut across the southern stacked-plate unit.

The present horizontal stress pattern is dominated by the 3rd harmonic. If Mars had a lithospheric plate system, then this pattern of compression and tension zones would delineate the plate edges. However, only a few surface features have been found which correlate with this pattern. Therefore, Mars has not yet experienced a history of plate tectonics as has the Earth; but the 3rd harmonic stress pattern and marginal correlations do suggest that such a plate system is incipient.

Details of this study, including the geologic history during the precursor 1st harmonic convection cell and the origin of the Tharsis and Elysium volcanic shields, can be found in the author's text *Geophysics of Mars* (Elsevier, Amsterdam, in press).

*Formerly, Space Sciences Laboratory, University of California, Berkeley.

basaltic magmas remain on the curve all the way to the surface and are erupted at approximately the f_{O_2} of the iron-wüstite buffer.

Based on solar nebula condensation models (e.g., Lewis, 1972), Mars is expected to contain a greater relative abundance of water in its mantle than does the Earth. If that is the case, then rising martian magmas are expected to depart from the indicated curve at a greater P and be extruded onto the surface at a higher oxidation state compared to the terrestrial case. Although this model predicts that martian basalts have a higher oxidation state than terrestrial basalts, it falls short of the goal of accounting for a f_{O_2} that approximates the (H-M) buffer by about 2 log units. Refinements are in progress.

References:

- Lewis, J. S. (1977) *Earth Planet. Sci. Lett.* 15, 286-290.
Moore, H. J. et al. (1977) *J. Geophys. Res.* 82, 4497-4523.
Sato, M. (1978) *Lunar Planetary Sci.* IX, 990-992.

Solar Wind Sputtering of the Atmosphere of Mars

C. C. Watson and P. K. Haff, A. W. Wright Nuclear Structure Laboratory, Yale University, New Haven, Connecticut 06520⁺, and W. K. Kellogg Radiation Laboratory, Caltech, Pasadena, California 91125.

We have investigated the mass loss and the chemical and isotopic fractionation implied by solar wind sputtering (SWS) of the martian atmosphere. A Monte Carlo calculation of proton and alpha particle impact and of the subsequent recoil collisions were performed. Primary proton and alpha collisions resulting in sputtering occur near or above the critical layer. Most sputtered particles are molecular rather than atomic. Proton and alpha particles are about equally effective in sputtering. Because all relevant collision processes occur at very high altitudes and because the sputtering yield is proportional to the path length in this region, ionospheric deflection of the SW may tend to increase the sputtering effects reported below.

Approximate equations were used to tie the Monte Carlo results for a CO₂ atmosphere to sputtering of nitrogen and its isotopes. Over a period of 4.5×10^9 y, SWS may have ejected a total mass roughly equal to that in the modern atmosphere. As much as 97% of the initial nitrogen content can be removed by SWS alone. This large number suggests that significant isotopic fractionation may have occurred. Preferential ejection of lighter elements and isotopes is due mainly to ordinary diffusive separation in the atmosphere and to the fact that the sputtering yield is inversely proportional to the mass of the sputtered particle. The relative enrichment factor for the $^{15}\text{N}/^{14}\text{N}$ ratio is calculated to be 2.2, assuming an initial ratio equal to the terrestrial value, while the value derived from Viking data is 1.75. These results imply that SWS has played an important role in the chemical and isotopic evolution of the atmosphere of Mars.

⁺Permanent address

Structural Sequence, Timing, and a Model for the Evolution of the Tharsis Province of Mars

D. U. Wise, M. P. Golembek, G. E. McGill, Dept. of Geology and Geography, Univ. of Mass., Amherst, MA. 01003.

The discovery and mapping of the Tharsis province of Mars, with its spectacular volcanoes, radial fault system, and great elevations, is among the major achievements of the Mariner and Viking explorers. The province covers ~25% of the planet, with the most distal portions of its radial fault system 10,000 km apart. Its history and origin are central to all martian tectonic syntheses.

Structural or stratigraphic superposition relations and crater statistics are used to place time limits on Tharsis history. All the crater data are reduced to a standard crater number (number of craters ≥ 1 km in diameter per 10^6 km²) using the standard curve of Neukum and Wise (1976). The exact relationship between crater number and absolute age is still debated; however most workers agree that the martian curve is within a factor of 2 of the lunar curve (informal conf., Planetary Geology Principal Investigators Meeting, Tucson, May 1978). The bulk of Tharsis events occur before crater number 5,000, in the extremely steep portion of the lunar curve. Thus the timing of these events is insensitive to the particular cratering model selected.

Martian tectonic history can be broken into several phases: 1) an early period of intense cratering of the crust yielding crater density numbers of 100,000-400,000 (4-4.5 b.y.b.p.), 2) destruction of the crust of the present northern third of Mars with isostatic lowering and resurfacing terminating at about crater number 50,000 (~4 b.y.b.p.), 3) rapid and permanent rise of Tharsis with development of the major radial fault system in the period of crater numbers 15,000-5,000 (3.5-4 b.y.b.p.), 4) volcanism with local intense faulting producing the giant volcanoes in the time from crater number 5,000 to present (last 3-3.5 b.y.). This last phase falls in the flat portion of the crater density vs. age curve, and thus its timing is very sensitive to the cratering model. For this reason, it is uncertain if the late volcanic phase is completed or if it represents an essentially continuous level of volcano-tectonic activity.

The rapid and early development of the two first-order asymmetries of Mars - the uncratered third followed closely by Tharsis - suggests a possible genetic link between them involving a change in some fundamental mantle process. A model is proposed (Wise et al., in review) involving sub-crustal erosion and foundering of the heavily cratered ancient crust to form the resurfaced northern third of Mars. This sub-crustal erosion is believed due to deep convection which ceased to be effective for resurfacing about 4 b.y. ago. Some of the lighter eroded material was then underplated and intruded beneath the Tharsis region. The resulting isostatic rise within the 3.5-4.5 b.y. time period produced a permanent and geologically rapid uplift of Tharsis. Shallow gravity sliding off the uplift formed the radial fault system. The deep underplate with excess heat and radioactive elements required a much longer time to affect the surface. Its major results have been the construction of the spectacular volcanic cones as the highlights of the last 3 b.y. of martian history.

References:

- Neukum, G. and D. U. Wise (1976) Mars: A standard crater curve and possible new time scale, *Science*, **194**, 1381-1387.
Wise, D. U., M. P. Golembek, and G. E. McGill, Tharsis province of Mars: Geologic sequence, geometry, and a deformation mechanism, *Icarus*, in review.

Topographic Mapping of Mars

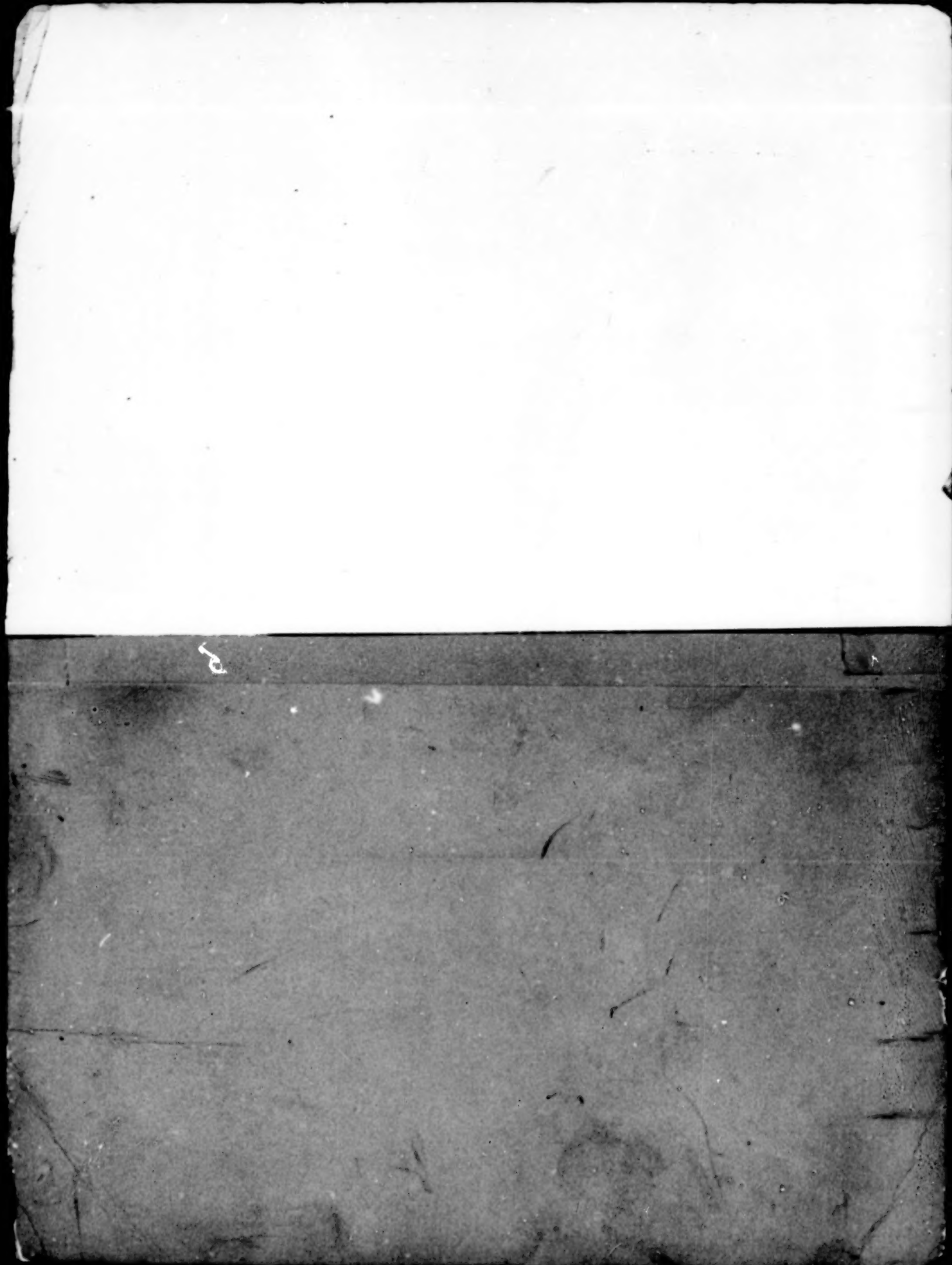
S. S. C. Wu, U. S. Geological Survey, Flagstaff, Arizona

Topographic mapping of Mars is described with three integrated parts including the global and local scales, and the close-up scale of areas surrounding the two Viking Landers.

By synthesis of imaging and non-imaging topographic information, a global topographic contour map of Mars is derived. This map represents the general topography and gives us a broad, quantitative view of the fascinating planet. It particularly shows a ring of high mountainous terrain along the equatorial belt of Mars which explains the phenomena that the martian flattening determined by optical measurements is always larger than that determined dynamically.

Using various resolution Viking Orbiter photographs, topographic contour maps of a broad range of prominent geologic features of Mars are compiled at intermediate scales. The topographic map of Tithonium Chasma shows an extensive landslide area with slopes varying from 20° to 28° at the canyon walls. The contour map which covers the grooved terrain at the northwest of Olympus Mons was compiled with a contour interval of 25 m and provides fine details of the aureole deposit materials around the volcanic feature.

Using imagery taken by the Lander facsimile cameras, special detailed close-up scale (1:10) topographic maps of the terrain surrounding the two landers have been compiled.



END

July 2, 1981